Development of Manufacturing Process and Testing for Thick Curved Thermoplastic Composite Tubes Made by Automated Fiber Placement

Chong Hui Song

A Thesis in

The Department

of

Mechanical and Industrial Engineering

Presented in Partial Fulfillment of the Requirements

For the Degree of Master Science at

Concordia University

Montreal, Quebec, Canada

February 2018

CONCORDIA UNIVERSITY
SCHOOL OF GRADUATE STUDIES

This is to certify that the thesis prepared,

By: **Chong Hui Song**

Entitled: "**Development of Manufacturing Process for Thick Curved Thermoplastic Composite Tubes and Testing Made by Automated Fiber Placement"**

and submitted in partial fulfillment of the requirements for the degree of

Master of Applied Science (Mechanical Engineering)

complies with the regulations of this University and meets the accepted standards with respect to originality and quality.

Signed by the Final Examining Committee:

_____Chair
Dr.

_____Examiner
Dr.

_____Examiner
Dr.

_____Supervisor
Dr. S. V. Hoa

Approved by

_____
Dr.

_____
Dean Amir Asif Faculty of Engineering & Computer Science

Date: _____

Abstract

Composite materials have numerous commercial and industrial applications, especially in aircraft and space where the weight-saving could be of significance. One of the important considerations is to make tubular skid landing gears for helicopter by using thermoplastic composite materials. Numerous works have been done to research the possibility of using thermoplastic composites to replace the aluminum, the principal material of landing gears for helicopter. Previous works [11, 12, 13] have shown that straight aluminum tubes could be replaced by straight tubes of thermoplastic composite material. The tubes have shown same strength and stiffness, and the composite tubes have less weight. This research aims to develop an effective and practical way in using Concordia lab facilities to manufacture thick curved thermoplastic tubes that can be used as cross tubes on helicopters.

The curved tubes were tested under three point loading. Strains and displacements were measured at different loads. Finite element analysis was carried out, and the calculated strains and displacements are compared with experimental values.

Keywords: manufacturing process, thermoplastic composites, automated fiber placement, thick curved tube, collapsible mandrel, water soluble materials

Acknowledgement

The author appreciates financial supports from the NSERC Industrial Research Chair project on Automated Composite Manufacturing, from the Natural Sciences and Engineering Research Council of Canada, Bell Helicopter Textron Canada Ltd., and Bombardier Aerospace. High tribute is paid to Bell Helicopter Textron Canada Ltd. for providing support.

I would like to express special thanks to my supervisor Dr. Suong Van Hoa for having allowed me to participate in this research. He is always ready and patient to offer necessary instructive advices and helpful comments, which is a great contribution to this research. This project could not have reached the present results without his consistent instructions.

Deep gratitude goes to Jeffery Fortin Simpson who is extremely experienced in automated fiber placement. His patient collaborations and suggestions played an important role in realization of this project, and are always highly appreciated.

Sincere appreciation should be paid to Xiao Cai and Jun Fei Li for their valuable assistances and advices in testing and finite element analysis.

I am very indebted to all the people in Concordia Center for Composites who gave me their assistance and time in this research. It is very pleased to have an opportunity to work in such a competent group.

I am most grateful to examining committee for reading this thesis and for the helpful comments.

Contents

List of Figures

List of Tables

Chapter 1. Introduction

1.1 Fiber-reinforced composite materials

Fiber-reinforced composite materials usually consist of two ingredients: fibers and matrix. Fibers of high strength and modulus, acting as the principal load-carrying members, are embedded in matrix. There are recognizable interfaces (boundaries) between fibers and matrix. In such a manner, the fibers offer reinforcement to the matrix, and the matrix provides multiple useful functions: keeping the fibers in desired location and orientation, and transferring loads between fibers, and protecting fibers from environmental damages caused by elevated temperature and humidity [1].

The two constituents of a composite, fibers and matrix, retain their own physical and chemical features, and produce a combination of properties that cannot be achieved with only fibers or matrix alone. Most fiber-reinforced composite materials have a combination of strength and modulus that are comparable to or better than many traditional metallic materials. The superior strength-weight ratios and modulus-weight ratios of a few composite materials are listed in Table 1.1[1].

Fiber-reinforced composite materials are anisotropic materials. Their properties strongly depend on the direction of measurement. Generally, the maximum tensile strength and modulus exist along the fiber direction, and the minimum strength and modulus are in the transverse direction, 90° to the fiber direction. (Figure1.1) There is also angular difference to other mechanical and thermal properties such as thermal conductivity, coefficient of thermal expansion, and impact strength. Such a unique nature of fiber-reinforced composite materials offers the design flexibility to increase the strength of a structure in a preferred direction where the major stress occurs, or to fabricate a structure with zero coefficient of thermal expansion. [1,2]

Compared with metals, composite materials have other distinct properties like lower coefficient of thermal expansion offering great dimensional stability; high internal damping that leads to better energy absorption; and noncorroding behavior. Table 1.2 presents the thermal properties of selected composites and metals. [1]

Table 1.1 Tensile properties of some metallic and structural composite materials [1]

Tensile Properties of Some Metallic and Structural Composite Materials

Material[a]	Density, g/cm^3	Modulus, GPa (Msi)	Tensile Strength, MPa (ksi)	Yield Strength, MPa (ksi)	Ratio of Modulus to Weight,[b] 10^6 m	Ratio of Tensile Strength to Weight,[b] 10^3 m
SAE 1010 steel (cold-worked)	7.87	207 (30)	365 (53)	303 (44)	2.68	4.72
AISI 4340 steel (quenched and tempered)	7.87	207 (30)	1722 (250)	1515 (220)	2.68	22.3
6061-T6 aluminum alloy	2.70	68.9 (10)	310 (45)	275 (40)	2.60	11.7
7178-T6 aluminum alloy	2.70	68.9 (10)	606 (88)	537 (78)	2.60	22.9
Ti-6A1-4V titanium alloy (aged)	4.43	110 (16)	1171 (170)	1068 (155)	2.53	26.9
17-7 PH stainless steel (aged)	7.87	196 (28.5)	1619 (235)	1515 (220)	2.54	21.0
INCO 718 nickel alloy (aged)	8.2	207 (30)	1399 (203)	1247 (181)	2.57	17.4
High-strength carbon fiber–epoxy matrix (unidirectional)[a]	1.55	137.8 (20)	1550 (225)	—	9.06	101.9
High-modulus carbon fiber–epoxy matrix (unidirectional)	1.63	215 (31.2)	1240 (180)	—	13.44	77.5
E-glass fiber–epoxy matrix (unidirectional)	1.85	39.3 (5.7)	965 (140)	—	2.16	53.2
Kevlar 49 fiber–epoxy matrix (unidirectional)	1.38	75.8 (11)	1378 (200)	—	5.60	101.8
Boron fiber-6061 A1 alloy matrix (annealed)	2.35	220 (32)	1109 (161)	—	9.54	48.1
Carbon fiber–epoxy matrix (quasi-isotropic)	1.55	45.5 (6.6)	579 (84)	—	2.99	38
Sheet-molding compound (SMC) composite (isotropic)	1.87	15.8 (2.3)	164 (23.8)		0.86	8.9

[a] For unidirectional composites, the fibers are unidirectional and the reported modulus and tensile strength values are measured in the direction of fibers, that is, the longitudinal direction of the composite.

[b] The modulus–weight ratio and the strength–weight ratios are obtained by dividing the absolute values with the specific weight of the respective material. Specific weight is defined as weight per unit volume. It is obtained by multiplying density with the acceleration due to gravity.

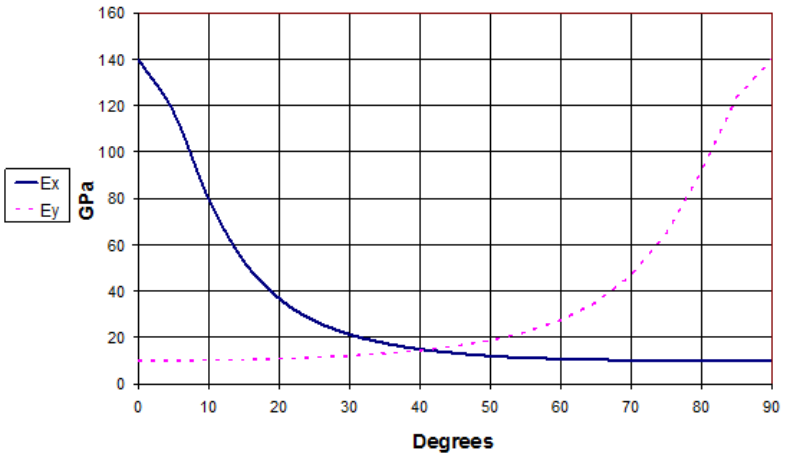

Figure 1.1 Angular variance of the stiffness [1]

Composite materials have increasing applications in commercial and military aircrafts where the weight-saving leads to significant benefits along with the development of the materials and the manufacturing technologies. Boeing 777 was introduced in 1995 when Boeing started to use composite materials in commercial aircraft in a large scale. [1] About 10% of this plane's structural weight was made of carbon fiber-reinforced epoxy and about 50% was made of aluminum alloys. The composite materials were employed to make the control surfaces, engine cowling, fuselage floor beam, and empennage. Figure 1.2 displays the application of composite materials in the Boeing 777. [1]

Table 1.2 Thermal properties of selected metals and composite materials [1]

Thermal Properties of a Few Selected Metals and Composite Materials

Material	Density (g/cm^3)	Coefficient of Thermal Expansion (10^{-6}/°C)	Thermal Conductivity (W/m°K)	Ratio of Thermal Conductivity to Weight (10^{-3} m^4/s^3 °K)
Plain carbon steels	7.87	11.7	52	6.6
Copper	8.9	17	388	43.6
Aluminum alloys	2.7	23.5	130–220	48.1–81.5
Ti-6Al-4V titanium alloy	4.43	8.6	6.7	1.51
Invar	8.05	1.6	10	1.24
K1100 carbon fiber–epoxy matrix	1.8	−1.1	300	166.7
Glass fiber–epoxy matrix	2.1	11–20	0.16–0.26	0.08–0.12
SiC particle-reinforced aluminum	3	6.2–7.3	170–220	56.7–73.3

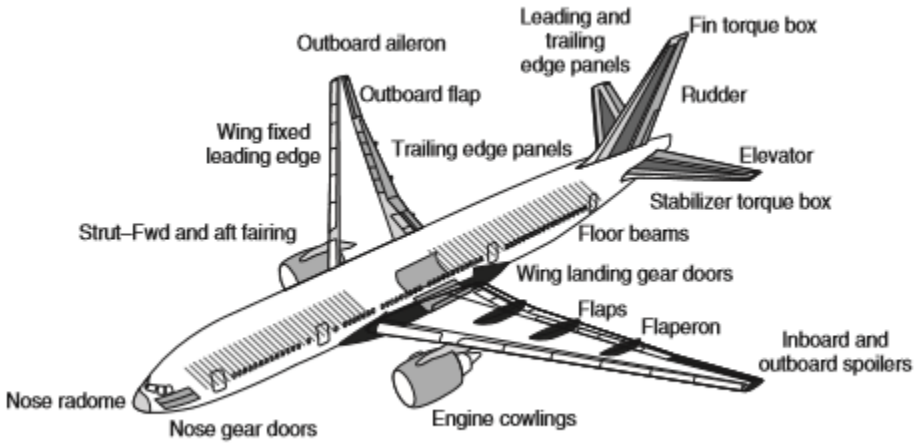

Figure 1.2 Use of fiber-reinforced polymer composites in Boeing 777 [1]

For the next generation of airplanes, the Boeing 787 Dreamlinear, about 50% of the structural weight is made of fiber-reinforced materials (Figure 1.2). [3]

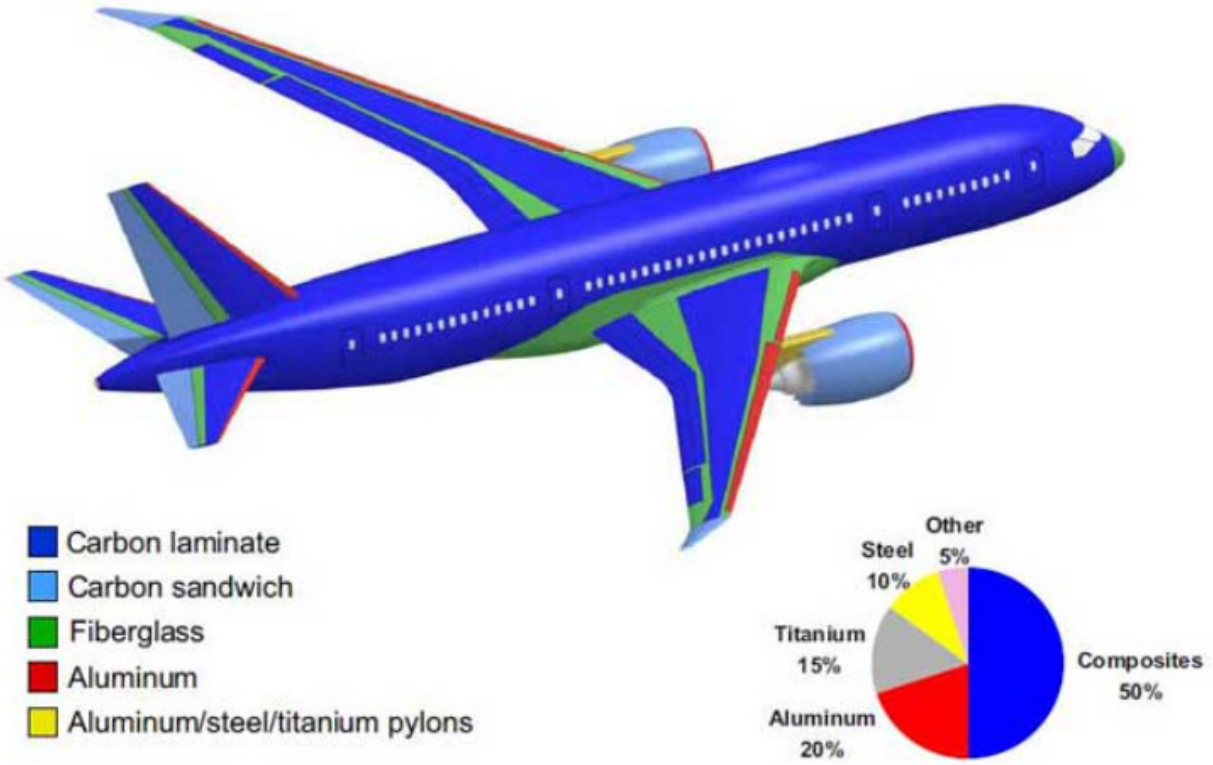

Figure 1.3 Boeing 787 Dreamlinear composite profile [3]

1.2 Thermoplastic composite materials

Fiber-reinforced polymer composite materials are classified as either thermoset composites or thermoplastic composites depending on the type of the polymeric matrix. The molecules in thermoset polymers are joined together by cross-links and need cross-linking chemical reactions to solidify. Once these cross-links are formed during the polymerization reactions (curing reactions), the themoset polymers cannot be melted and reshaped by applying heat and pressure. [2, 5, 6]

On the other hand, thermoplastic polymers do not have cross links. Their molecules are kept in place by weak secondary bonds (molecular forces and physical entanglement). When heat and pressure are applied, these bonds in solid thermoplastic polymer can be broken and the molecules can move to new positions. Upon cooling the molecules are frozen in the new positions and form a new shape. This heating-cooling process can be done as many times as desired. Figure 1.4 shows the schematic presentation of thermoplastic and thermoset composites. [2, 5, 6]

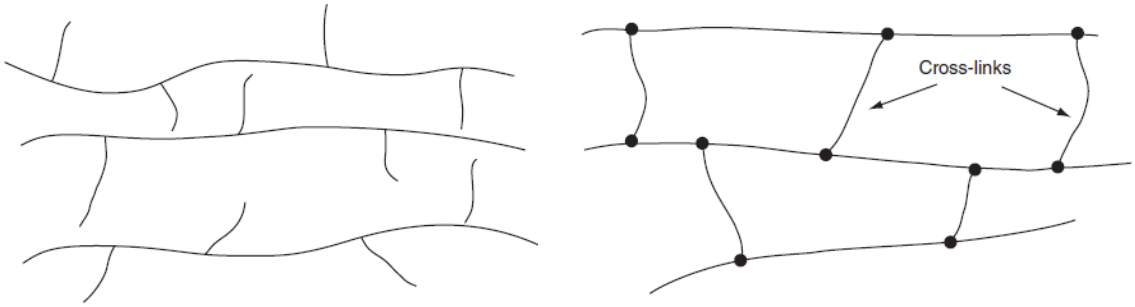

(a) Thermoplastic (b) Thermoset

Figure 1.4 Presentation of thermoplastic and thermoset polymer [1]

Thermoplastic composites materials employ the thermoplastic polymer as matrix. Their stiffness and strength are provided by the size of molecule which are non-reactive, and by the degree of entanglement of polymer chains. Due to the high molecular length, it is very difficult for these molecules to move around at a moderate temperature. High temperature must be applied so that the molecules could move relative to each other. Compared with thermoset polymer, thermoplastic resins exhibit very high viscosity even at high temperature. Table 1.3 shows that Polyetheretherketone (PEEK) has viscosity of 10^6 cP at 400 °C. [2]

Table 1.3 Viscosity of some composite materials [2]

Viscosity (in centipoise) of a Few Thermoset and Thermoplastic Materials (1 Pa-sec = 10 Poise = 1000 centipoise).

Material	20°C	25°C	T°C
Air	0.0187		
Water	1		
Polyester	100–300		
Vinyl ester	100–300		
#10 Motor oil	500		
Golden syrup	2,500		
Epoxy (Shell Epon 828-14 phrMPDA, 15 phr BGE)	600		
Epoxy (Shell 826 16 phr MPDA, 10phr BGE)	750		
Epoxy (Dow 332-16 phr MPDA, 10 phr BGE)	500		
Molasses		10^5	
Epoxy 5208			100 @ 177°C
BMI			1000 @ 150°C
Ryton (thermoplastic)			10^7 @ 313°C
PEEK (thermoplastic)			10^6 @ 400°C
Utem (thermoplastic)			10^8 @ 305°C
Torlon (thermoplastic)			10^9 @ 350°C

The processing temperature of thermoplastic composites is higher than that of thermoset composites, which requires that the mandrel used in manufacturing must be able to withstand high temperatures. Table 1.4 lists the processing temperature of common thermoplastic polymers.

Table 1.4 Common thermoplastic polymers [7]

Polymer	Morphology	T_g (°C)	T_m (°C)	$T_{process}$ (°C)	Cost (Relative)
PBT	Semi-crystalline	56	223	250	$$
PA-6	Semi-crystalline	48	219	245	$
PA-12	Semi-crystalline	52	176	224	$
PP	Semi-crystalline	-20	176	190	$
PEEK	Semi-crystalline	143	343	390	$$$
PEI	Amorphous	217	---	330	$$
PPS	Semi-crystalline	89	307	325	$
PEKK	Semi-crystalline	156	306	340	$$

Due to the difference of the polymer matrix, thermoplastic and thermoset composite materials demonstrate different properties and processing conditions. Table 1.5 displays the processing conditions of two types of composite materials.

Table 1.5 Processing properties of thermoplastic and thermoset composites [8]

Feature	Thermoplastic matrix	Thermose matrix
Fiber impregnation	Difficult	State-of-the-art
Shel life	Unlimited	Limited
Handling	Usually difficult	Usually easier
Industrial health	Easy	Critical
Mechining effort	High	High
Processing time	short tovery short	Medium to long
Recycling	Possible	Under certain conditions

Low viscosity is the main reason for the predominance of thermoset matrix composites. The development of very low void thermoplastic unitapes and advanced manufacturing technologies such as automated fiber placement system bring more interest and applications for thermoplastic composite materials. Figure 1.5 shows the trends in materials used in aerospace, which shows the increasing applications of the thermoplastic composite materials.

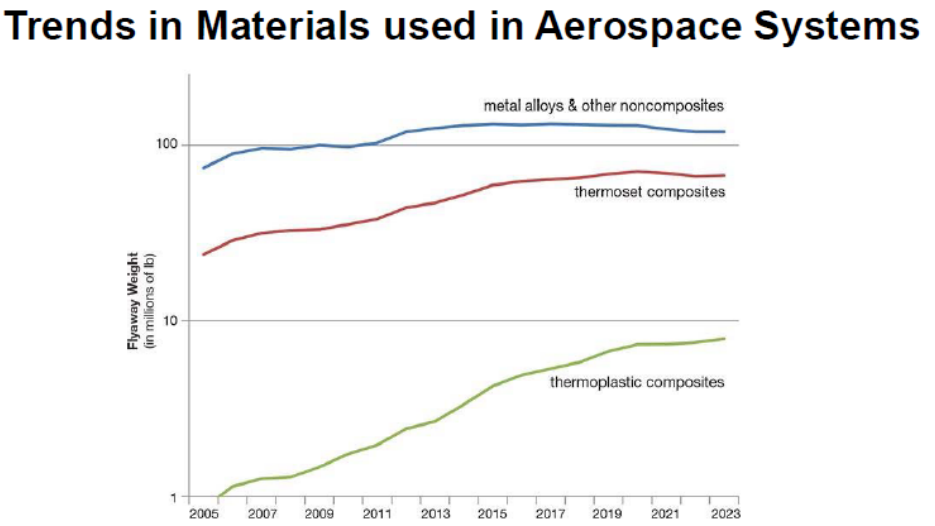

Red, C., *The Outlook for Thermoplastics in Aerospace Composites, 2014-2023*, in *High-Performance Composites*. 2014, Gardner Business Media, Inc.: Cincinatti, Ohio. p. 54-63.

Figure 1.5 Trends in materials used in aerospace system [8]

1.3 Automated fiber placement (AFP)

AFP, known as automated fiber placement or advanced fiber placement, is one of the most advanced technologies of manufacturing composite parts. This technology enables the fabrication of large complex composite parts of a large variety of size and shape. It can be used to manufacture complex structures that are not possible to manufacture with any other methods

Figure 1.6 illustrates the automated fiber placement system. In the system, the required number of tows of composite tape is loaded into a creel system. When the tows are fed, they pass in front of a process heat source (hot gas torch or other heat source) and under a consolidation device (roller or other types). The heat melts the thermoplastic matrix, or makes the thermoset tape more sticky, allowing the incoming tape to adhere onto the previous ply when pressed down by the consolidation device. At the end of each band, the tows in process are cut and the robot moves to the next band. The process is repeated band-by-band until each ply is completed. The process continues ply-by-ply until the final part is achieved, and no further processing is required, thus manufacturing time is reduced. [9]

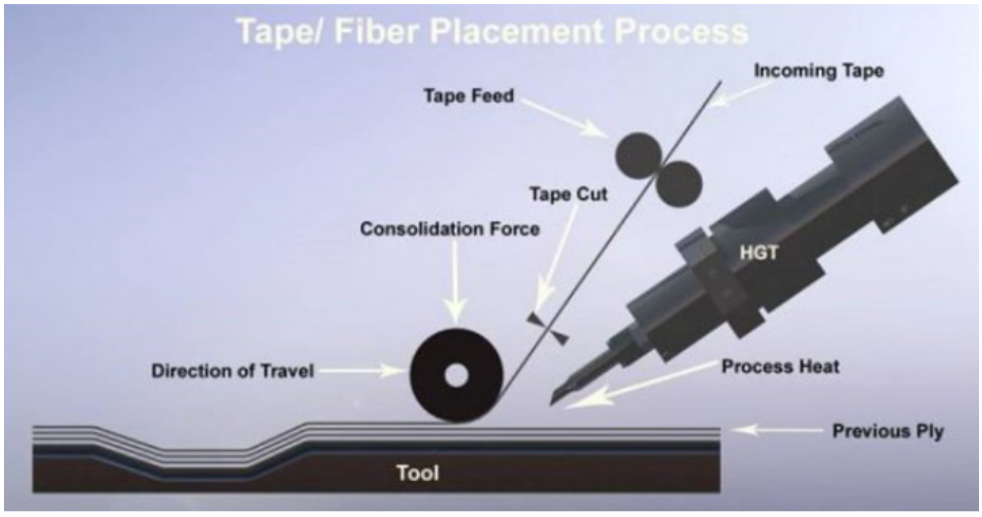

Figure 1.6 Automated fiber placement system [9]

Parts manufactured with advanced fiber placement system reach the net-shaped, so the material scrap rate is greatly reduced. It is reported that the fiber placement manufacturing produces typically 2% to 15% scrap, as compared to 50% to 100% for the traditional fabrication techniques [10]. The precise fiber orientation control of this system offers the possibility to optimize product performance by tailoring or by applying local reinforcements.

Figure 1.7 shows the automated fiber placement machine at Concordia Center for Composites, fabricated by Automated Dynamics. This system is used to offer support to fundamental research and service to industry, and has principal features as:

(1). 6 axis Kawasaki articulated arm robot;

(2). 125 kg payload;

(3). Interchangeable processing heads;

(4). Work envelope: 48 inches of OD, 120 inches by length;

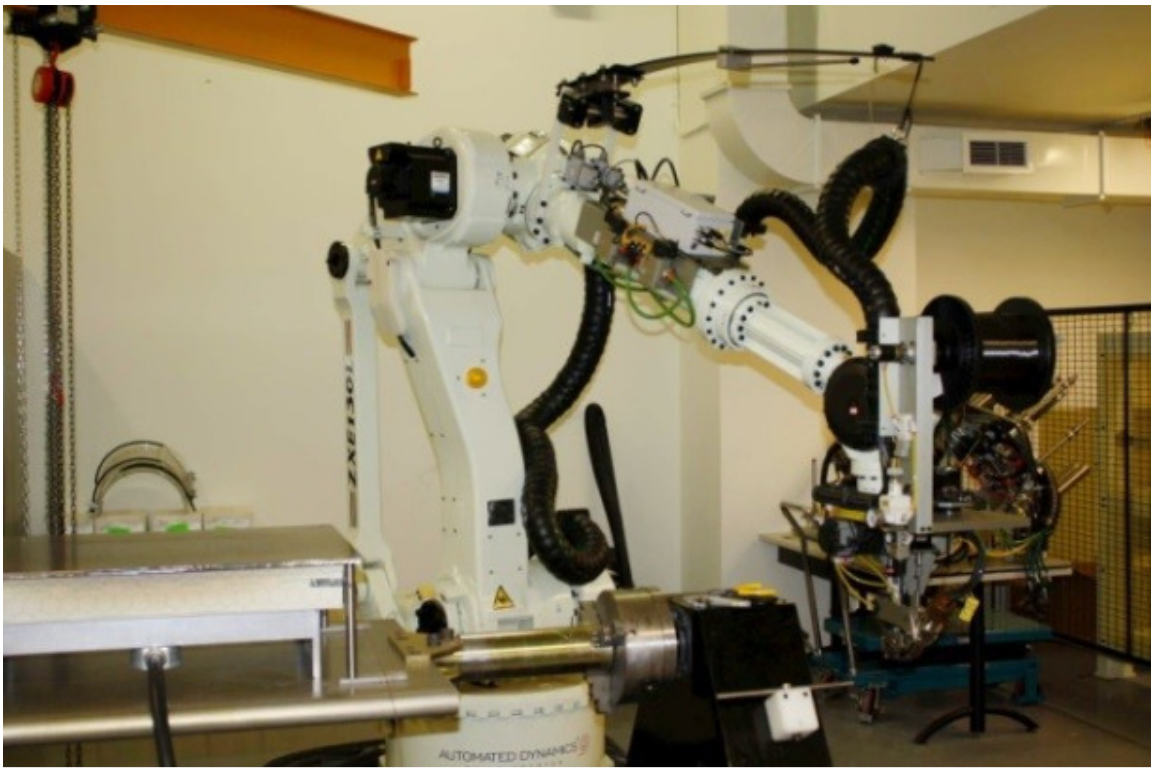

Figure 1.7 ADC fiber placement system in CONCOM

Along with the advantages of automated fiber placement technology, the distinct properties of thermoplastic composites provide the possibility of manufacturing thick curved thermoplastic composite tubes used as landing gear for helicopter.

1.4 Objective and plan of the research

Previous researches have been done showing that a straight aluminum circular tube could be replaced by a straight composite tube, which offer the possibility to fabricate composite skid type landing gear for helicopter instead of using aluminum. Based on the previous research works, the manufacturing of curved thermoplastic tubes becomes the principal part of this dissertation.

Focusing on the experimental aspect, the research presented in this thesis aims to develop a manufacturing process to make a thick curved thermoplastic composite tube using automated fiber placement. This thesis includes the following objectives:

1.) Development of a process to fabricate thick curved thermoplastic tube by using automated fiber placement;

2.) Applying the process to manufacture thick curved thermoplastic tubes;

3.) Bending test of the curved tube and result analysis.

4.) Comparison of the experimental data and FEA analysis results.

1.5 Literature review

Conventional skid type landing gear for helicopter is made of high strength aluminum. It consists of skid tubes and cross tubes (Figure 1.8). The cross tubes absorb energy with plastic deformation in hard landing, and the skid tubes provide stability to the helicopter. The aluminum skid landing gears serve well on helicopters for decades despite a few shortcomings: difficulty in fabrication, spot corrosion in normal landing, high maintenance cost, etc. One solution to overcome these shortcomings is to develop new skid landing gear using fiber reinforced composite materials. [11]

Compared with aluminum, composite materials have higher strength-to-weight ratio and stiffness-to-weight ratio (Table 1.1), but have smaller limit strain. When fiber angle changes, the limit strain varies. It is reported that AS4/PEKK, carbon fiber thermoplastic composite, has strain limit of 1.45% for samples of $(0°)_{4s,}$ and 6% for samples of $(\pm 45°)_{2s}$ with a sacrifice of stiffness from 140 GPa to 18 GPa [12,13]. This unique angular difference of properties gives the design flexibility to design skid landing gear that is comparable or better than aluminum skid landing gear.

Figure 1.8 Cross tube for landing gear in helicopter (Bell 206L) [3]

There has been significant amount of work done on composite tubes. These are usually made using filament winding method.[14], and they are used for making pipes or pressure vessels[15]. These tubes are usually made using thermoset composite materials. There has been limited amount of work done on thick thermoplastic composite tubes. Even though filament winding using thermoplastic composites has been carried out [16], it is usually difficult to process thermoplastic composites into complex shapes. The advent of automated fiber placement (AFP) machine has provided a breakthrough on this problem. AFP machines using either hot gas torch or laser have been used to make tubes out of thermoplastic composites. Taking advantage of this advanced technology, the fabrication of thick thermoplastic tubes has been done.

Bijan Derisi [11] showed that thermoplastic composite material can be used to make the composite landing gear for helicopter since the thermoplastic polymers have higher toughness and deformability that could contribute to the deformation of the composite tube. His research showed that a 140-layer straight composite tube made of AS4/PEKK with a stacking sequence of $[(90)_{20}/ (\pm25)_{20}/ (90)_5/ (\pm30)_{25}/ (90)_5/ (\pm45)_{10}]$ have the same strength and stiffness as that of aluminum tube with significant amount of elongation (Figure 1.9). In this composite tube, the layers that could sustain large deformation ([±45°]) are placed on the outside, and those layers with small deformation ([±25°]) are located close to the neutral axis. Layers with different strain limits are separated with composite plies of 90°. [11]

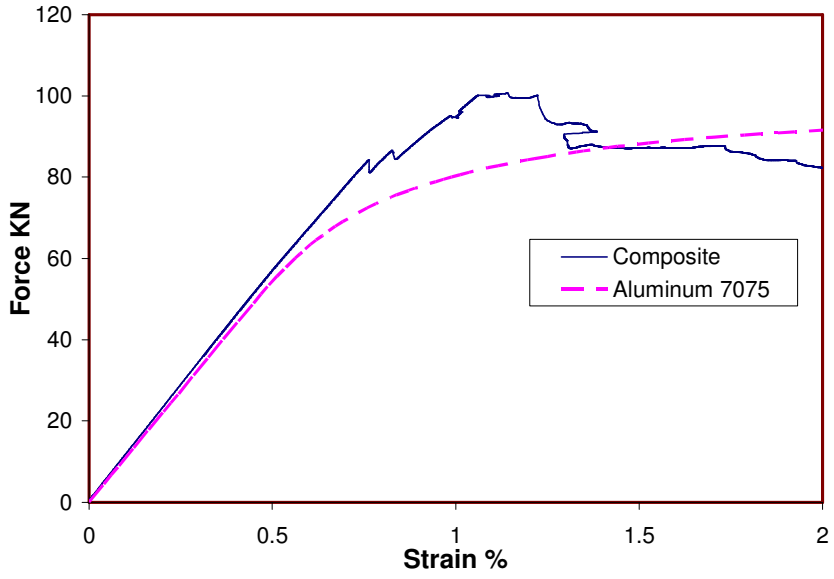

Figure 1.9 Experimental force-strain curve of aluminum and composite tube [11]

In the research of bending behavior of thick-walled composite tube [17], *Mohamed Ibrahim El-Geuch*y defined a new parameter, named effective extensional stiffness of nth composite layer, to present the layer mechanical properties contribution in bending stiffness of the composite tube, and there is excellent agreement between the theoretical and experimental bending stiffness properties of thick-walled curved composite tube.

Zhang and Hoa [18] proposed an efficient method to analyze the straight tube of anisotropic layers including special angles (0° and 90°) under pure bending. They introduced new unified coefficients and their nonsingular parameters to overcome the problem from singular parameters in the previous research for pure bending. The obtained flexural stiffness can match the results from NASTRAN.

Work done by a few previous researchers mentioned dealt with straight tubes. These have been successful in demonstrating the feasibility of composite tubes that can exhibit not only high stiffness, high strength, and light weight, but they can also exhibit a good degree of elongation required for the flexibility of the helicopter landing gear. There has been recent interest from the industry (Bell Helicopter) to develop cross piece for the landing gear of helicopters. The cross piece is used to support the body of the helicopter and it is usually curved. The configuration of a typical cross piece is shown in Figures 1.10 and 1.11.

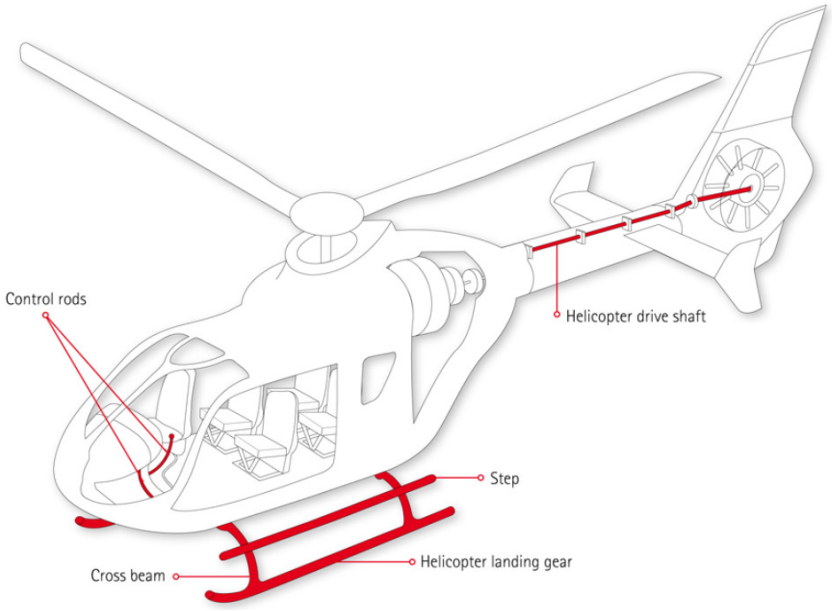

Figure 1.10 Helicopter with cross piece [3]

The cross piece typically has a straight section in the middle, and two straight sections at the ends. These are connected by curved sections. In order to bring the technology to industrial application, it is necessary that the curved tubes be developed.

There are two challenges associated with the development of curved thermoplastic composite tubes for helicopter landing gear applications: Design challenge and Manufacturing challenge. The design challenge relates to the ability of the tube to exhibit good resistance to loading, and also exhibiting the ability to show large deformation. The Manufacturing challenge refers to the ability to process thermoplastic composite (processing temperature at 400 °C) onto curved mandrel which can be removed after the processing.

The work in this thesis focuses on the development of the manufacturing procedure to process the thermoplastic composite to make the thick curved tubes.

Based on the above mentioned accomplishments, it is imperative to find a practical method to make thick curved thermoplastic composite tubes, and this method should be adapted to the laboratory conditions. Since the curved tube has a required inner diameter of only 2.5 inches, the design of the mandrel can be a big challenge. The combination of segmented metal shafts covered with breakable or dissolvable material is a good choice for designing a mandrel for curved thermoplastic composite tubes.

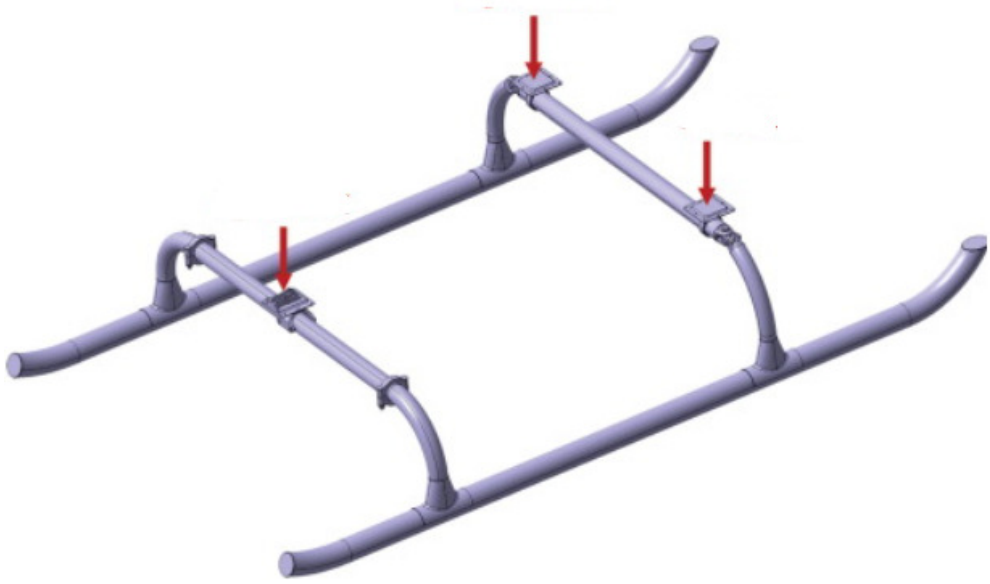

Figure 1.11 Schematic of a crosspiece [3]

The curved configuration of the tube creates challenges for the manufacturing process. The main challenge is to have mandrels that are stiff enough to sustain the load imposed by the fiber placement head. The mandrels then need to be removed from the part. A segmented mandrel was made of many pieces of steel rods which have diameter much smaller than the inner diameter of the tube. Subsequently, plaster of Paris was deposited over the steel rods. The diameter of the jacket of plaster of Paris is the same as the inner radius of the thermoplastic composite tube. A few layers of thermoset composites were deposited on the surface of the plaster of Paris. This helps to prevent indentation of the depositing head of the AFP machine into the plaster. Later, thermoplastic composite layers were deposited on top of the thermoset composite layers. After all composite layers were deposited, the finished curved tube with mandrel was put into an oven with a temperature of 200 °C, and stayed in the oven for about 16 hours so the gypsum would be dehydrated. After the dehydration, certain amount of water was added to soak the plaster facilitate the removal of the mandrel.

The optimized process parameters for manufacturing thermoplastic composite structure of AS4/PEEK using automated fiber placement were identified by *Cai* [10]. Process induced defects and environmental influences that can affect the mechanical strength of the composite structure were also estimated.

Chapter 2. Development of Manufacturing Procedure

There are three challenges in manufacturing thick curved thermoplastic composite tubes by using automated fiber placement.

(1). A force of 80 lbs is imposed on to the mandrel during the deposition of thermoplastic composite tapes, thus the mandrel should have sufficient stiffness to sustain this force.

(2). The processing temperature of carbon/PEEK is about 400 °C, so the mandrel should be able to withstand this temperature.

(3). The mandrel needs to be removed once the tube is finished.

Since it is comparatively easy to find a material that can provide adequate strength to take the pressure and withstand a temperature of 400 °C, the most critical challenge of manufacturing a curved thermoplastic tube is how to remove the mandrel when the curved tube is fabricated.

2.1 Design of the mandrel

In general there are four types of removable mandrel that can be used to fabricate composite tubes. Each has its own particular features and applications

2.1.1 Extractable mandrels

Metal shaft or tube could be used as mandrels for manufacturing straight composite tubes; once the composite is cured, the mandrel can be extracted with a winch. Figure 2.1 shows a mandrel for straight pipe.

If the composite tube is a curved one, but has only one constant radius, the mandrel could also be directly extracted from the tube by using auxiliary devices. (Figure 2.2)

Figure 2.1 Extraction of straight mandrel [2]

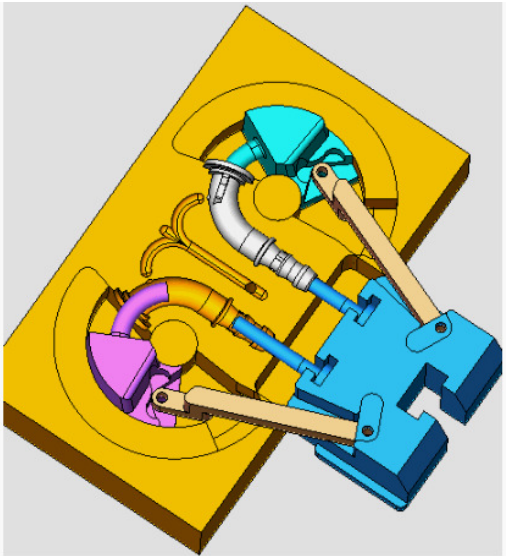

Figure 2.2 Extraction of curved mandrel [29]

2.1.2 Collapsible mandrels:

These types of mandrels consist of segmented surface made of several pieces that are connected with collapsible linkages. The mandrel can be expanded to form the final shape of the part (Figure 2.3a). When the part is cured, the mandrel is collapsed and be removed (Figure 2.3b).

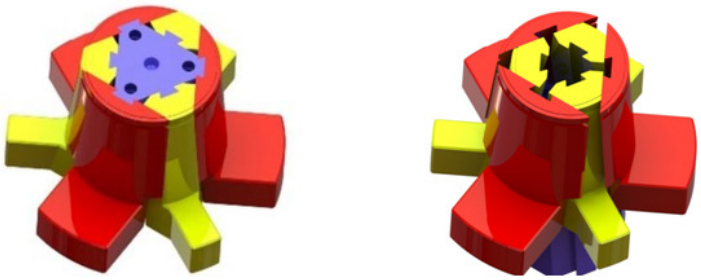

(a) Mandrel expanded (b) Mandrel collapsed

Figure 2.3 Collapsible mandrel [29]

2.1.3 Breakable mandrels

Any breakable material which can be machined or molded to form the shape of final part could be used as this kind of mandrels. Usually plaster or glass is used to make breakable mandrels. When the composite tube is cured, the mandrel is broken and removed, and then the final tube is completed.

Since the materials used for breakable mandrel are always brittle, it is of concern that this kind of mandrels may break during the automated fiber placement.

2.1.4 Dissolvable mandrels

The materials for dissolvable mandrels can be dissolved in solution or can melt at a temperature that is lower than the working temperature of the tube, such as water soluble sand, low melting alloy that is suitable to small vessels or eutectic salts which can be melted at a moderately high temperature. The disposable mandrel could be dissolved, melted or broken into small pieces for removal. The water soluble plaster is the most preferred material, since it could be directly washed way with cold tap water or hot water.

The approach taken in this work is a combination of a segmented mandrel made from steel, and a jacket made of plaster which is partially dissolvable and breakable. The procedure is described below.

2.2 Mandrel for manufacturing curved tube

Due to the constraint of the size of the AFP machine at Concordia Center for Composites, curved tubes of overall dimensions as shown in Figure 2.4 are to be made. The arcs of the tube have radius of 27 inches. The inside diameter would be 2.5 inches. The outside diameter depends on the layup sequence required for the performance of the tube under loading.

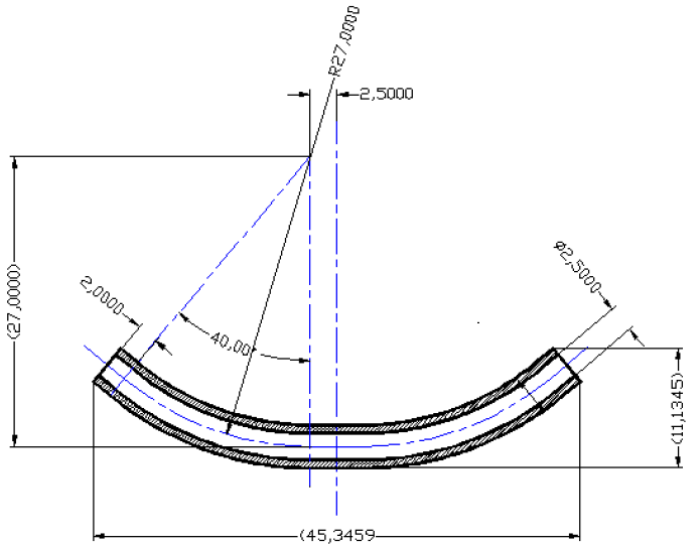

Figure 2.4 Dimensions of the tubes to be made (in inches)

Since the curved thermoplastic composite tube in this research has an inner diameter of 2.5 inches, there will be little possibility to use a collapsible mandrel, and the complex shape of this tube does not allow the mandrel to be removed by simply sliding or extraction, so the dissolvable mandrel and segmented mandrel are considered for this curved composite tube.

Shown in Figure 2.5a, the combination of segmented metal shaft is covered with buffer material that can provide enough strength to take the manufacturing force and sustain the high processing temperature. When the curved tube is made and cured, the plaster is dissolved or washed away so there will be space for the segmented metal core to be removed. (Figure 2.5b)

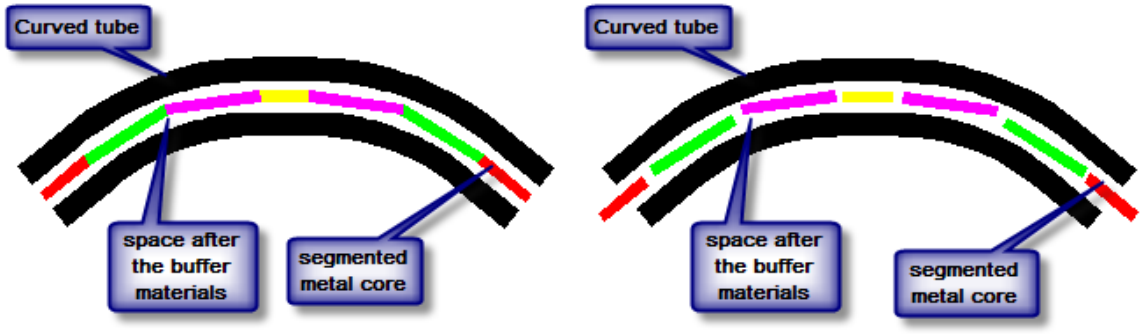

(a) Segmented shafts covered with buffer material (b) Removal of segmented shafts

Figure 2.5 Concept of mandrel for curved tube

The maximum length of each segment is determined by the curvature of the inner wall of the tube, such that the segment can be moved out after processing. Two metal shafts are used to form the curved portion of the tube, the arc with radius of 27 inches and an angle of 40° which is shown in Figure 2.6. The length and diameter of the metal shafts are determined as:

(1) The maximum length of the shafts:

Lmax=2*L3=2*(27.0000+2.5000/2)*sin(10)=9.8111 (ins)

(2) The minimum length of the shafts:

Lmin=2*L4=2*(27.0000-2.5000/2)*tan(10)=9.0808 (ins)

(3) The maximum diameter of the shafts:

Dmax=L2-L1=(27.0000+2.5000/2))*cos(10)-(27-2.5000/2)=2.0708 (.ins)

The actual diameter of the metal shafts is 1.5 in., and the actual maximum length is about 9.7 in..

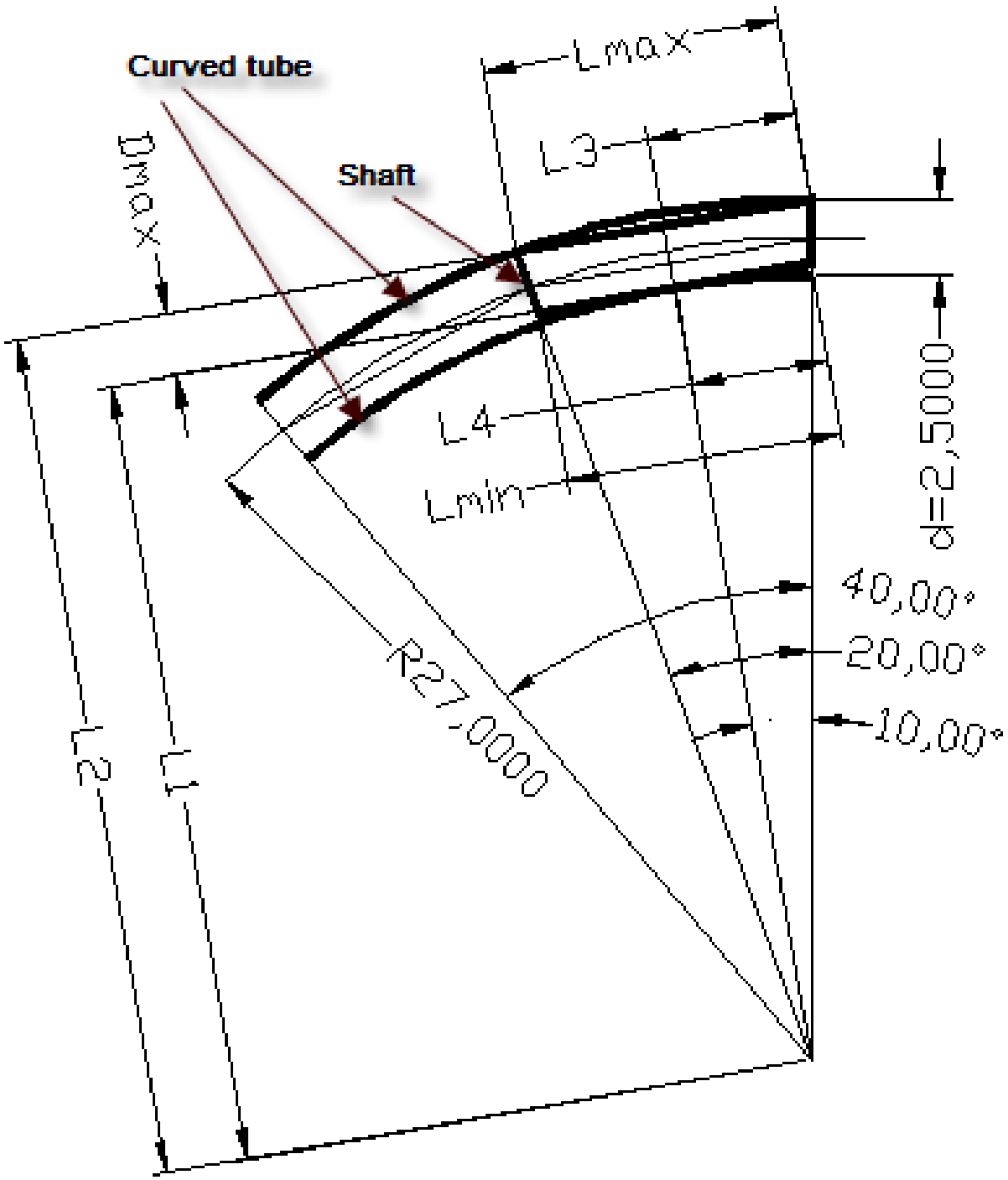

Figure 2.6 Determination of dimensions for metal shafts (in inches)

The selection of the ideal buffer material becomes the key point of the development of a manufacturing process for a curved tube.

2.3 Selection of buffer material

It is important to select a suitable breakable or dissolvable material to make the mandrel that is required for manufacturing curved thermoplastic tubes. Aqua products, notably water soluble materials, can be regarded as one choice [19-22]. The other solution is to use gypsum plaster (Plaster of Paris, $CaSO_4$ $0.5H_2O$). The gypsum phenomenon describes that gypsum plaster is transformed to gypsum ($CaSO_4$ $2H_2O$) and forms a hard mass when it contacts with the appropriate amount of water at room temperature, and also gypsum loses its water of hydration at elevated temperature. This enables the gypsum plaster be a good choice for making breakable or dissolvable mandrels. [23-28]

Required characteristics of an ideal buffer material are depicted as:

(1). Strong enough to take manufacturing force;

(2). Can be machined and is easy for molding;

(3). Ability to withstand high temperature;

(4). Breakable or water-soluble; water- soluble is preferred;

(5). Environment impact is a consideration;

There are two water soluble materials that can be selected as buffer material for fabricating the curved composite tubes. One is known for its water solubility, the aqua products provided by Advanced Ceramics Manufacturing. The other is gypsum plaster (plaster of Paris) which can react with water to form gypsum (calcium sulfate dihydrate), and the gypsum can be heated to lose its water of hydration to form gypsum plaster again. This is known as gypsum technology that leads to a wide range of industrial applications of gypsum plaster.

2.3.1 Aqua products [19-22]

Aqua products, provided by Advanced Ceramics Manufacturing, seem to be the best water soluble materials for dissolvable mandrel. Three aqua products, Aquapour™, Aquacore™ and Aquacore™ premium have distinct features listed as.

(1). Easily mixed with water;

(2). Pourable and injectable;

(3). Environmentally friendly; no special disposal procedures required;

(4). Washes away in cold tap water;

(5). Compatible with all commercial resins and pre-preg compounds;

(6.) Makes complex part manufacturing possible;

(7). Easily dried in a convection oven;

(8). Easily repaired;

(9). Takes less time, labor and money;

The compressive strengths of these products vary from 4-7 MPa at 70 °F/21 °C. This could provide enough resistance to withstand the low pressure exerted by the automated fiber placement system. These products are thermally stable, but can only withstand a temperature of 200 °C which is much lower than 390 °C, the processing temperature of PEEK. These products are not ideal buffer material for manufacturing curved thermoplastic tube because there is no information showing that these products are still water soluble after having withstood a temperature up to 400 °C or higher.

Figure 2.7 displays the procedure that the aqua products work as water soluble mandrels.

Figure 2.7 Preparation of mandrels using aqua products [20]

2.3.2 Gypsum plasters (Plaster of Paris) [23-29]

When dry gypsum plaster powder with molecular formula of $CaSO_4.0.5H_2O$, is mixed with water, its hemihydrate particles react with the water, rehydrating and becoming a hard mass by an exothermic reaction shown as formula (1)

$$CaSO_4 \cdot 0.5H_2O + 1.5H_2O \longrightarrow CaSO_4 \cdot 2H_2O \quad (1)$$

This reaction is explained that, when mixed with water, the hemihydrates ($CaSO_4.0.5H_2O$) are dissolved in water, forming a saturated solution of Ca^{2+} and $SO_4{}^{2-}$ ions, followed by precipitation of acicular dihydrate crystals ($CaSO_4.2H_2O$), so the crystallization nuclei are formed and around it the crystals grow, forming an interlocking net of long crystals providing the strength of the materials. The resulting materials is calcium sulfate dihydrate ($CaSO_4.2H_2O$) having the same chemical nature of the natural gypsum. The setting time starts about 10 minutes after mixing and is complete in about 45 minutes; but not fully set for 72 hours.

There are five usual physical tests carried on the hardened plasters for their performance in actual use:

(1) Normal consistency

The normal consistency is defined as " the number of parts of water, by weight, required to produce a slurry of definite fluidity when mixed with 100 parts of plaster, by weight, and at a definite temperature." This property guides all other working properties and has been considered an important criterion for classifying plaster.

(2) Crushing strength

The crushing strength of plaster is indicative of its resistance to pressure, mechanical shocks, and rough handling in actual working conditions. This value, expressed in psi or MPa, is determined from the force required to crush a sample acting on an area of the sample. The crushing strength of plaster varies from 800 psi to 1700 psi (5.6 MPa to 12 MPa). [28]

(3) Surface hardness

This hardness is a measure of the resistance to abrasion and to wear and tear in use. Since plaster is soft, if the test is conducted by impressing a 23 mm diameter steel ball on the surface of samples at a pressure of 100 psi and measure the diameter of the indentation formed, the hardness of plaster measured in this way is about 4.25 to 7.5 mm. This value has been used for comparing the degree of surface hardness, assuming that the softer the surface is, the larger would be the diameter. [28]

(4) Density

Density of the plaster was calculated from the naturally dried weight of sample and its volume. The value is expressed in lbs/ft^3or kg/m^3 . The density of the hardened plaster is about 70-92 lbs/ft^3. [28]

(5) Setting time

The setting time of a plaster is the interval between the moment the plaster and water come in contact and when the setting plaster is able to support a pre-determined weight. It indicates the period within which the plaster-water mix remains in a workable condition so as to give a desired shape.

(6) Water absorption

Absorption of water by the plaster mould is a very important characteristic which determines its usefulness in the ceramic industry since the mould is used for absorbing water from the casting slip or from the soft body during jiggering. The absorption was determined on a 1-inch inch cube, prepared from plaster using water equivalent to the normal consistency, by immersing the dry cube in water at room temperature until it reached constant weight and calculating the percentage gain in weight on its dry weight.

The most unique properties of gypsum is its ability to lose the water of hydration at elevated temperature and then recombine with appropriate amount of water at low temperature to form the original hardened dehydrate. When gypsum is heated up to a range of 130 °C-200 °C, it is dehydrated to calcium sulfate hemihydrate. The formula is given as:

$$CaSO_4 \cdot 2H_2O \xrightarrow{heat} CaSO_4 \cdot 0.5H_2O + 1.5H_2O \quad (2)$$

There are also other calcium sulfate phases resulting from different interactions such as temperature; water pressure of calcinations environment inside the kiln; particle size distribution and residence time. The presence of each calcium sulfate phase provides the final gypsum plaster with different behaviors, changing the kinetic of hydration reactions and, consequently, their mechanical properties.

The above mentioned two properties are described as gypsum phenomena, which enables the gypsum plaster to work as the first choice of buffer materials in making thick curved thermoplastic composite tubes. The reason for this application can be explained in Figure 2.8.

Step 1		Step 2		Step 3
Plaster of Paris		Gypsum		Wrap 4 thermoset layers
$CaSO_40.5H_2O$	Water	$(CaSO_4.2H_2O)$		Cure 4 thermoset layers
(Powder)		Form hard mass		

Step6		Step 5		Step 4
Form gypsum		Heat the gypsum to 200 °C, 12 hrs		Wrap thermoplastic layers
and become soft	Water	Gypsum dehydrated to	Heat	
Easily removed		$(CaSO_40.5H_2O)$		
before it is set		Brittle,hard		

Figure 2.8 Application of plaster of paris as buffer materials for curved tubes

The DAP plaster of Paris shown in Figure 2.9 is used as buffer material for making a thick curved thermoplastic composite tube. The tests of normal consistency and crushing strength of this plaster are performed in this project.

Figure 2.9 Plaster of Paris used for making curved tube.

2.4 Characterization of gypsum

2.4.1 DSC test of gypsum plaster

DSC, Differential Scanning Calorimetry, is a thermo-analytical technique in which the difference in the amount of heat required to increase the temperature of a sample and a reference is measured as a function of temperature. Both the sample and reference are maintained at the same temperature throughout the experiment. Generally, the temperature program for a DSC analysis is designed such that the sample holder temperature increases linearly as a function of time. The reference sample should have a well-defined heat capacity over the range of temperatures to be scanned. [30]

Figure 2.10 displays the DSC test. Two small containers having same weight are used. One holds the sample; the other is empty and works as reference. The weight of the sample is precisely measured. The measuring cell is heated to the required temperature and DSC curve could be obtained, see Figure 2.11.

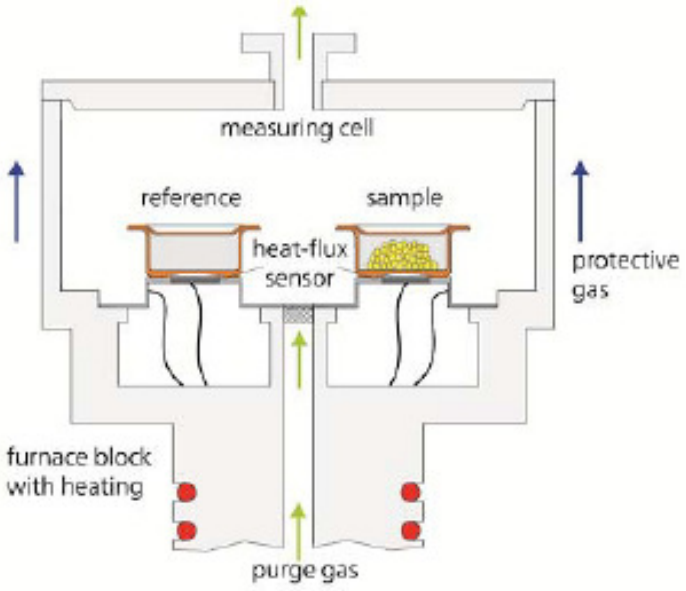

Figure 2.10 Schematic of DSC test [30]

When the sample undergoes a physical transformation such as phase transitions, more or less heat is needed than the reference to maintain both at the same temperature. The DSC curve in Figure 2.11 shows that exothermic process for crystallization, cross-linking and oxidation; and endothermic process for melting where more heat is absorbed to melt the sample.

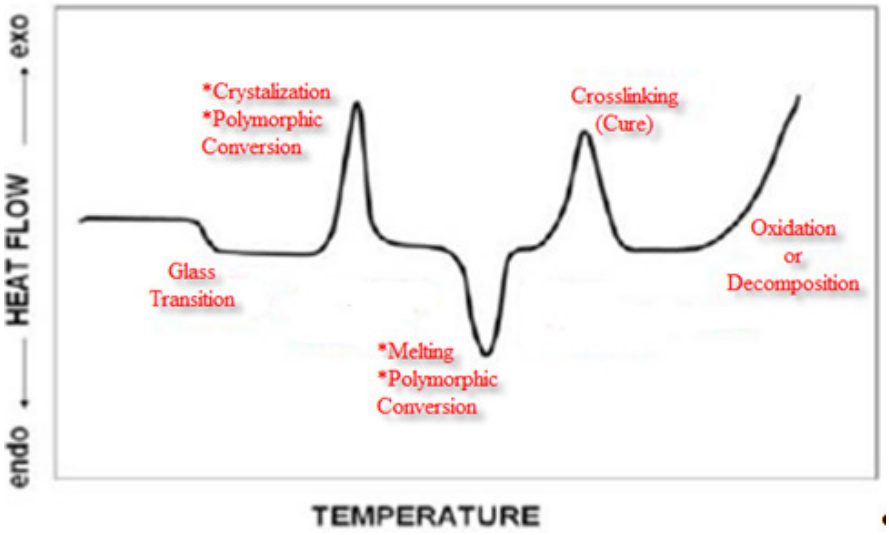

Figure 2.11 Typical DSC curve [30]

From the DSC curve of gypsum depicted in Figure 2.12, it is found that an endothermic process occurs at the temperature range of 110 °C to 180° C. More heat is needed to flow into the sample than to the reference. The required amount of heat reaches the maximum at 165 °C. which means a physical transformation happens within this temperature range. And this verifies the dehydration of the gypsum given as:

$$CaSO_4 \cdot 2H_2O \longrightarrow CaSO_4 \cdot 0.5H_2O + 1.5H_2O$$

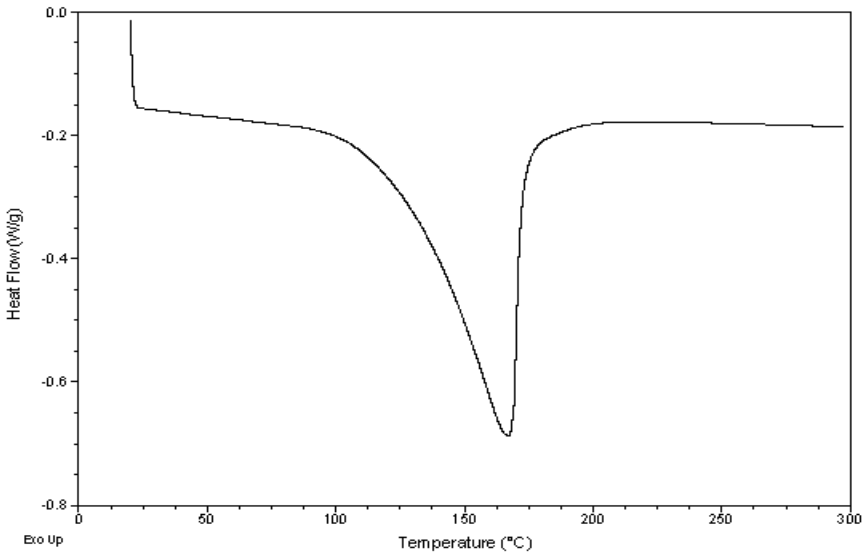

Figure 2.12 DSC curve of gypsum plaster

2.4.2 Normal consistency (Water needed for pourable mix)

In this step, weight-to-weight ratio between water and Plaster of Paris is used. A ratio of 1:2.42 shown in Figure 2.14 means that 100 grams of water will be mixed with 242 grams of Plaster of Paris, the normal consistency of this ratio is about 42. Instructions for casting the plaster of Paris are given as:

(1). Pre-measure the quantity of the water and plaster with different ratio;

(2). Add the water to the plaster all at one time, stir them immediately;

(3). Stir for 3-5 minutes and get rid of lumps and bubbles;

(4). Carefully pour the plaster into the pre-prepared mold.

(5). Leave the casted samples to set up for 72 hours.

Figure 2.13 Unclosed mold for casting plaster

It is found that the maximum ratio of 1:2.55 , normal consistency of 39, is acceptable to an unclosed mold shown in Figure 2.13. And a ratio of 1:2.42, normal consistency of 42, could obtain a hard mass with good surface finish (Figure 2.14).

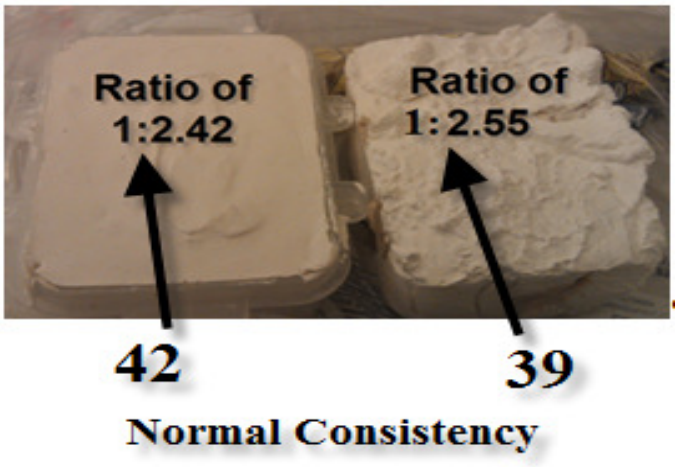

Figure 2.14 Different normal consistency for molding

For closed mold, a smaller ratio should be used so that the plaster could reach every corner of the mold, and holes or gaps must be considered so the air could escape. Figure 2.15 shows the Plaster of Paris casted into a spring water bottle. With a ratio of 1:2, normal consistency of 50, small features can be obtained.

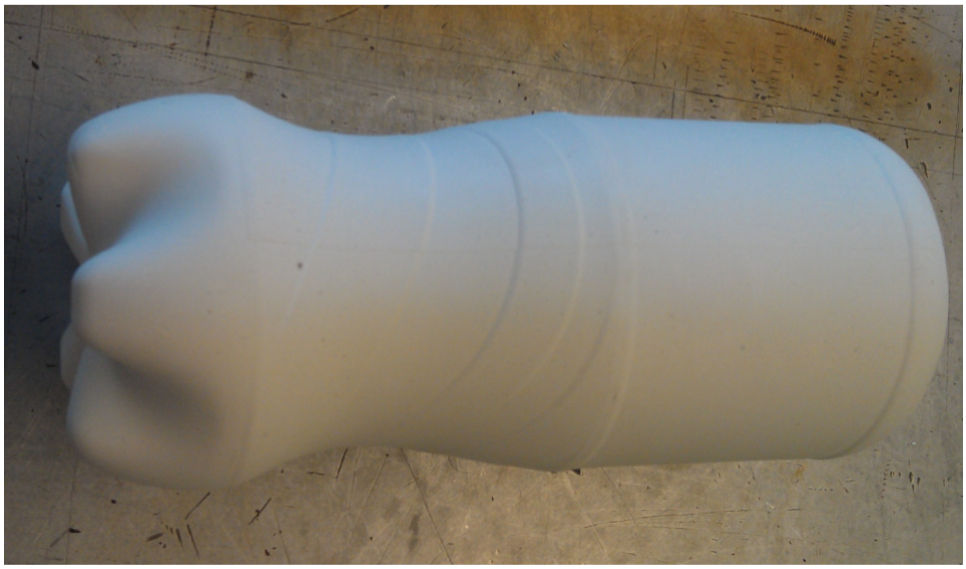

Figure 2.15 Casted plaster of a weight ratio of 1:2

2.4.3 Compressive strength (Crushing strength)

As mentioned before, when the Plaster of Paris is mixed with water, its hemihydrate particles react with water and become a hard mass. It is necessary to measure the compressive strength of the hard mass to verify if it has enough resistance to withstand the force during manufacturing.

Five samples are cut from the cast plaster of a ratio of 1:2.42 (normal consistency of 42), and each sample is heated to different temperatures and held at the temperature for 1 hour. Then all samples are tested on MTS machine (Figure 2.16). The force at which the samples are crushed is recorded, and the compressive strength of each sample is calculated. The compressive strength and dimensions of all samples are recorded and shown in Table 2.1.

It is found that the compressive strength of the gypsum ($CaSO_4.2H_2O$) is much higher than that of aqua products (4-7 Mpa). The sample dehydrated at 120 °C has the minimum compressive strength which is still comparable to that of aqua products.

Figure 2.16 Compression test of the plaster

During the manufacturing of curved tube, the temperature of hot gas torch is about 900 °C, which will cure only the surface of the plaster. After the first ply is completed, the composite ply will help to take the high temperature. It can be concluded that the gypsum ($CaSO_4.2H_2O$, hard mass in step 2, Figure 2.8) has enough resistance to withstand the manufacturing force, and the high processing temperature does not affect the compressive strength of gypsum ($CaSO_4.2H_2O$).

Table 2.1 Compressive strength of the plaster

Sample	1	2	3	4	5
Heat temperature (°C)	Non-heated	65	120	180	230
Area (mmXmm)	18.95X19.04	30.3X30.6	26.9X33.9	30.4X30.96	27.93X31.96
Area (mm^2)	361	927.18	911.91	941.84	894.56
Height (mm)	20.5	67.6	64.67	59.77	59.77
Force (N)	4094	4792	4017	4094	7581
Compressive Strength (MPa)	11.3	5.2	4.4	6.5	8.5

Since there is only one sample tested for each temperature, there is no tolerance for the compressive strength shown in table 2.1

2.4.4 Water dissolvability

The cast plaster is calcium sulfate dihydrate ($CaSO_4.2H_2O$). When it is heated to certain temperature, it will be dehydrated to calcium sulfate hemihydrates ($CaSO_4.0.5H_2O$) which is the main constituent of plaster of paris. The formula is given as:

$$CaSO_4 \cdot 2H_2O \longrightarrow CaSO_4 \cdot 0.5H_2O + 1.5H_2O$$

Samples shown in Figure 2.17a have a size close to 1 inch cube, are cured at different temperatures for 1 hour:

Sample 1: non-dehydrated;

Sample 2: dehydrated at 65 °C;

Sample 3: dehydrated at120 °C;

Sample 4: dehydrated at 180 °C;

Sample 5: dehydrated at 230 °C;

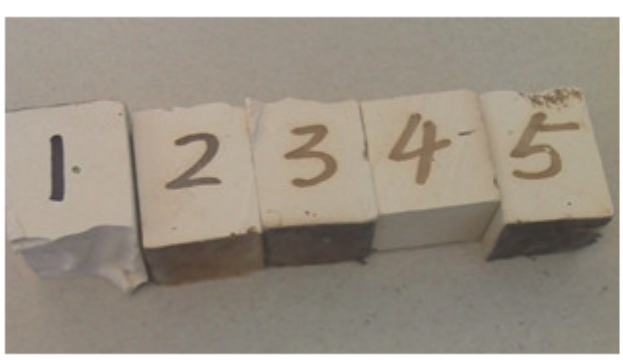

(a) Dehydrated sample

(b) Dehydrated samples softened in water

Figure 2.17 Water dissolvable in the gypsum

Five samples were immersed in cold tap water for about 20 minutes, and four dehydrated samples were softened in the water and could be crushed with very small force applied by fingers (Figure 2.17b). Sample 5 was dehydrated at 230 °C, and became much softer than sample 2 which was dehydrated at 65 °C. The non dehydrated sample was still hard and could not be easily damaged. This phenomenon offers the possibility to wash away the cured plaster.

2.4.5 Coefficient of Thermal expansion

The CTE, coefficient of thermal expansion, of the cast plaster is measured and shown in Table 2.2. Figure 2.18 demonstrates the measurement, TMA Q400, for measuring coefficient of thermal expansion. During the test, a flat-tipped standard expansion probe is placed on the sample, and the sample is heated to 250 °C, cooled down to room temperature and heated to 250 °C again. The probe movement records sample expansion or contraction, as shown in Figure 2.19 to Figure 2.22. With the recorded probe movements, the coefficient of thermal expansion can be obtained.

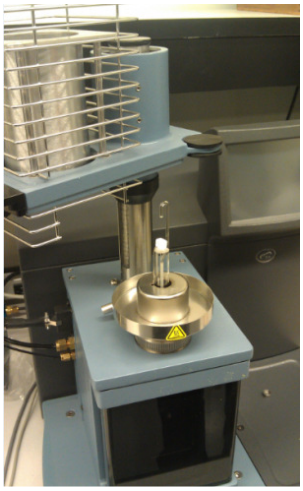

Figure 2.18 CTE measurement, TMA Q400

It can be found that cast Plaster of Paris has thermal stability. All samples have almost same coefficient of thermal expansions. At a temperature range of 0-399 °C, the mild steel has a coefficient of thermal expansion of 16.2 (10^{-6} m/m °C).

Table 2.2 CTE of different samples

Sample	1	2	3	4
Heat temperature (°C)	Non-heated	65	120	180
Height (mm)	3.481	7.7711	6.4038	2.4783
CTE (10^-6 m/m°C)	7.924	8.519	8.788	7.932

The CTE test curves are shown in Figure 2.18 to Figure 2.21. The difference in these curved can be explained as different degrees of cure of casted plaster, since the $CaSO_4.H_2O$ system has five phases and four are known to exist at room temperature. [24]

All the samples are heated from 20°C to 250 °C (point A to B), then cooled down to 20 °C or lower (point B to C and to D), and then be heated to 250 °C again (point D to E and to F). It can be found that, compared with the curves in Figures 2.20, 2.21, and 2.22; there is big difference of the curve of first heating-up shown in Figure 2.19. This can be explained that, for the non cured sample of gypsum plaster, there is more water bonded between the molecules of $CaSO_4.2H_2O$. During the first heating up, more heat is needed so that the water between molecules of $CaSO_4.2H_2O$ will evaporate. But for the cured samples, the water has lost before the CTE test starts.

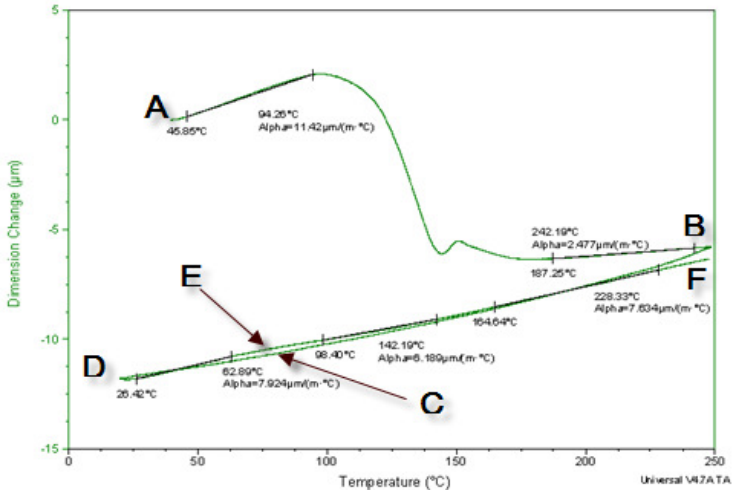

Figure 2.19 CTE of sample non cured, 7.924 (10^{-6} m/m °C)

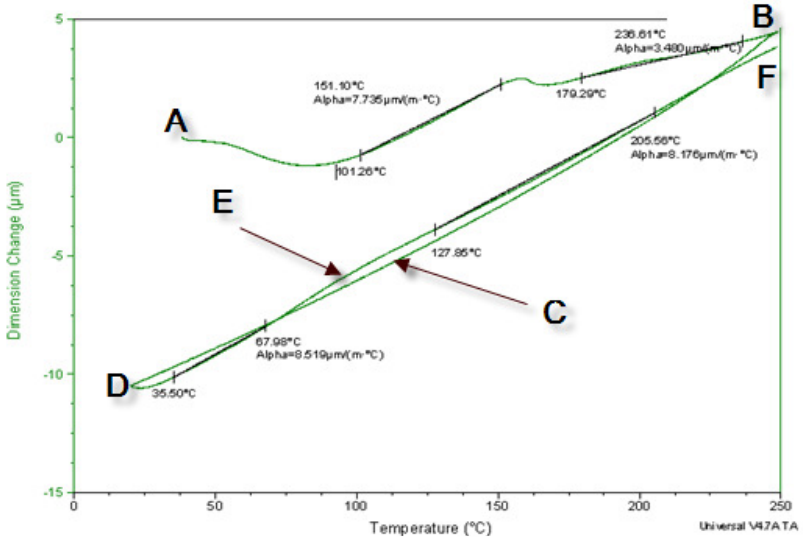

Figure 2.20 CTE of sample cured at 65°C for 1hr, 8.519 (10^{-6} m/m °C)

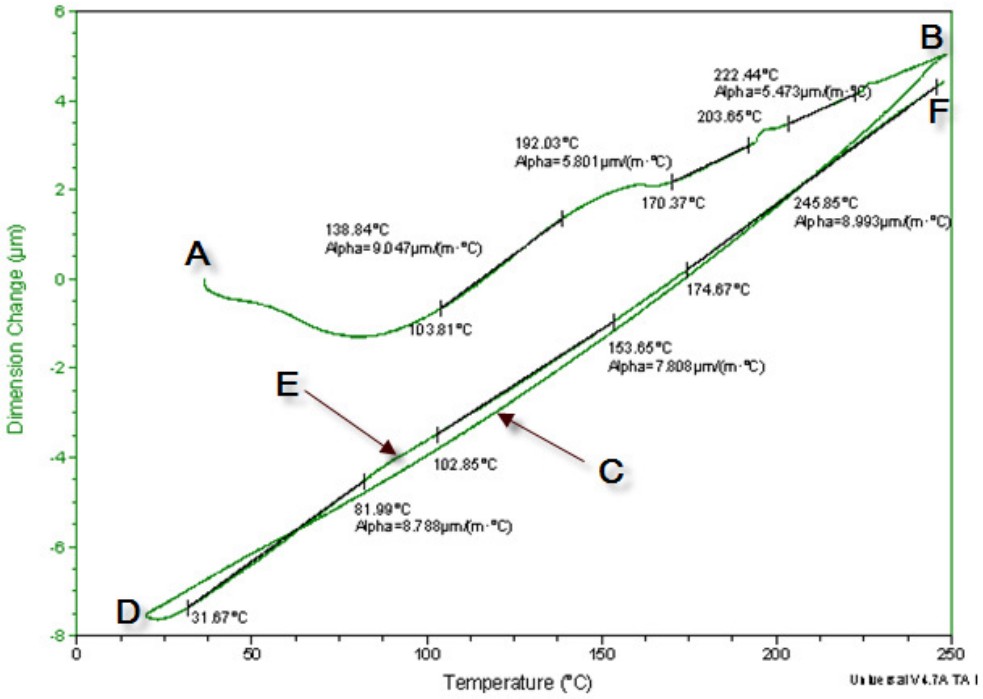

Figure 2.21 CTE of sample cured at 120°C for 1hr, 8.788 (10^{-6} m/m °C)

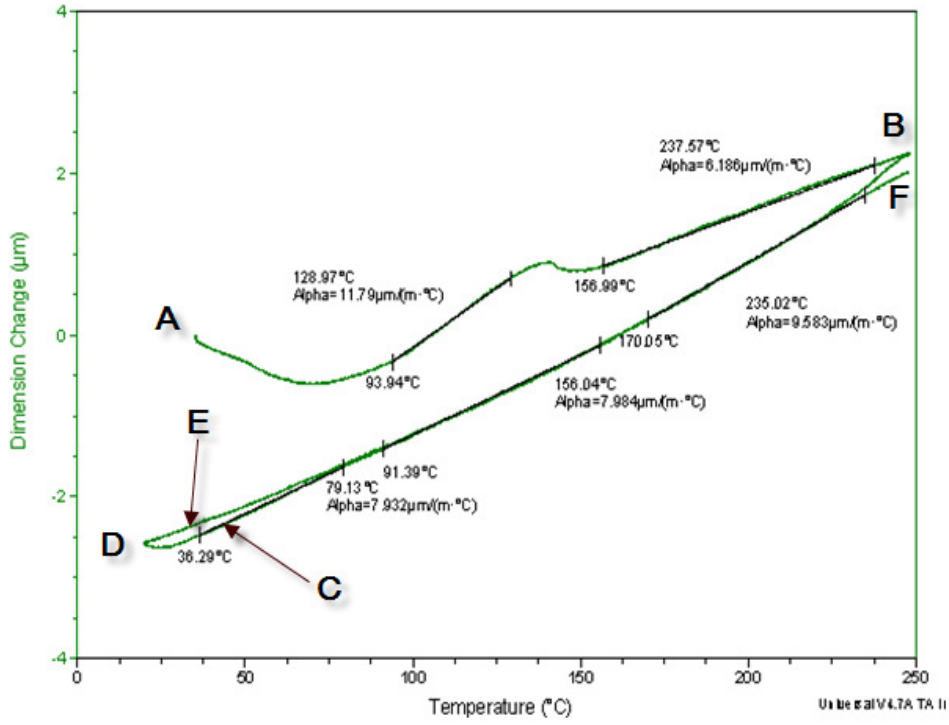

Figure 2.22 CTE of sample cured at 180°C for 1hr, 7.932 (10^{-6} m/m °C)

2.4.6 A trial straight tube

A straight metal shaft consisting of three segments is covered with gypsum ($CaSO_4.2H_2O$, plaster of paris mixed with water), and the plaster is machined to a shaft with diameter of 2.5 inches after the plaster is fully set up, as shown in Figure 2.23a.

Figure 2.23b illustrates the joint that connects the segmented shaft. Three dowel pins are used: the one in the middle with 0.5 inches diameter positions the segmented shafts in the right position and withstand the manufacturing force; other two pins with 1/8 inches diameter are used to take torsion.

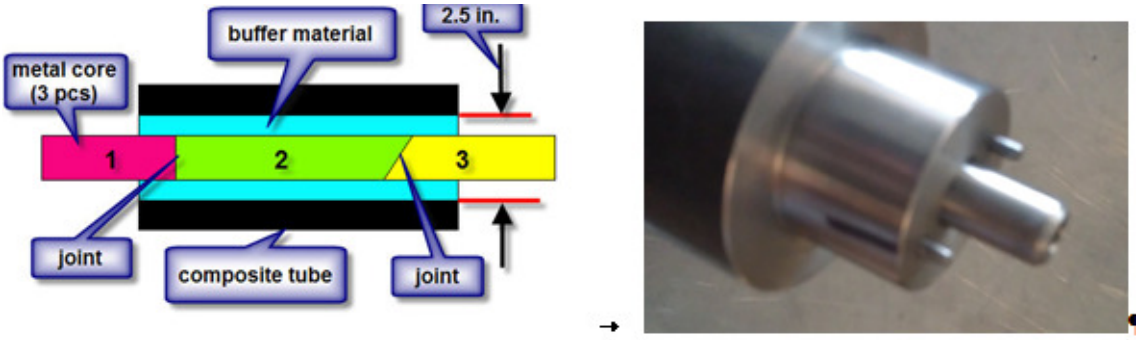

(a) Mandrel for straight tube (b) Joint used to connect segmented shafts

Figure 2.23 Segmented mandrel and plaster for straight tube

Firstly, the mandrel is wrapped with 4 layers of thermoset composite (Carbon/epoxy) at 90 degrees by AFP machine, then the mandrel with plaster and thermoset composite layers are cured in autoclave. (Thermoset composite material of Tencate TC250 is used for this purpose, and the wrapped composite layers are cured at 130 °C for 2hrs). These cured thermoset composite layers will help the first thermoplastic layer be bonded onto the mandrel, and assist the plaster to withstand the exerted pressure during the deposition of thermoplastic layers.

Secondly, 10 layers of thermoplastic composite are deposited on the mandrel. Afterwards the mandrel with plaster and thermoplastic composite layers is heated to 200 °C and stays at this temperature for 6 hours, so that the gypsum could be dehydrated to $CaSO_4.0.5H_2O$.

When the dehydrated plaster ($CaSO_4.0.5H_2O$) contacts water, it absorbs water and becomes to gypsum ($CaSO_4.2H_2O$), and softens. This softened gypsum can be easily damaged. Figure 2.23a demonstrates the crushed plaster when the thermoset composite layers are stretched out. The rest of the plaster can be washed away with cold tap water. (Figure 2.24b)

Figure 2.25 shows finished the straight thermoplastic composite tube.

When the dehydrated plaster ($CaSO_4.0.5H_2O$) contacts water, it absorbs water and becomes to gypsum ($CaSO_4.2H_2O$), and softens. This softened gypsum can be easily damaged. Figure 2.23a demonstrates the crushed plaster when the thermoset composite layers are stretched out. The rest of the plaster can be washed away with cold tap water. (Figure 2.24b)

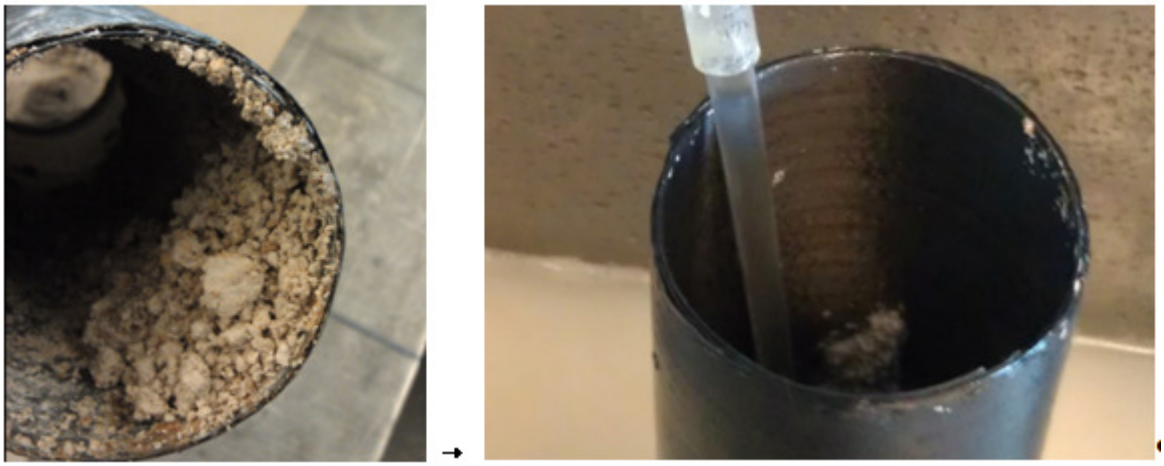

(a) (b)

Figure 2.24 The removal of plaster

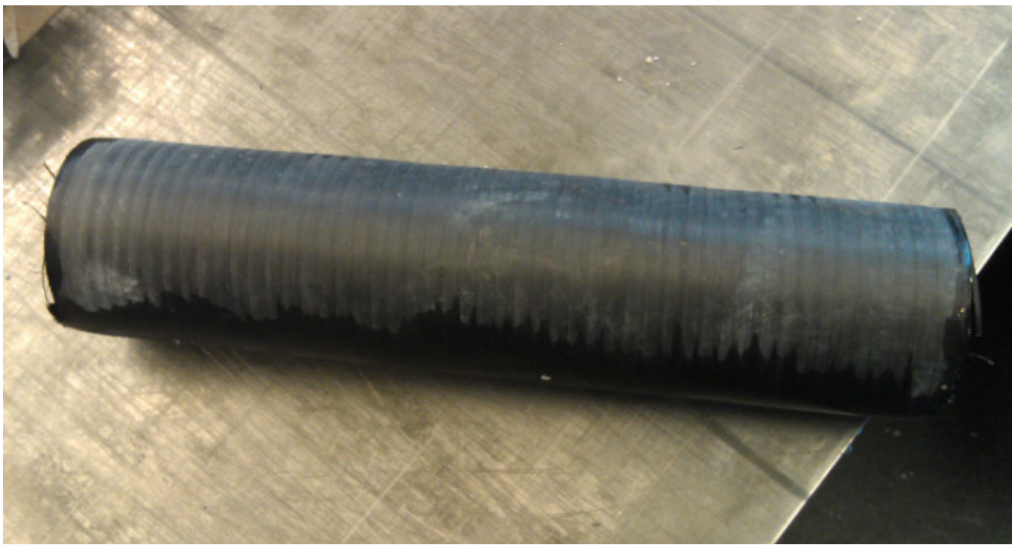

Figure 2.25 Finished thermoplastic straight tube

It is concluded that the plaster of Paris can be used as buffer material for making a curved thermoplastic composite tube. It is not fully dissolvable, but breakable when contacts with water after dehydrated.

Chapter 3. Manufacturing of curved tube

3.1 Curved tube design

3.1.1 Curved tube with constant thickness

Based on the size limitation of the Automated Fiber Placement machine at Concordia, maximum OD of 48 inches and length of 120 inches, it is not possible to produce a curved tube of full size. Instead, a smaller tube with sufficient degree of complexity was designed and made. Figure 3.1 shows the schematic of the design of the tube. The tube has constant inner diameter of 2.5 inches, and outer diameter varies with the number of thermoplastic layers.

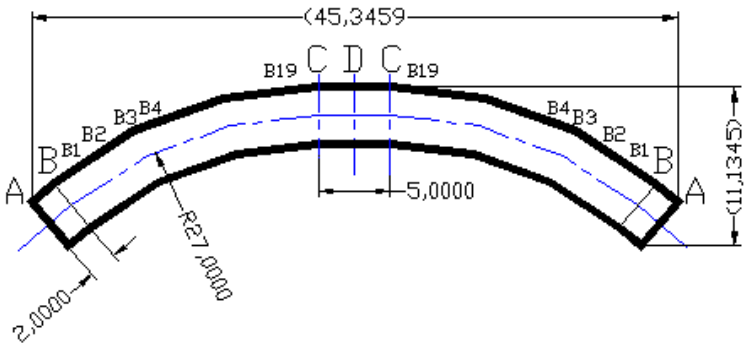

Figure 3.1 Overall dimensions of curved tube (in inches)

With the dimensions shown in Figure 3.2, the mandrel has a total length of 102 inches, and maximum working envelope of 35 inches (2*17.5) for 140 composite layers (OD varies with the number of layers). The size of mandrel is very close to the size limit of AFP machine in the lab (Figure 3.2).

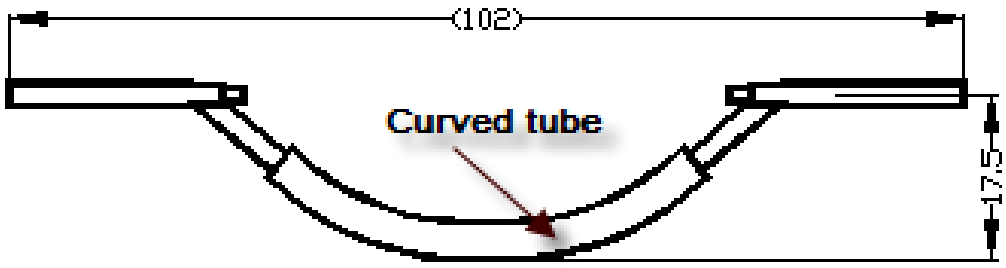

Figure 3.2 Size of mandrel (in inches)

This tube is intended to have 140 layers, and have a layup sequence of [11]

$[(90)_{20}/ (\pm25)_{20}/ (90)_5/ (\pm30)_{25}/ (90)_5/ (\pm45)_{10}]$

3.1.2 Curved tube with variable thickness

This curved tube also has an inner radius of 2.5 inches and the geometrical shape as the tube with constant thickness. But it has least layers at both ends (portion AB in Figure 3.1), and the number of layers gradually increases to the middle portion. The variation of thickness is proposed by Dr. Suong Van Hoa, director in Concordia Composite Center, and is described in following details. (Refer to Figure 3.1 and starting from inside)

This curved tube is divided into five portions:

(1) Two straight portions A-B on two ends, with length of 2 inches;

(2) One straight portion C-C in the middle, with length of 5 inches;

(3) Two curved portions B-C on two sides, with curvature of 27 inches;

The length of the curved portion of this tube can be obtained as:

$$L_{BC} = 2 * \pi * 27 * 40/360 = 18.85 \text{ inches}$$

This length is divided into 19 portions, named:

Portion B1: Point B+1 inch towards point C;

Portion B2: Point B1+1 inch towards point C;

Portion B3: Point B2+1 inch towards point C;

.....

Portion B18: Point B17+1 inch towards point C;

Portion B19: Point B18+0.85 inch towards point C;

Point B19 coincides with point C.

The layup sequence is described as

1.) **Portion A-A, covering the whole length of the mandrel:**

Segment 1 (AA): with a length of 2 inches: $[(90)_{20}/(\pm25)_{20}/(90)_5]$: 65 layers

2.) Portion B-B:

Segment 2: From point B1L to point B1R: $[(90)_{20}/(\pm25)_{20}/(90)_5/(\pm30)_2]$: 69 layers

Segment 3: From point B2L to point B2R: $[(90)_{20}/(\pm25)_{20}/(90)_5/(\pm30)_4]$: 73 layers

Segment 4: From point B3L to point B3R: $[(90)_{20}/(\pm25)_{20}/(90)_5/(\pm30)_6]$: 77 layers

Segment 5: From point B4L to point B4R: $[(90)_{20}/(\pm25)_{20}/(90)_5/(\pm30)_8]$: 81 layers

Segment 6: From point B5L to point B5R: $[(90)_{20}/(\pm25)_{20}/(90)_5/(\pm30)_9]$: 83 layers

Segment 7: From point B6L to point B6R: $[(90)_{20}/(\pm25)_{20}/(90)_5/(\pm30)_{10}]$:85 layers

Segment 8: From point B7L to point B7R: $[(90)_{20}/(\pm25)_{20}/(90)_5/(\pm30)_{11}]$: 87 layers

Segment 9: From point B8L to point B8R: $[(90)_{20}/(\pm25)_{20}/(90)_5/(\pm30)_{12}]$: 89 layers

Segment 10: From point B9L to point B9R: $[(90)_{20}/(\pm25)_{20}/(90)_5/(\pm30)_{13}]$: 91 layers

Segment 11: From point B10L to point B10R: $[(90)_{20}/(\pm25)_{20}/(90)_5/(\pm30)_{14}]$: 93 layers

Segment 12: From point B11L to point B11R: $[(90)_{20}/(\pm25)_{20}/(90)_5/(\pm30)_{15}]$: 95 layers

Segment 13: From point B12L to point B12R: $[(90)_{20}/(\pm25)_{20}/(90)_5/(\pm30)_{16}]$: 97 layers

Segment 14: From point B13L to point B13R: $[(90)_{20}/(\pm25)_{20}/(90)_5/(\pm30)_{17}]$: 99 layers

Segment 15: From point B14L to point B14R: $[(90)_{20}/(\pm25)_{20}/(90)_5/(\pm30)_{18}]$: 101 layers

Segment 16: From point B15L to point B15R: $[(90)_{20}/(\pm25)_{20}/(90)_5/(\pm30)_{19}]$: 103 layers

Segment 17: From point B16L to point B16R: $[(90)_{20}/(\pm25)_{20}/(90)_5/(\pm30)_{20}]$: 105 layers

Segment 18: From point B17L to point B17R: $[(90)_{20}/(\pm25)_{20}/(90)_5/(\pm30)_{21}]$: 107 layers

Segment 19: From point B18L to point B18R: $[(90)_{20}/(\pm25)_{20}/(90)_5/(\pm30)_{22}]$: 109 layers

Segment 20: From point B19L to point B19R: $[(90)_{20}/(\pm25)_{20}/(90)_5/(\pm30)_{23}]$: 111 layers

3.) Portion CC:

This portion has a length of 5 inches and has the full layup sequence, i.e.

$[(90)_{20}/ (\pm25)_{20}/ (90)_5/ (\pm30)_{25}/(90)_2]$: 117 layers

4.) **Overwrap the whole tube (portion A-A):**

Overwrap the whole tube with $[(90)_3/ (\pm45)_{10}]$: 23 layers overwraps.

Thus the thickness increases from both ends towards the middle. In the middle portion (portion C-C), where the maximum thickness exists, there are140 layers and a stacking sequence of

$[(90)_{20}/ (\pm25)_{20}/ (90)_5/ (\pm35)_{25}/ (90)_5/ (\pm45)_{10}]$

At the two ends of the tube (portion A-B1), there are 88 layers and a stacking sequence of:

$[(90)_{20}/ (\pm25)_{20}/ (90)_8/ (\pm45)_{10}]$

3.2 Preparation of mandrel for curved tube

As shown in Figure 2.5 and Figure 2.22, the mandrel for curved tube consists of segmented metal shafts covered with Plaster of Paris. The metal shafts provide stiffness for the mandrel to withstand the manufacturing force, and the Plaster of Paris forms the inner diameter of 2.5 inches. (Figure 3.3) When the plaster is dissolved or washed away, the segmented shaft collapses and could be removed.

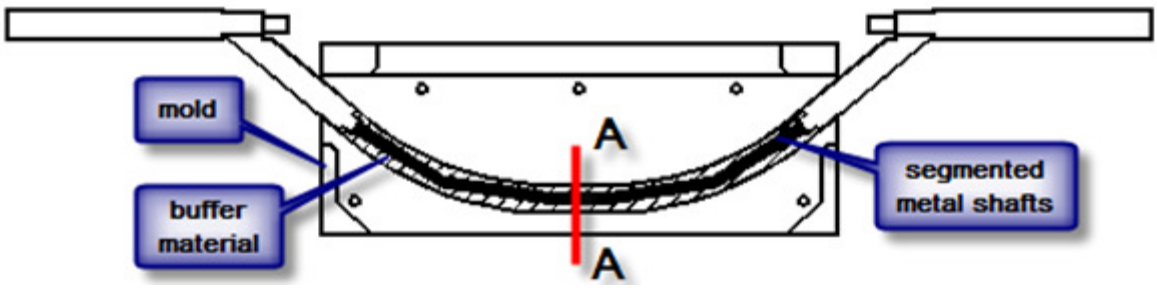

(a) Mandrel for curved tube (with mold)

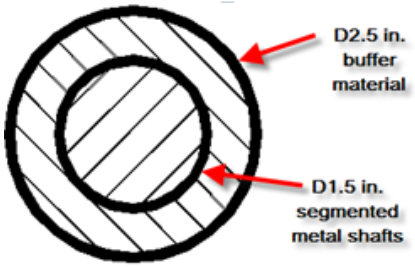

(b) Cross section of the mandrel

Figure 3.3 Schematic of mandrel for curved tube

3.2.1 Segmented metal shafts

For the tube shown in Figure 3.1, there are five segments forming the metal core: two straight portions at ends (AB, 2 pieces); two portions for each arc (BC, 2 pieces), and one for the straight portion in the middle (CD). All segments have diameter of 1.5 inches so that there will be adequate section area for three dowel pins, and this diameter can offer sufficient rigidity to the whole mandrel. The determination of diameter and length of metal shafts is shown in Figure 2.6.

The joint used to connect the segmented metal shafts is shown in Figure 2.22b. The connected segmented shaft is shown in Figure 3.4.

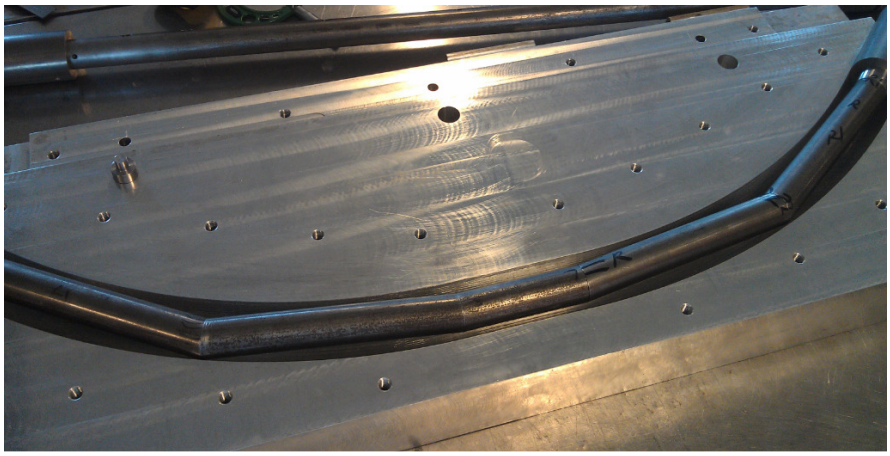

Figure 3.4 Segmented mandrel for curved tube

3.2.2 Casting the plaster

A mold is fabricated to cast the plaster. The two plates of this mold, top and bottom, are guided and positioned by 4 pins of 1 inch diameter. Five holes of 1 inch diameter are evenly located along the length of the mandrel, two of which work as injection gate and other three offer paths for the air to come out. As shown in figure 3.5, gates 2 and 4 work as injection gate, and gates 1-3-5 provide space for air escaping.

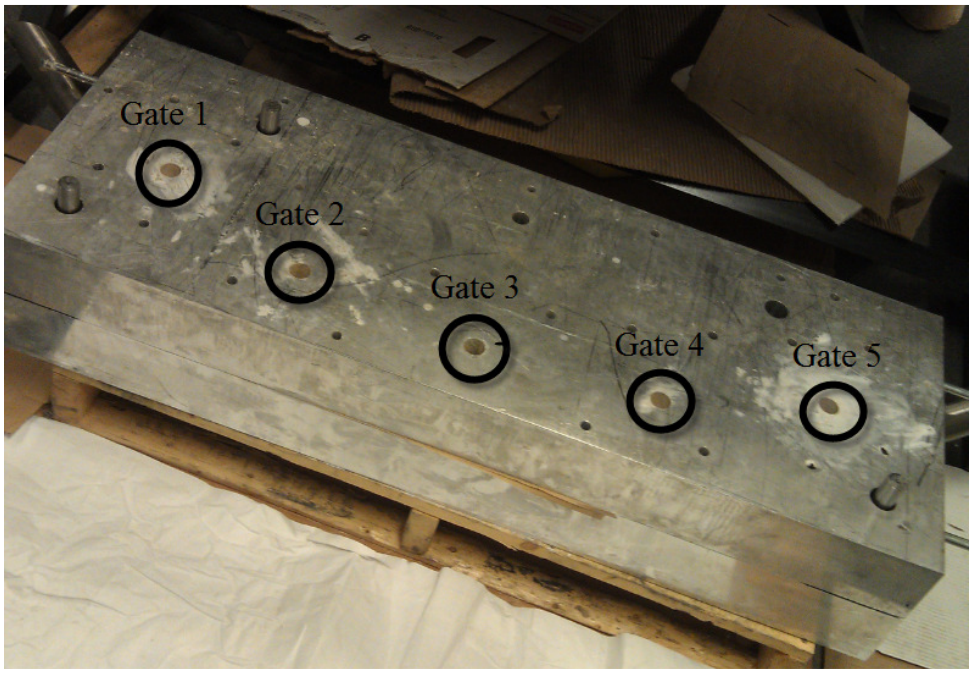

Figure 3.5 Mold for casting the plaster

It is calculated that 3.2 kg of gypsum plaster is required to cast this curved mandrel. With a weight-to-weight ratio of 1:2, 1.6kg water was used. The amounts of gypsum plaster and water are divided into four portions: 800g plaster and 400g of water for each portion.

All gypsum plaster and water were brought to the mold and the curved mandrel was carried by following the steps:

(1). Take first portion of the plaster and water: 800g plaster and 400g water;

(2). Add the water to the plaster all at one time, stir them immediately;

(3). Stir for 3-5 minutes to get rid of lumps and bubbles;

(4). Carefully pour the plaster into the mold through gate 2;

(5). Take second portion, and repeat steps 1-3, and pour the plaster through gate 4;

(6). Repeat steps 1-5 till the plaster comes out of five injecting holes.

(7). In 20 minutes, remove the plaster in five holes using tubes of 1 inch outer diameter .

(8.). Leave the cast samples to set up for 24 hours.

(9). Remove the top part of mold and clean injection mark.

(10). Leave the mandrel in to set up for 24 hours more;

(11). Take off the bottom part of mold.

The injection mark can be easily cleaned with a blade, and the finished injection marks are shown in Figure 3.6.

Figure 3.6 Casting mark on the mandrel

3.2.3 Thermoset layers to protect the plaster

The thermoplastic composite materials are not easy to be directly deposited onto the surface of the plaster. To accommodate this, thermoset composite layers were wrapped onto the plaster by AFP or by hand and cured in autoclave. With these thermoset composite layers, the cast plaster is well protected. Meanwhile the deposition of thermoplastic composite material became less difficult. Generally 4 layers of thermoset composite layers were employed to serve these purposes. Figure 3.7 illustrates the mandrel protected with thermoset composite materials.

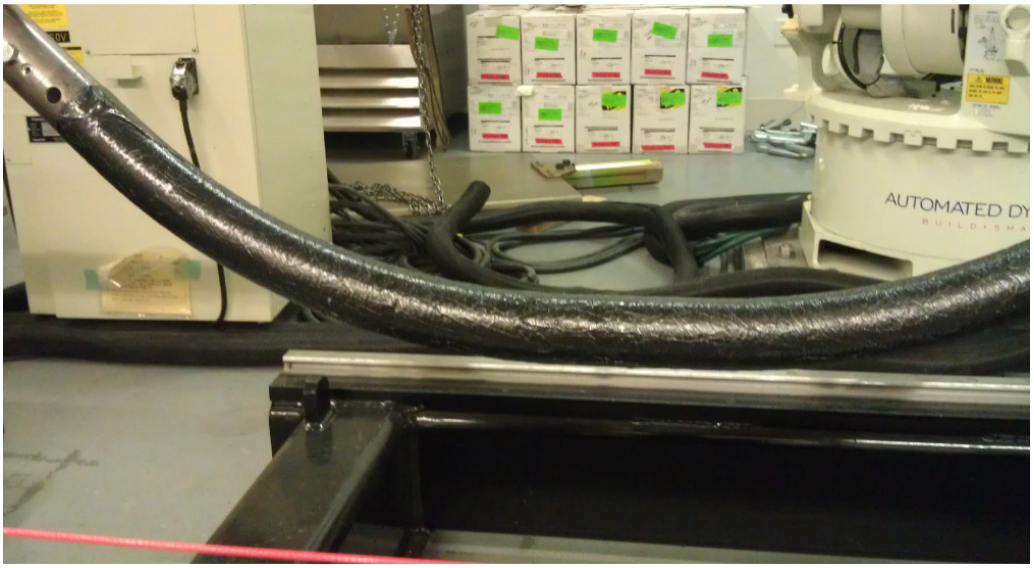

Figure 3.7 Mandrel wrapped with thermoset composite layers

3.3 Fabricating of curved tube using AFP

3.3.1 Materials and manufacturing parameters

The curved tube with constant thickness has 140 layers, and its stacking sequence is suggested by Bijan Derisi. [11]

$$[(90)_{20}/(\pm 25)_{20}/(90)_5/(\pm 30)_{25}/(90)_5/(\pm 45)_{10}]$$

This tube is made of 0.25" wide AS-4/PEEK slit tape supplied by Cytech Engineered Materials. The material has been used in several previous projects in Concordia Composites Center. It has distinct features as:

(1). Semi-crystalline thermoplastic matrix;

(2). Service temperature up to 500 °F/260 °C;

(3). High toughness and damage tolerance;

(4). Excellent environment resistance

(5). Indefinite shelf life at ambient conditions;

It is recommended that the optimum parameters for manufacturing AS4/PEEK on the automated fiber placement system are given as: [10]

(1). Nozzle Temperature: 925 °C

(2). Process Rate: 50.8 mm/s

(3). Compaction Force: 40 kgf

(4). Nozzle distance to Nip Point: 11.38 mm

Due to the complexity of the curved tube, the process speed was reduced to 25.4 mm/s (1 in/s) to avoid frequent rapid motion changes of the motors on AFP machine.

3.3.2 Manufacturing steps

1.) Simulate the tool path on the computer.

The mandrel surface is modeled and meshed in Solidworks, and the ply layup and part boundaries are defined in FPM, Fiber Placement Manager, which is installed on AFP machines. The simulated tow paths can be viewed in FPM. Figure 3.8 and Figure 3.9 demonstrate the tool paths of tows of 25 degrees and 45 degrees.

(a) Paths of all tows of 25 degrees

(b) Path of one tow of 25 degrees

Figure 3.8 Tool paths of 25 degrees

2.) Dry run to verify the tool path and to find any potential collisions or interferences.

3.) Start wrapping the first a few layers by less compaction forces.

4.) Increase the compaction force to 80 lbs and wrap all plies. See Figure 3.10.

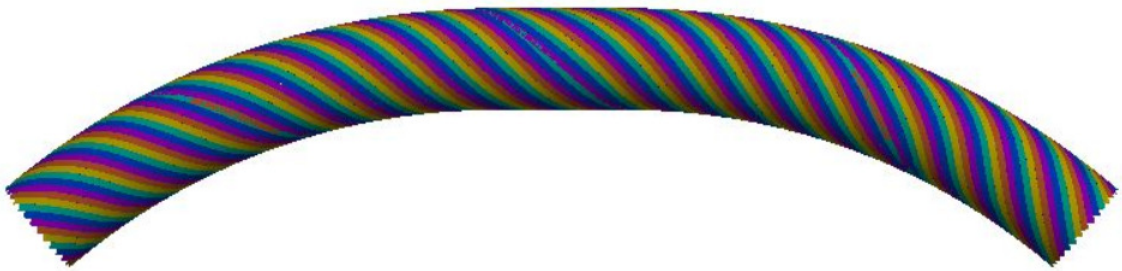

(a) Paths of all tows of 45 degrees

(b) Path of one tow of 45 degrees

Figure 3.9 Tool paths of 45 degrees

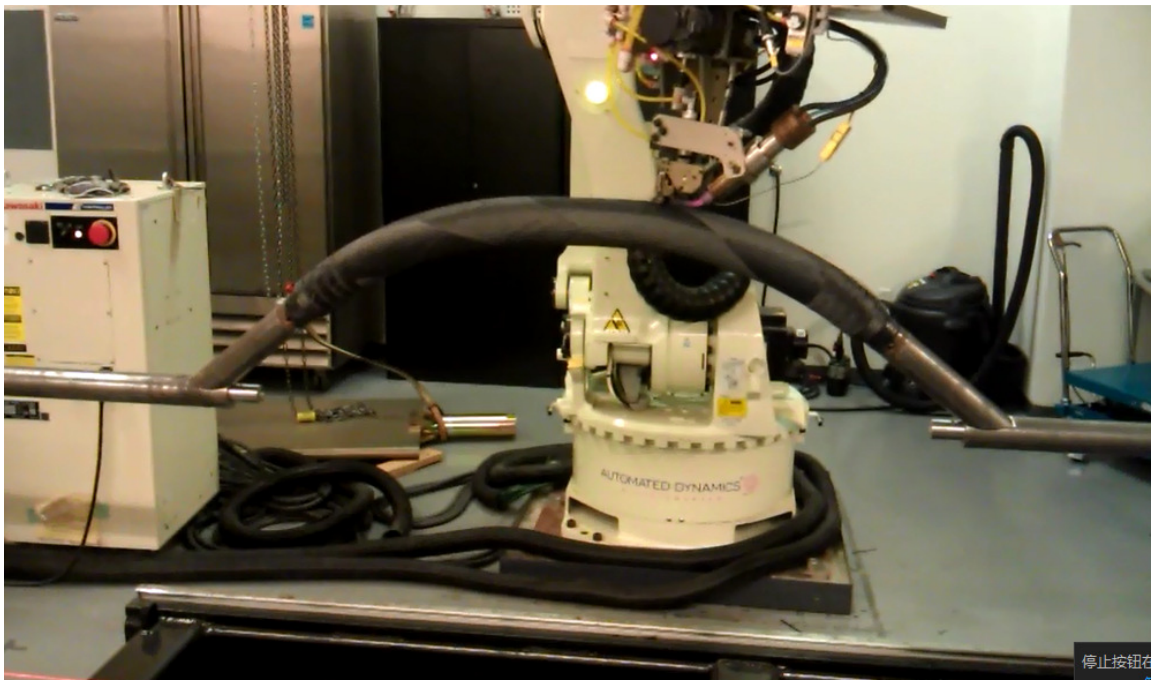

Figure 3.10 Wrapping thermoplastic composite layers

3.3.3 Time for layup

It is preferred to find the way to estimate the time for wrapping the thermoplastic composite, since this time plays a large portion in calculating the manufacturing cost. The time can be calculated with the following method:

Length of the curved tube: L=47 ins; (in the center)

Inner diameter: D_0 =2.5 ins;

Deposition rate: V=1 ins/s; (surface speed)

Width of tape: W=0.25 ins;

Thickness for slit tap: h=0.005 ins;

After the Nth layer, the outside diameter for calculation would be:

D_n=[2.5+2*(N-1)*h]=(2.49+0.01*N) (ins).

Area should be wrapped for the Nth layer:

$A_n = \pi * D_n * L$=3.14*(2.49+0.01*N)*47=(367.4742+1.4758*N) (in^2)

The deposition area rate is:

A=V*W=1*0.25 in^2=0.25 (in^2/s)

Then the time for Nth layer could be calculated as:

$t_n = A_n / A$=(367.4742+1.4758*N)/0.25=1469.8968+5.9032*N (s)

t_1 =1469.8968+5.9032*1=1475.8 (s)=24.6 min.

t_2 =1469.8968+5.9032*2=1481.7 (s)=24.7 min

t_3 =1469.8968+5.9032*3=1487.6 (s)=24.8 min

.....

t_{140} =1469.8968+5.9032*140=2296.34 (s)=38.3 min

Total time for 140 layers is about (24.6+38.3)*70/60=74 hrs:

3.4 Removal of the mandrel

When the wrapping of thermoplastic composites was finished, the tubes with plaster and segmented metal shafts were placed in an oven, and left them at a temperature of 200 °C for 12 hours so that the plaster could be completely dehydrated. The time for curing the plaster was determined from experiment.

Subsequently, adequate amount of water was added into the dehydrated plaster, and then the plaster absorbed the waster and softened. When the softened plaster was broken by rotating the segmented metal shaft or by other tools, the segmented shaft collapsed and was removed. The rest of the plaster was cleaned with cold tap water.

Figure 3.11 shows the curved tube with constant thickness and Figure 3.12 displays the curved tube with variable thickness.

Figure 3.11 Curved tubes with constant thickness, 110 layers
(Layup sequence: $[(90)_{15}/ (\pm35)_{20}/ (90)_5/ (\pm35)_{10}/ (90)_{10}/ (\pm45)_{10}]$)

Figure 3.12 Curved tube with variable thickness, 140 layers in the middle
(Layup sequence in middle: $[(90)_{20}/ (\pm25)_{20}/ (90)_5/ (\pm35)_{25}/ (90)_5/ (\pm45)_{10}]$)

Chapter 4. Testing and Results

4.1 Microscopic test

A process should meet with certain requirements so that it could be employed to manufacture composite parts. These requirements could be described as: [6]

(1). Good bonding between matrix and fibers;

(2). Proper orientation of fibers;

(3). Good amount of volume fraction of fibers;

(4). Uniform distribution of fibers within the matrix;

(5). Appropriate curing or solidification of the resin;

(6). Limited amount of voids and defects;

(7). Good dimensional control for final parts.

With automated fiber placement system, continuous slit tape is laid down on a mandrel under pressure and temperature, and the tape is consolidated as it is being placed. Good bonding between fiber and matrix, uniform fiber distribution needs to be ensured within the slit tape. Microscopic test is used here to detect the voids and gaps between layers caused during processing.

Four samples were cut from one end of first curved tube, the one with constant thickness. All samples are fixed in cured epoxy and are polished as required, shown in Figure 4.1

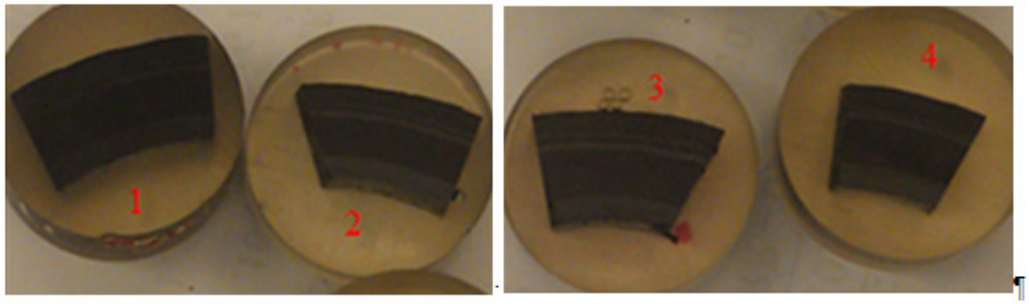

Figure 4.1 Samples for microscopic test

From the micrographs shown in Figure 4.2, 4.3, 4.4 and 4.5, it is found that fibers are uniformly distributed within one layer, but some resin rich areas exist between layers.

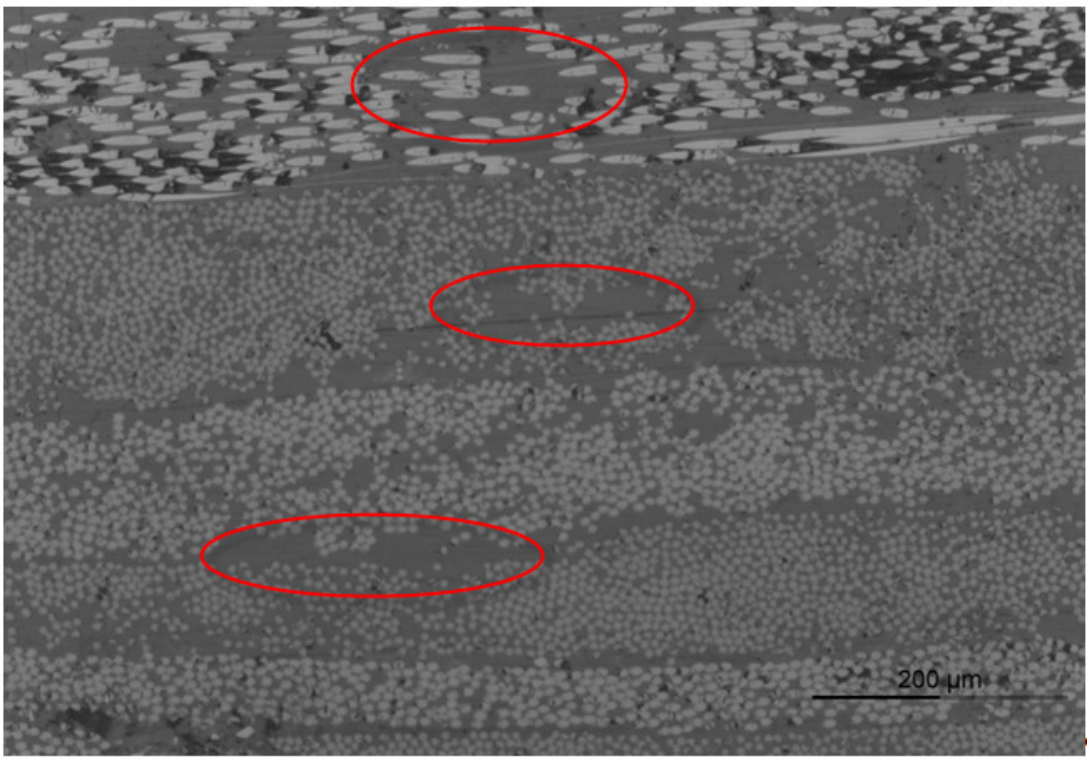

Figure 4.2 Micrograph 1

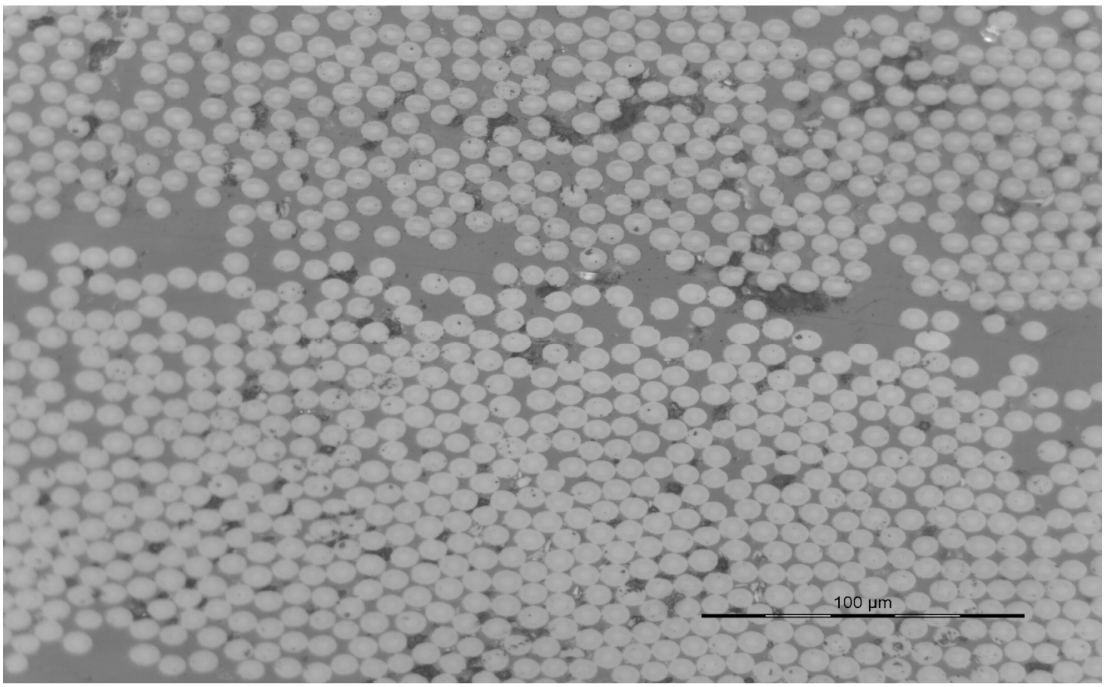

Figure 4.3 Micrograph 2

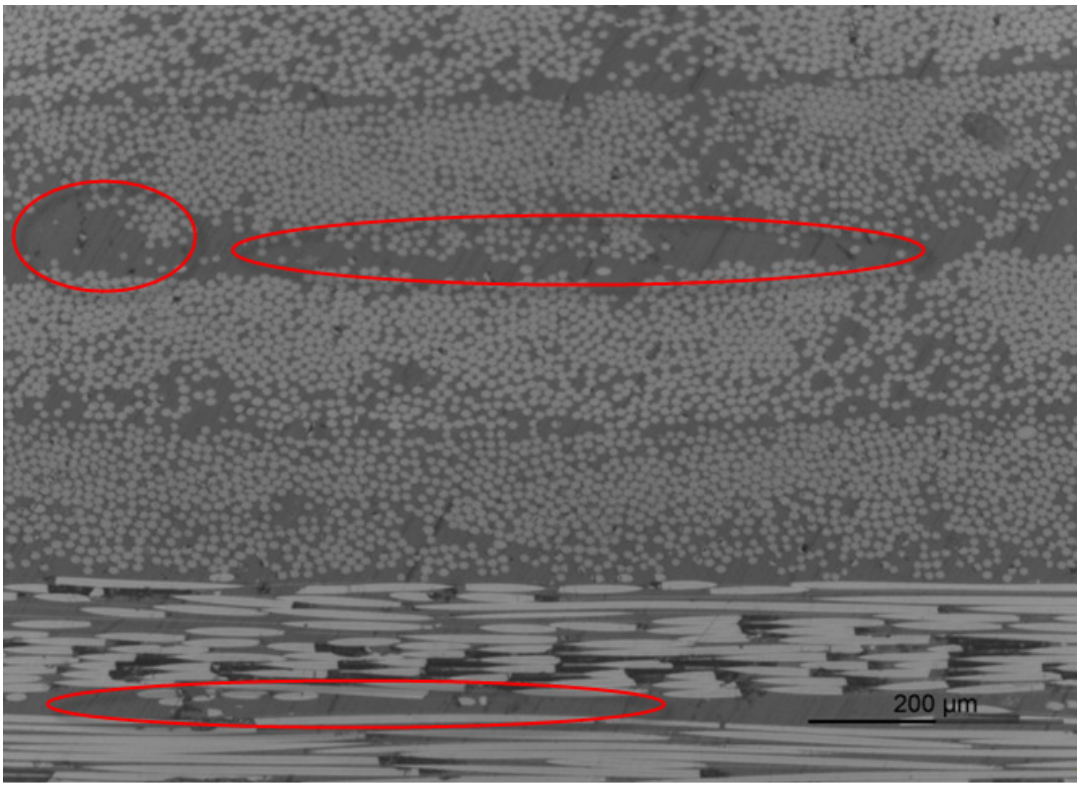

Figure 4.4 Micrograph 3

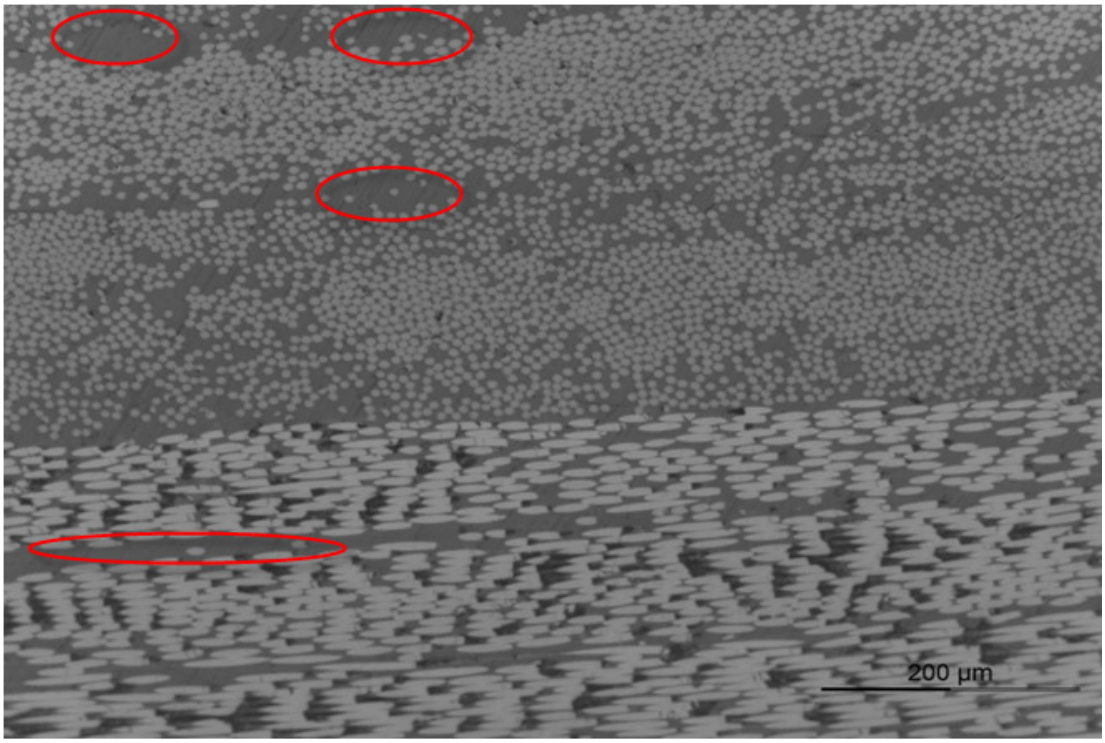

Figure 4.5 Micrograph 4

4.2 Three-point bending test

The tube was tested in three point bending test. Both ends and middle portion of each curved tube were strengthened by thermoset composite materials to prevent local damages caused by force concentration. Generally 20 thermoset composite layers were added on each portion. (Figure 4.6)

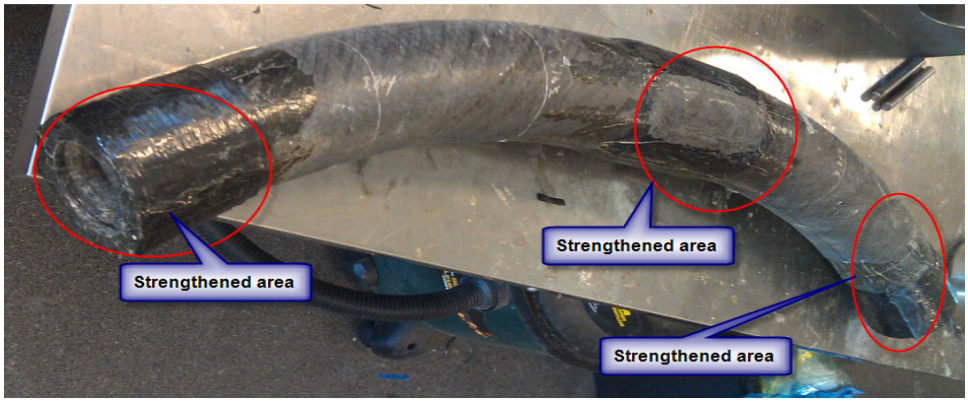

Figure 4.6 Locations of load application and supports are strengthened

4.2.1 Fixture for bending test

For the test, the tube was held in the middle portion by an adapter, where the bending force was applied. Both ends of the tube were supported by two metal pins which could rotate and move simultaneously with the ends of tube when force is applied. Figure 4.7 illustrates the schematic of test fixture.

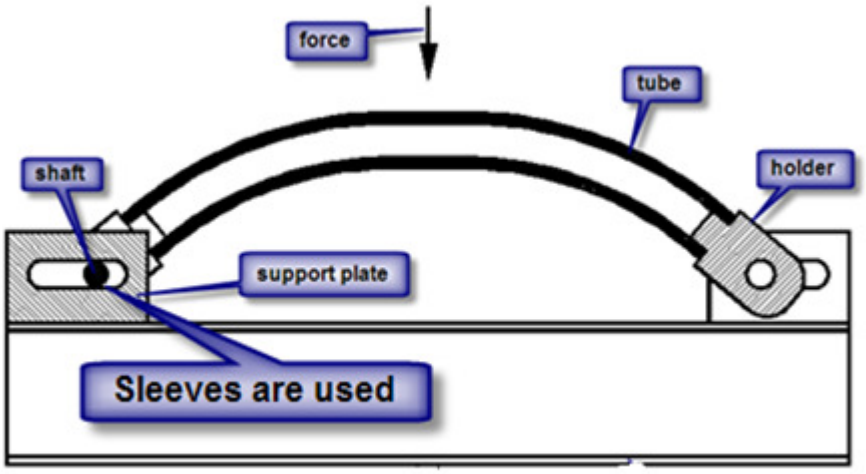

Figure 4.7 Test fixture

All parts for the fixture are shown in Figure 4.9, there are 14 pieces in total:

(a) adapter 2 pieces

(b) Pin: 2 pieces

(c) Sleeve: 4 pieces

(d) Plate: 4 pieces

(e) Holder: 2 pieces

The sleeves are made of steel with HRC of 35-45, and all other parts are made of mild steel with HRC of 18-25. Figure 4.8 illustrates the curved tube mounted on the test fixture, only upper part of the adapter is displayed.

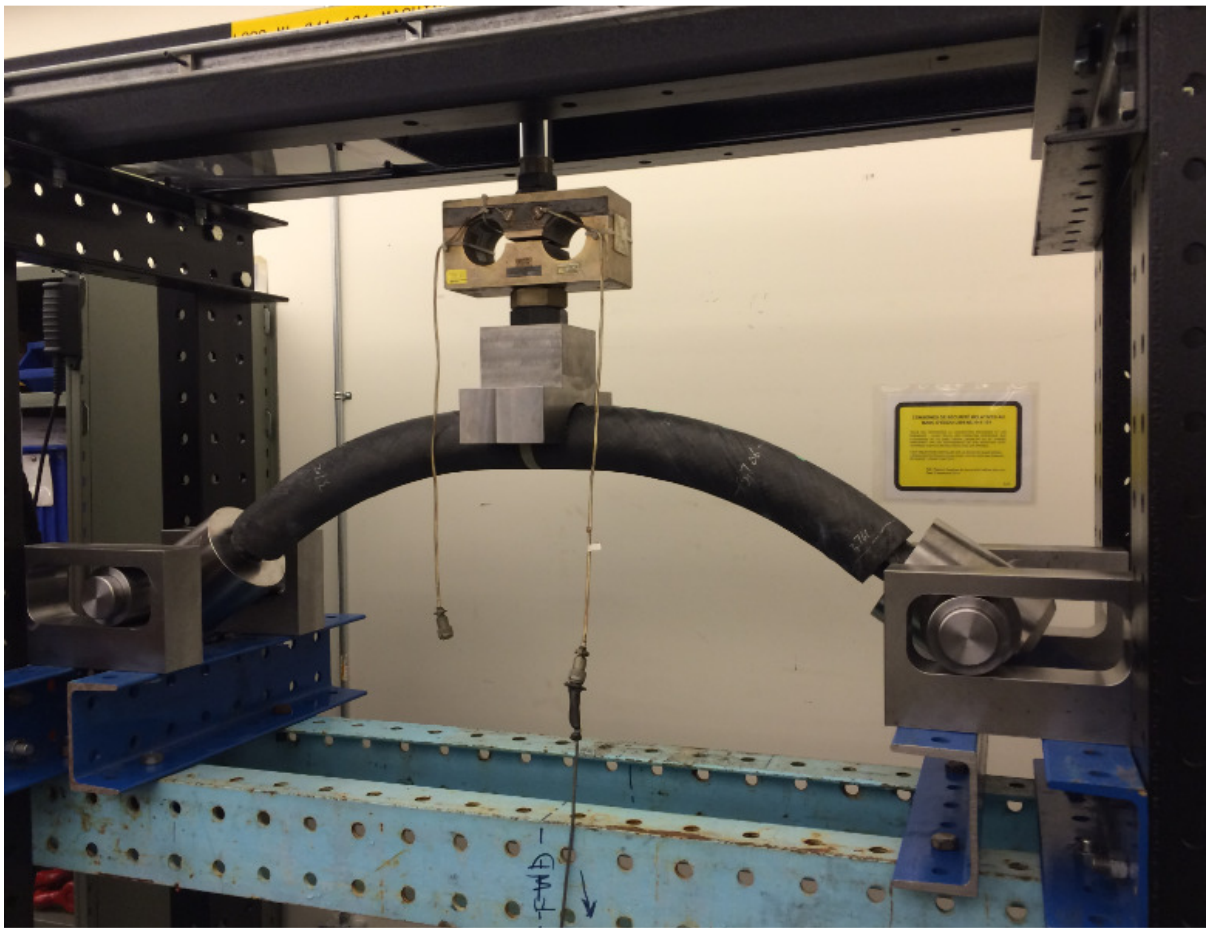

Figure 4.8 Curved tube mounted on test fixture (w/o strain gauges)

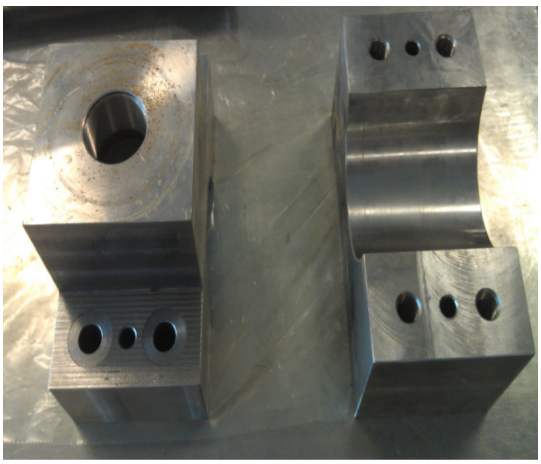

(a) Adapter

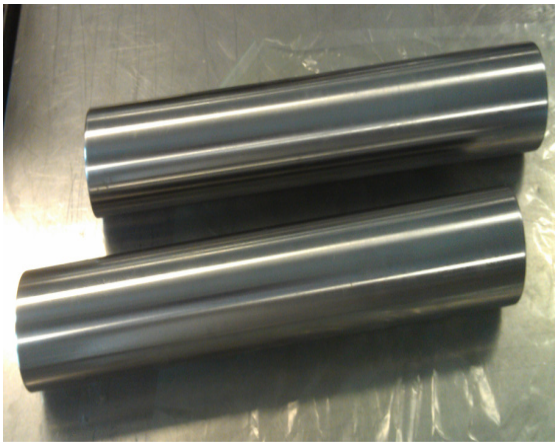

(b) Pins

(c) Sleeves

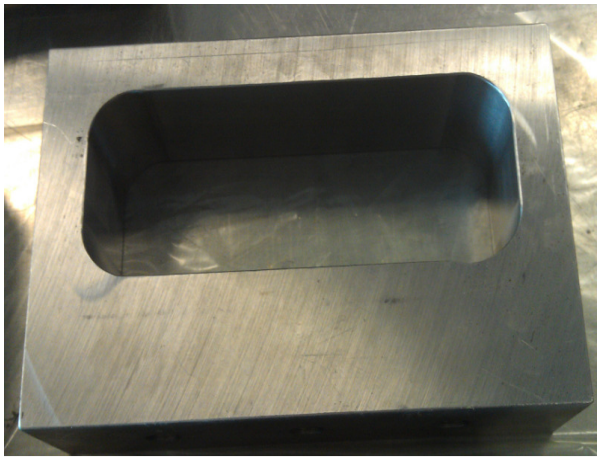

(d) Supporting plate

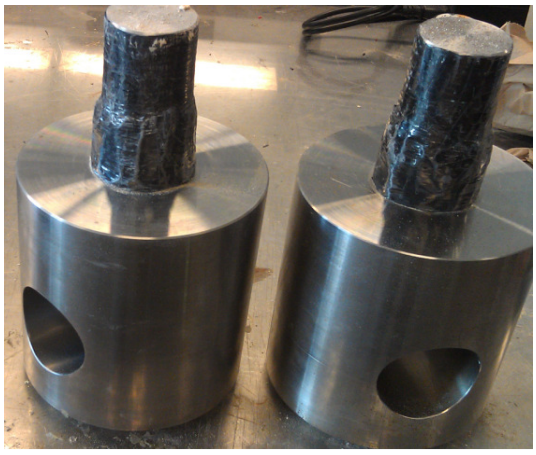

(e) Holder

Figure 4.9 Parts for test fixture

4.2.2 Installation of strain gauges

For each tube, there are 24 strain gauges, from 8 rosettes, attached to the locations as shown in Figure 4.10. It is suggested that the surfaces for the rosettes were polished with sandpaper of size 80, and then be completely cleaned with acetone and alcohol.

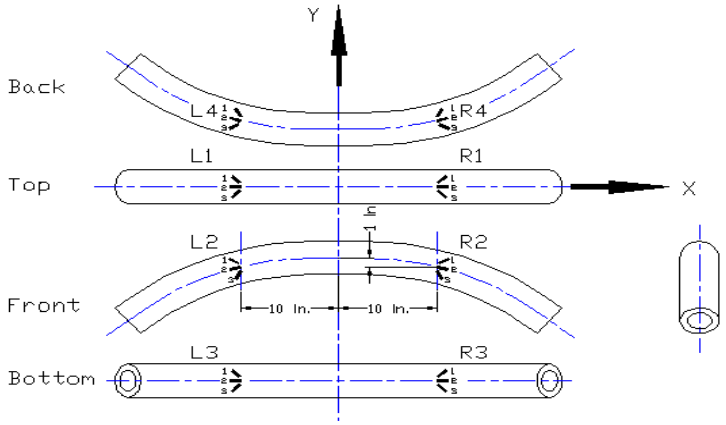

Figure 4.10 Location of strain gauges

Four rosettes are located on the left and named L1, L2, L3, L4, and the rosettes located on the right are labeled R1, R2, R3 and R4. Table 4.1 shows the positions of the strain gauges on the right, and Table 4.2 displays the gauges on the left. All angles are referred to X-axis shown in Figure 4.10. Strain gauges L1-2 and R1-2 locate at centerline on top, and L3-2, R3-2 locate at the centerline at the bottom. Gauges R2-2, R4-2, L2-2 and L4-2 locate at the centerline on front and rear surface and are tangent to the centerline. This describes how the angles shown in Table4.1 and Table 4.2 are determined.

Table 4.1 Strain gauges on the right side

Rossette	Gauge	X (ins.)	Angle	Sketch	Channel	Card
R1	R1-1	10	45	Right Top	1	1
	R1-2	10	0		2	1
	R1-3	10	-45		3	1
R2	R2-1	10	29	Right Front	4	1
	R2-2	10	-16		5	1
	R2-3	10	-61		6	1
R3	R3-1	10	-45	Right Bottom	7	1
	R3-2	10	0		8	1
	R3-3	10	45		9	2
R4	R4-1	10	-61	Right Back	10	2
	R4-2	10	-16		11	2
	R4-3	10	29		12	2

Table 4.2 Strain gauges on the left side

Rossette	Gauge	X (ins.)	Angle	Sketch	Channel	Card
L1	L1-1	-10	-45	Left Top	13	2
	L1-2	-10	0		14	2
	L1-3	-10	45		15	2
L2	L2-1	-10	-29	Left Front	16	2
	L2-2	-10	16		17	3
	L2-3	-10	61		18	3
L3	L3-1	-10	45	Left Bottom	19	3
	L3-2	-10	0		20	3
	L3-3	-10	-45		21	3
L4	L4-1	-10	61	Leftt Back	22	3
	L4-2	-10	16		23	3
	L4-3	-10	-29		24	3

Figure 4.11 shows the installed strain gauges and how their connecting wires are fixed so that the wires and gauges would not damaged during transportation.

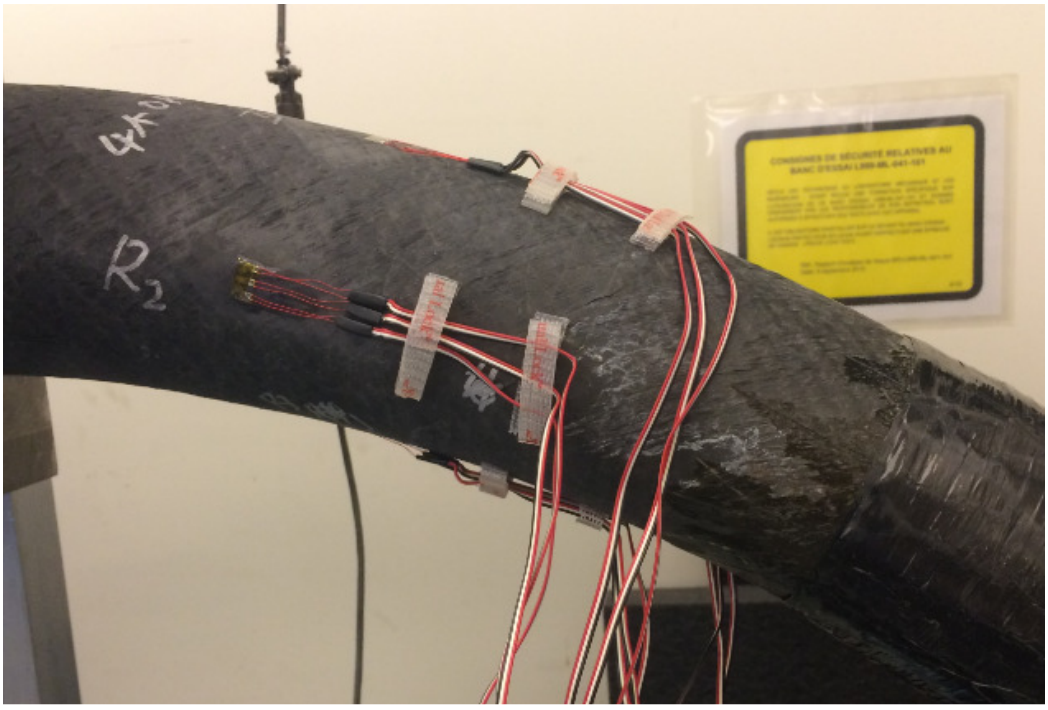

Figure 4.11 Strain gauges attached on the tube

Testing was done on a hydraulic set located at Bell Helicopter Textron Canada Ltd. Figure 4.12 shows that 24 strain gauges were attached on the tube, and all gauges have already been connected to data acquisition system. It could be seen that two aluminum beams were used to prevent the side motion when forces were applied.

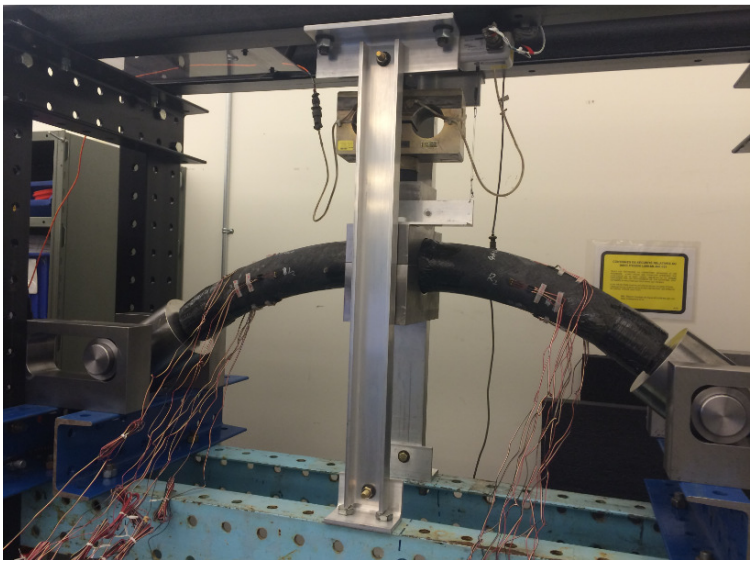

Figure 4.12 Tube ready for test

When test began, force was slowly applied using a hydraulic pump. Loading, displacement and strain values were automatically recorded with a data acquisition system. The loading continued till the tube was broken.

Two tubes were broken at the right side where strengthened area ends, see Figure 4.13.

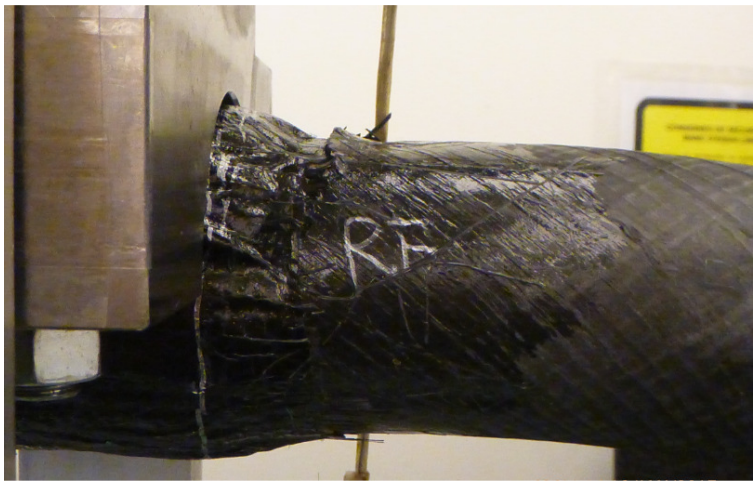

Figure 4.13 Damage on the tested tubes

4.3 Bending test results

4.3.1 Curved tube with constant thickness (tube 1)

The tube with constant thickness has 110 layers and has a stacking sequence of

$$[(90)_{15}/\ (\pm35)_{20}/\ (90)_5/\ (\pm35)_{10}/\ (90)_{10}/\ (\pm45)_{10}]$$

This tube broke at a load of 16000 lbs. Figure 4.14 shows the linear behavior between load and deflection.

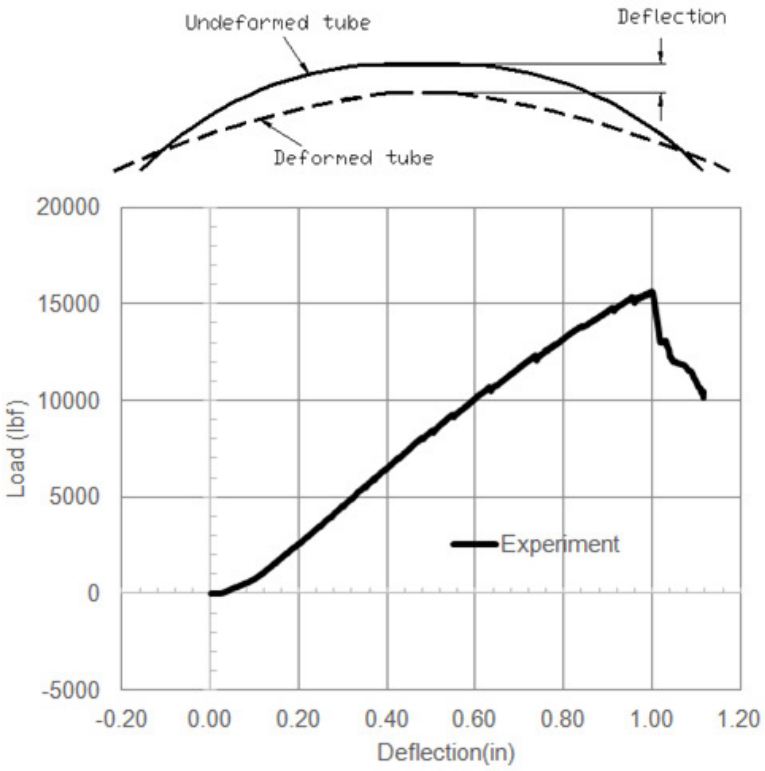

Figure 4.14 Load versus deflection on tube 1

Strains on all strain gauges are shown in Figure 4.15 to Figure 4.21. Since one recording channel was damaged, strains on seven rosettes are shown in Figure 4.15 to 4.21, (three strain gauges for each rosette), and no strains on rosette R2 were recorded. One graph in each figure indicates the location of rosette (In the meantime the locations of strain gauges are shown), and the other indicates the strains.

Since gauges R1-2 (Figure 4.15b) and L1-2 (Figure4.18b) are supposed to be in the symmetric locations, they should exhibit the same values under one load. The small difference of their maximum strain shows that these two gauges have almost the same strains, which mean the two gauges are well located at the symmetrical position.

Rosette R1 is on the right-top side displaying compressive strains. Strain gauge R1-2 is located at the center line and exhibits the maximum compressive strain of 7500 micro strain. Strain gauges R1-1 and R1-3 are located at positions symmetrical to center line, and both gauges display small compressive strains.

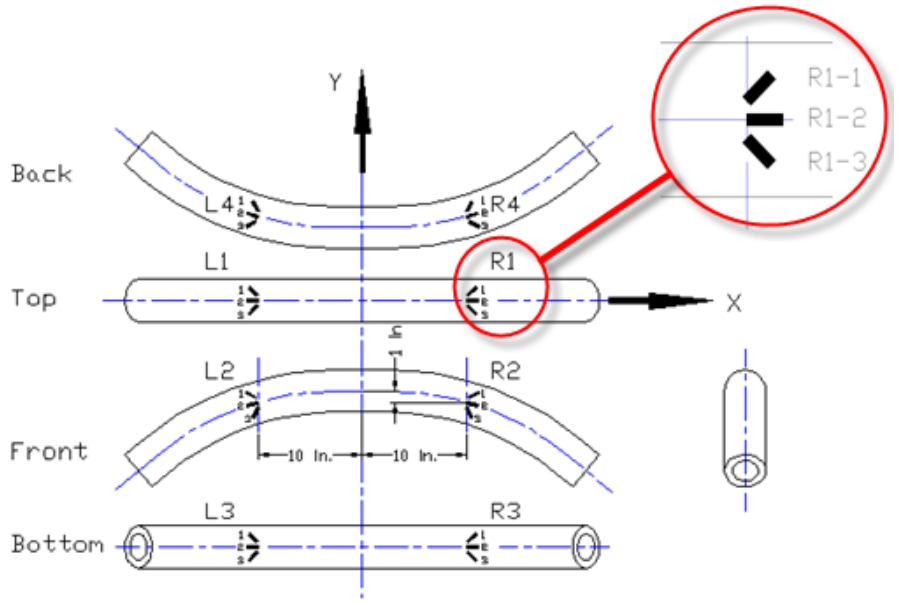

(a) Locations of strain gauges on rosette R1, tube 1

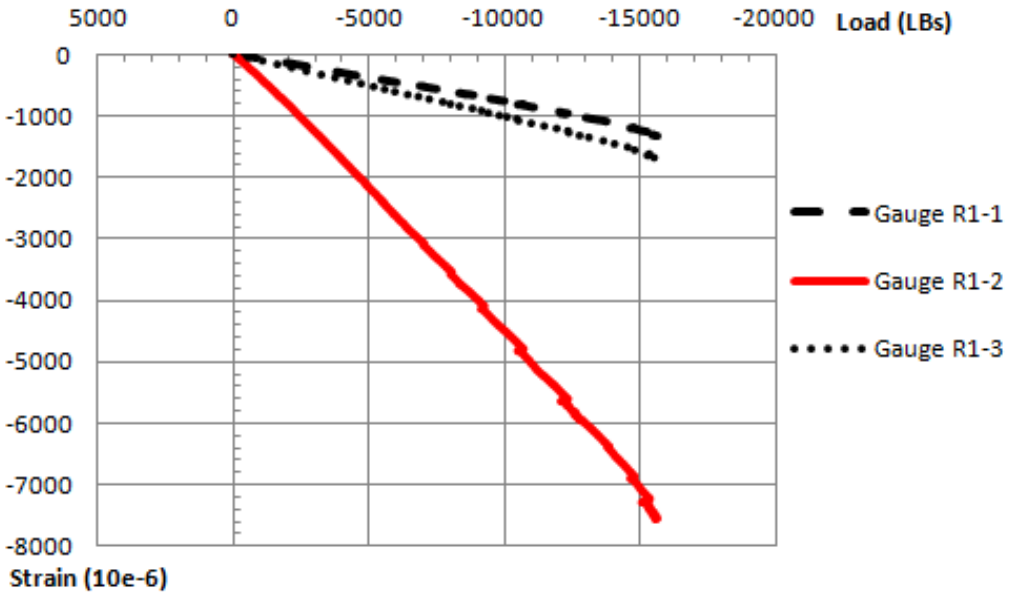

(b) Strains of Rosette R1, tube 1

Figure 4.15 Strains versus load of rosette R1 (tube 1)

Rosette R3 is at the right-bottom side displaying tensile strains. Strain gauge R3-2 is positioned at center line and showing maximum tensile strain of 7500 micro strain. Strain gauges R3-1 and R3-3 are located at positions symmetrical to center line, and both gauges display small tensile strains.

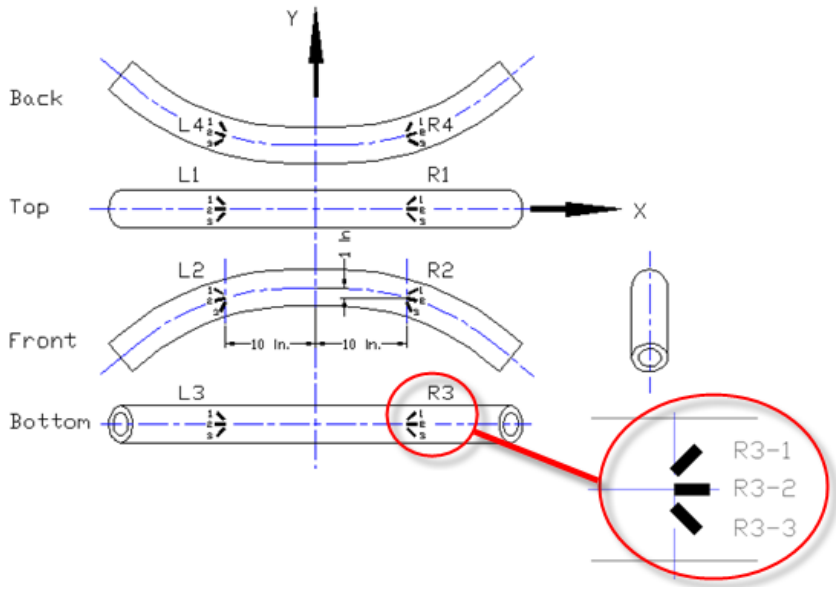

(a) Locations of strain gauges of rosette R3, tube 1

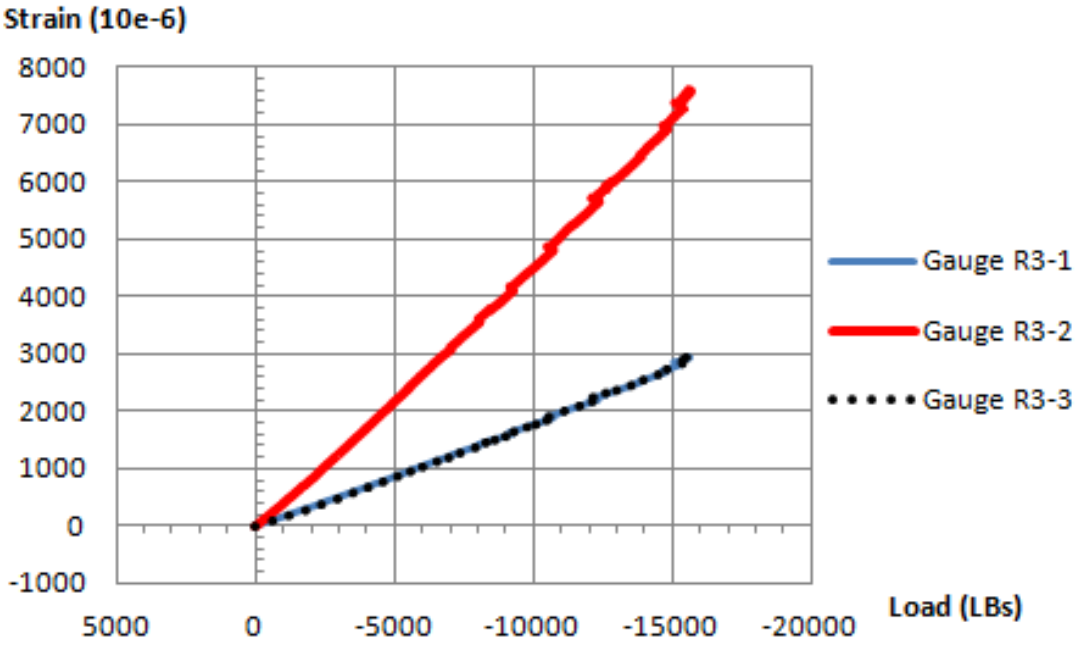

(b) Strains of Rosette R3, tube 1

Figure 4.16 Strains versus load on rosette R3 (tube 1)

Rosette R4 is at the right-rear side. Strain gauge R4-2 is tangent center line. Three strain gauges of this rosette display small compressive strains.

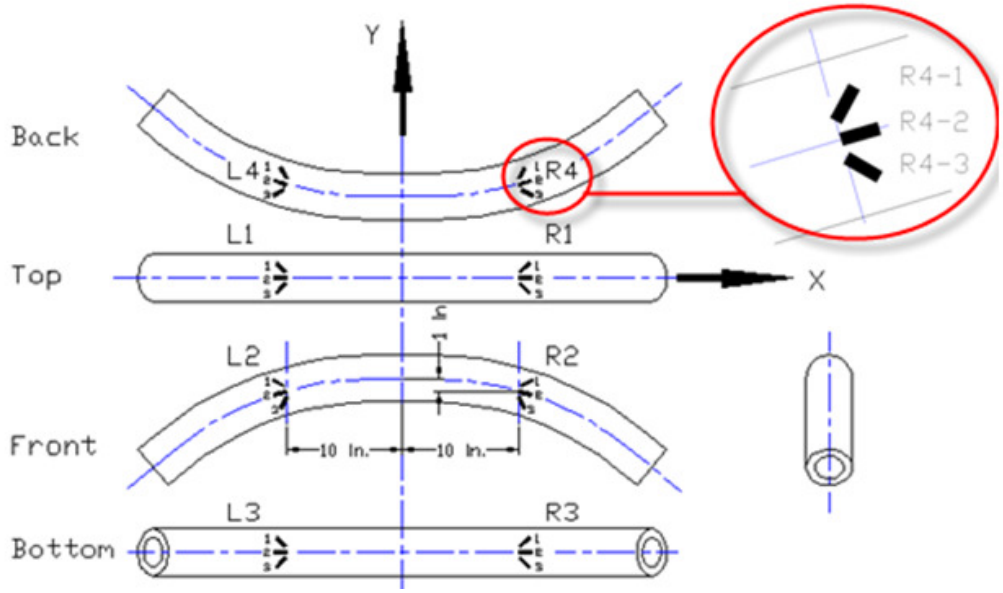

(a) Locations of strain gauges of rosette R4, tube 1

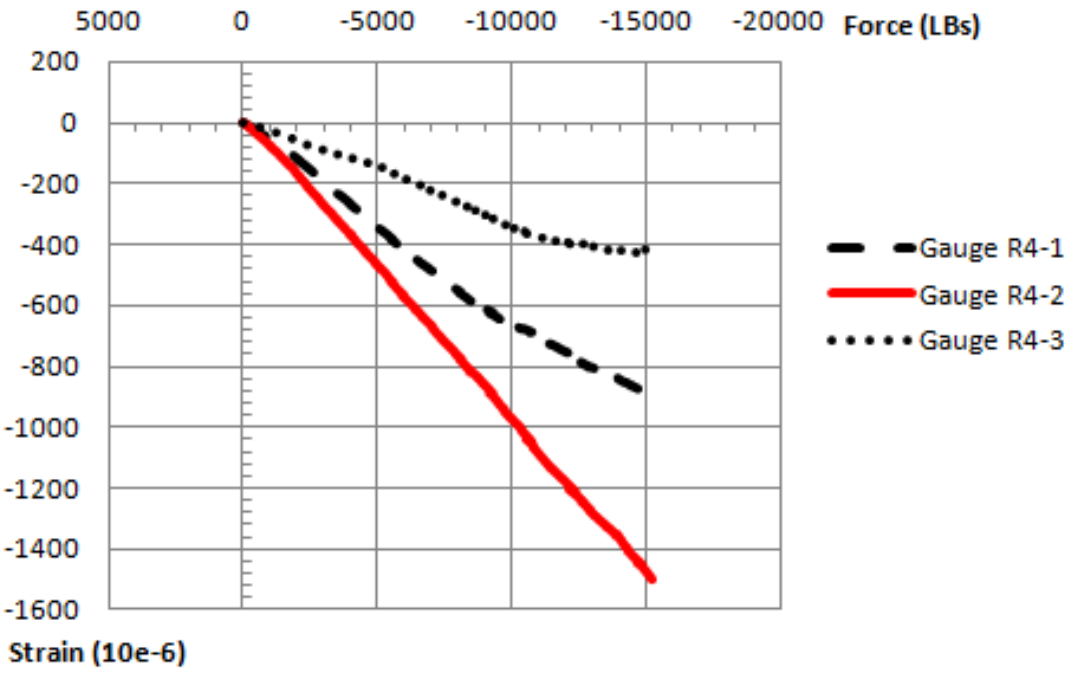

(b) Comparison of strains on Rosette R4, tube 1

Figure 4.17 Strains versus load on rosette R3 (tube 1)

Rosette L1 is on the left-top side displaying compressive strains. Strain gauge L1-2 is located at the center line and exhibits the maximum compressive strain of 8000 micro strain. Strain gauges L1-1 and L1-3 are located at positions symmetrical to center line, and both gauges display small compressive strains.

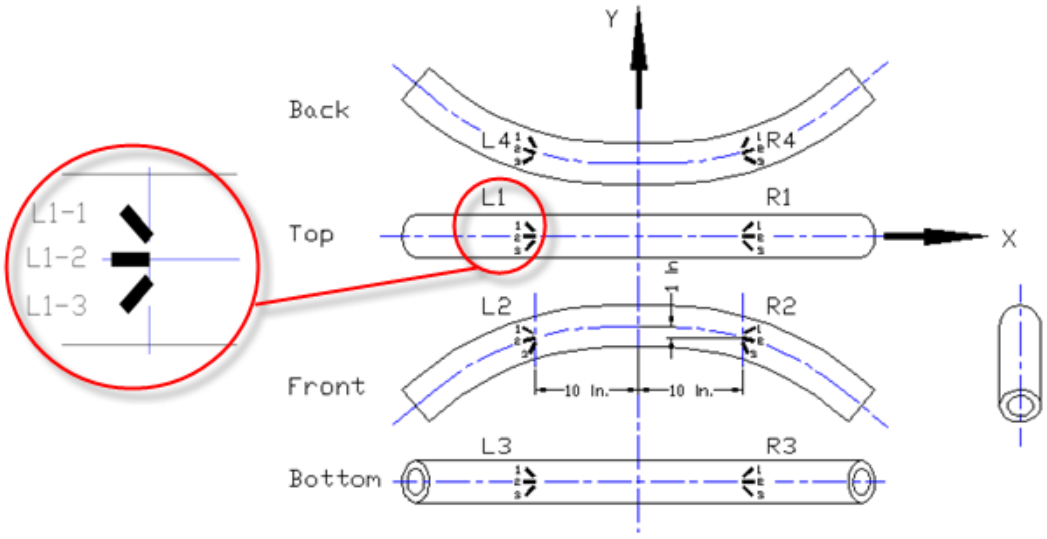

(a) Locations of strain gauges of rosette L1, tube 1

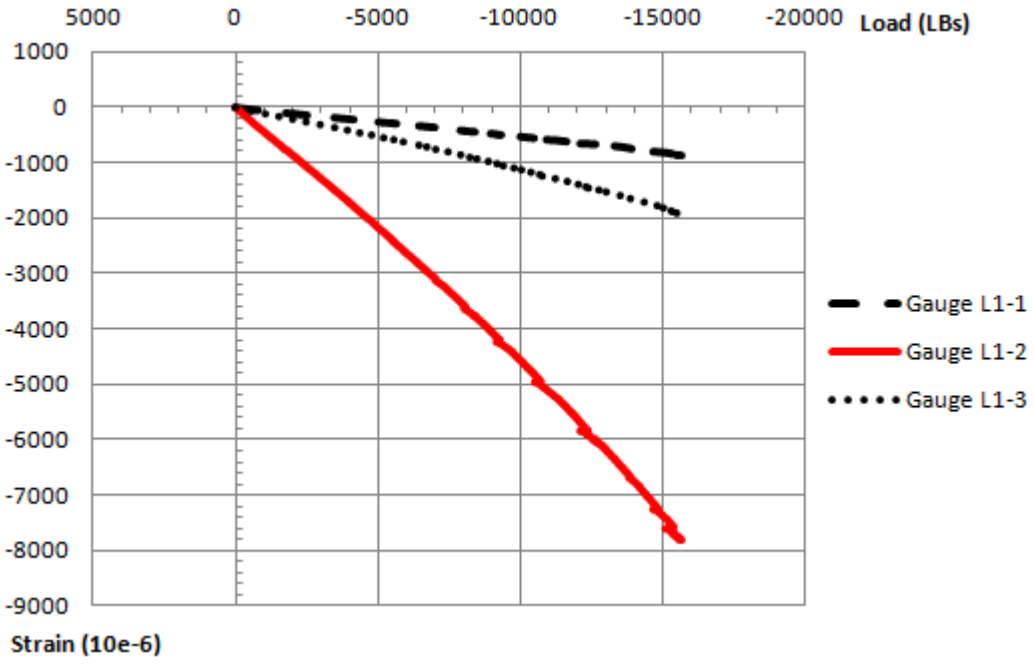

(b) Strains of Rosette L1, tube 1

Figure 4.18 Strains versus load on rosette L1 (tube 1)

Rosette L2 is at the left-front side. Strain gauge L2-2 is tangent center line and displays very small tensile strains, and strain gauges L2-1 and L2-3 exhibit small compressive strains.

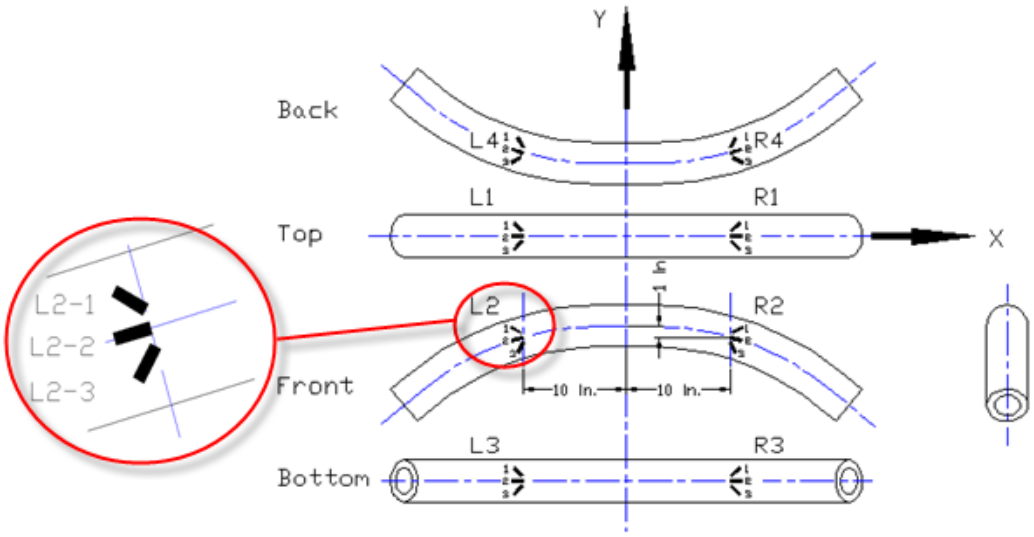

(a) Locations of strain gauges of rosette L2, tube 1

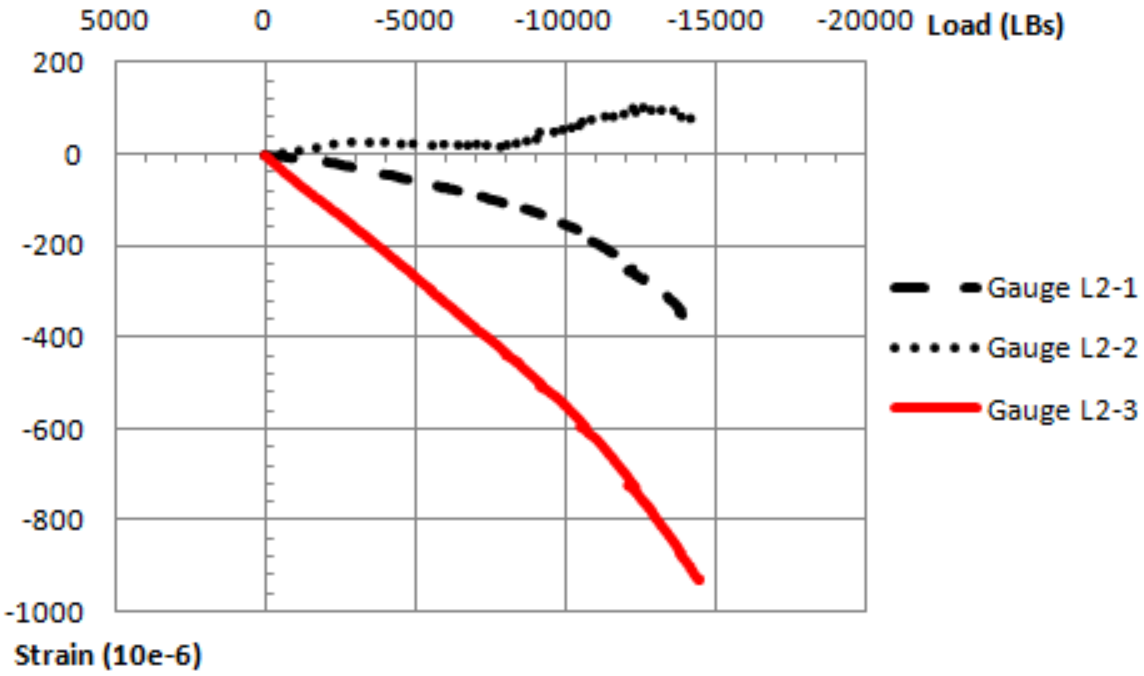

(b) Strains of Rosette L2, tube 1

Figure 4.19 Strains versus load on rosette L2 (tube 1)

Rosette L3 is at the left-bottom side showing tensile strains. Strain gauge L3-2 is positioned at center line and showing maximum tensile strain of 10000 micro strain. Strain gauges L3-1 and L3-3 are located at positions symmetrical to center line, and both gauges illustrate small tensile strains.

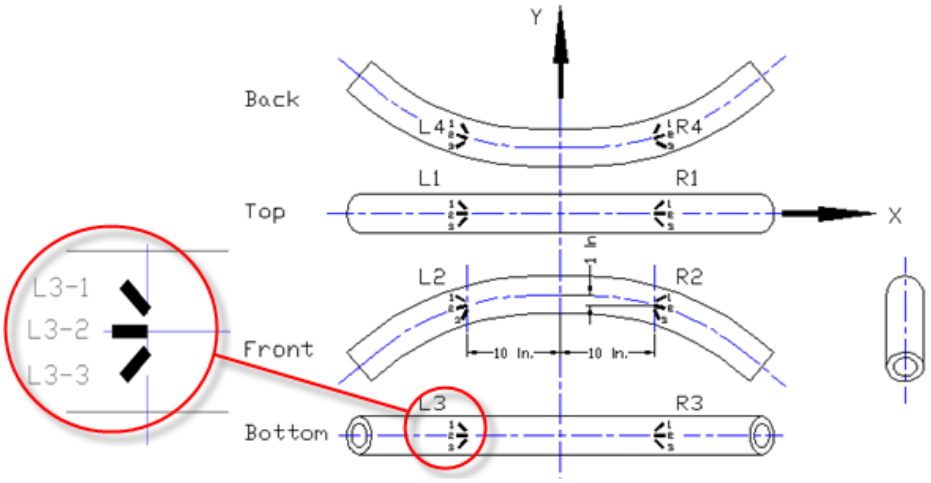

(a) Locations of strain gauges of rosette L3, tube 1

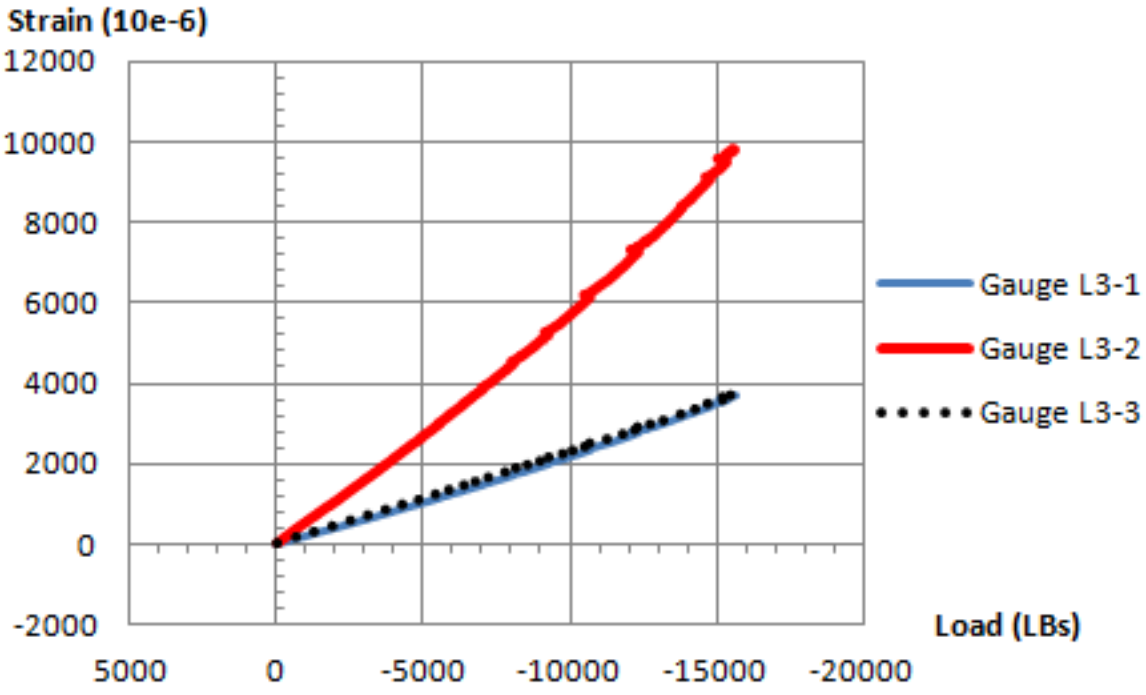

(b) Strains of Rosette L3, tube 1

Figure 4.20 Strains versus load on rosette L3 (tube 1)

Rosette L4 is at the left-rear side. Strain gauge L4-2 is tangent center line. Strain gauge L4-1 displays very small compressive strains, and strain gauges L4-2 and L4-3 exhibit small tensile strains.

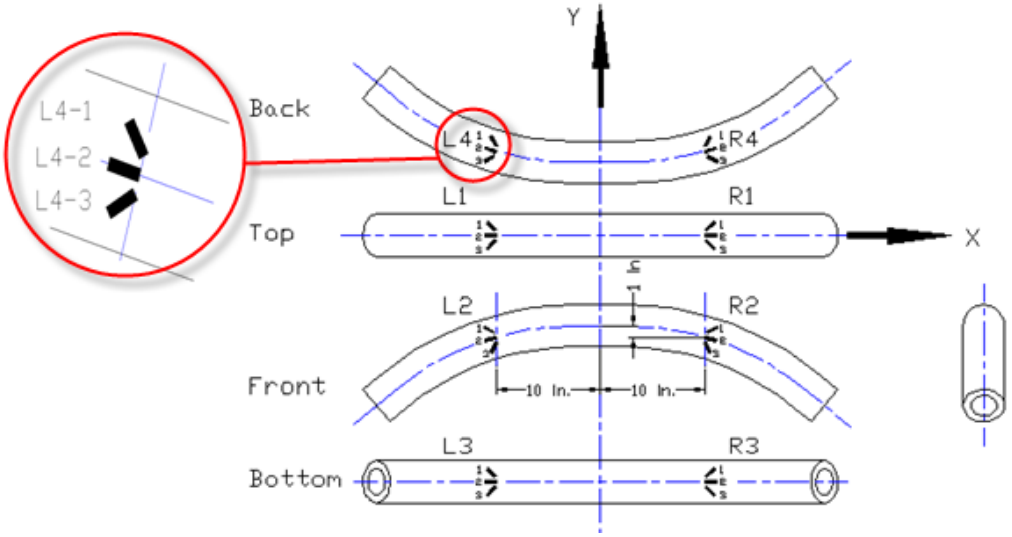

(a) Locations of strain gauges of rosette L4, tube 1

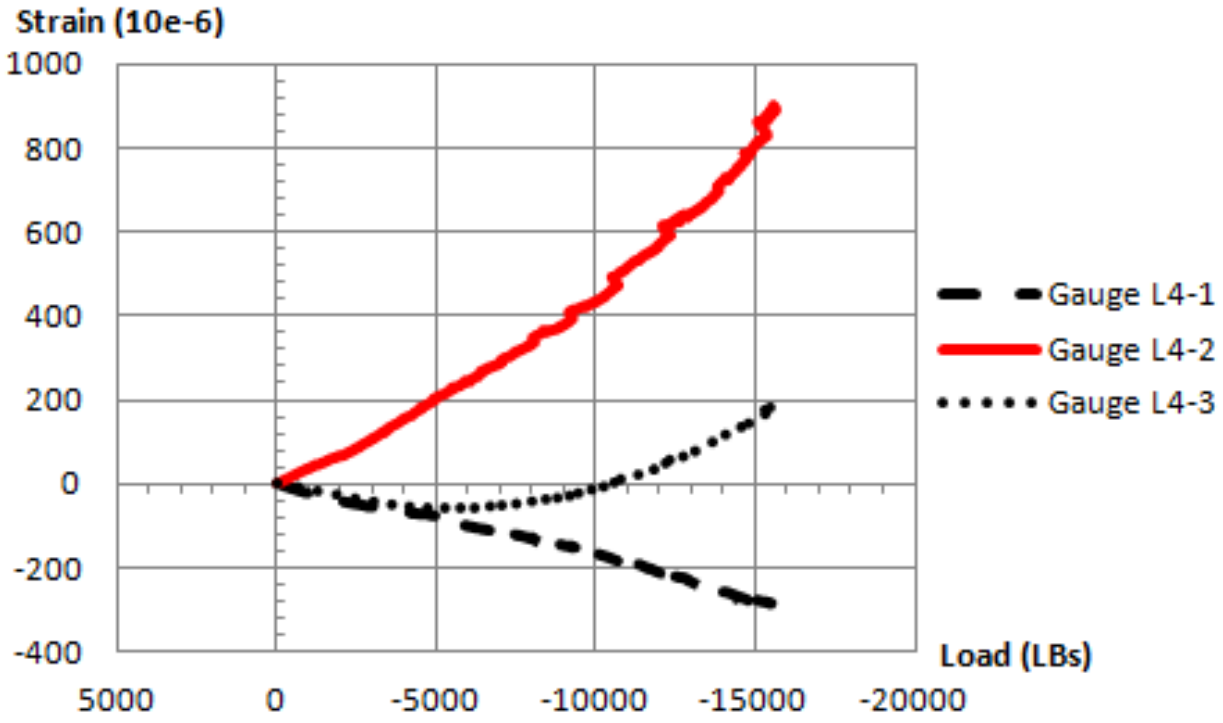

(b) Strains of Rosette L4, tube 1

Figure 4.21 Strains versus load on rosette L4 (tube 1)

4.3.2 Curved tube with variable thickness(tube 2)

The tube with variable thickness has 140 layers, and its layup sequence in the middle is

$$[(90)_{20}/\ (\pm30)_{20}/\ (90)_5/\ (\pm30)_{25}/\ (90)_5/\ (\pm45)_{10}]$$

There is also linear behavior before the maximum load of 22000 lbs. After the peak load, the force decreases while the deflection increases due to some failures inside the tube. The tube is broken when the force decreases to 17000 lbs. (Figure 4.22)

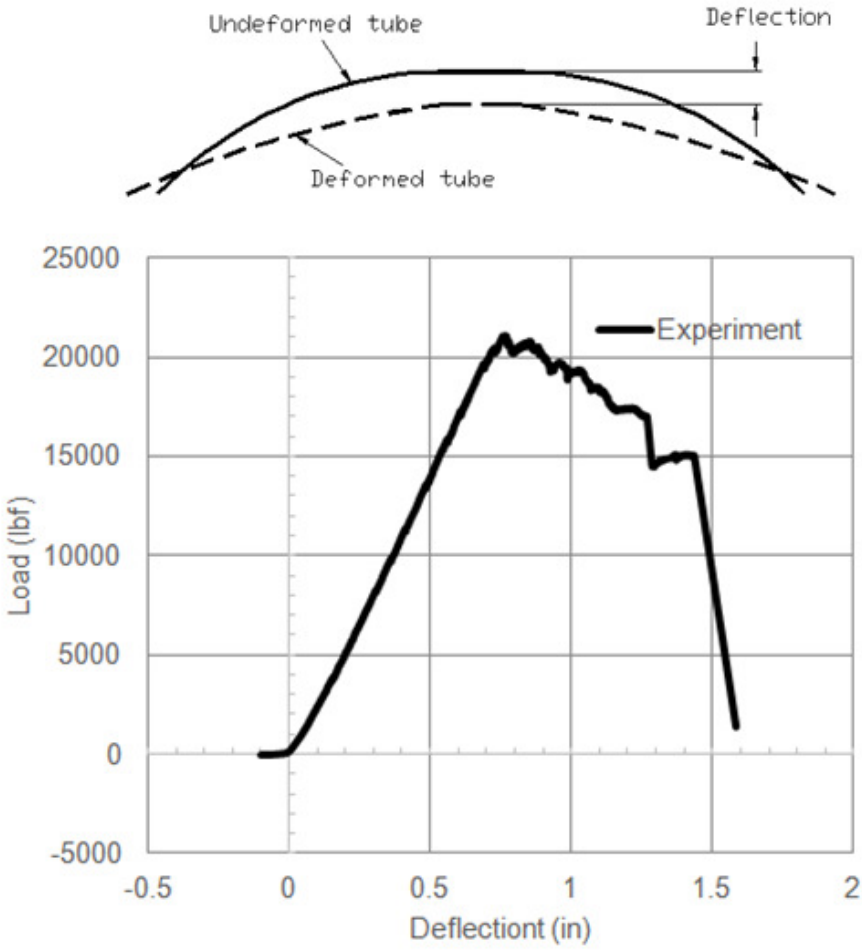

Figure 4.22 Load versus deflection on tube 2

Strains on all strain gauges of this curved tube are shown in Figure 4.23 to Figure 4.29. Only strains on seven rosettes are shown. There are two graphs in each figure. One graph in each figure indicates the location of rosette (In the meantime the locations of strain gauges are shown), and the other indicates the strains of each strain gauge.

Rosette R1 is on the right-top side displaying compressive strains. Strain gauge R1-2 is located at the center line and exhibits the maximum compressive strain of 6000 micro strain. Strain gauges R1-1 and R1-3 are located at positions symmetrical to center line, and both gauges display very small compressive strains.

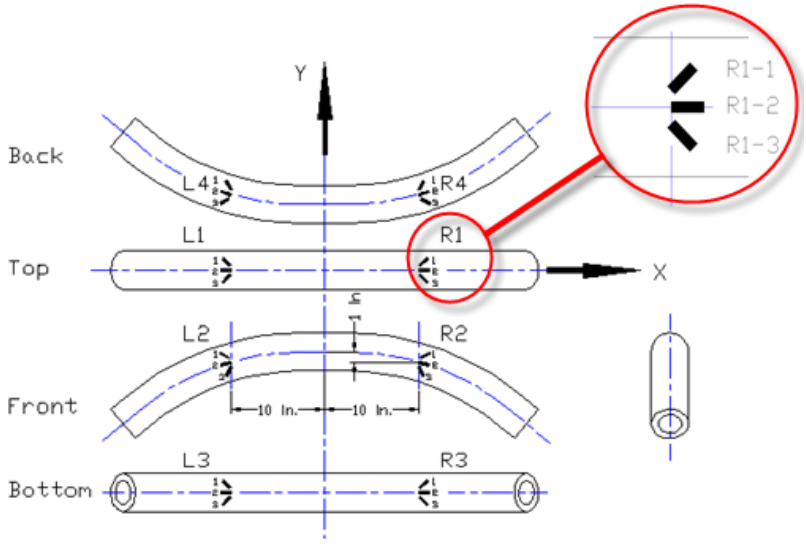

(a) Locations of strain gauges of rosette R1, tube 2

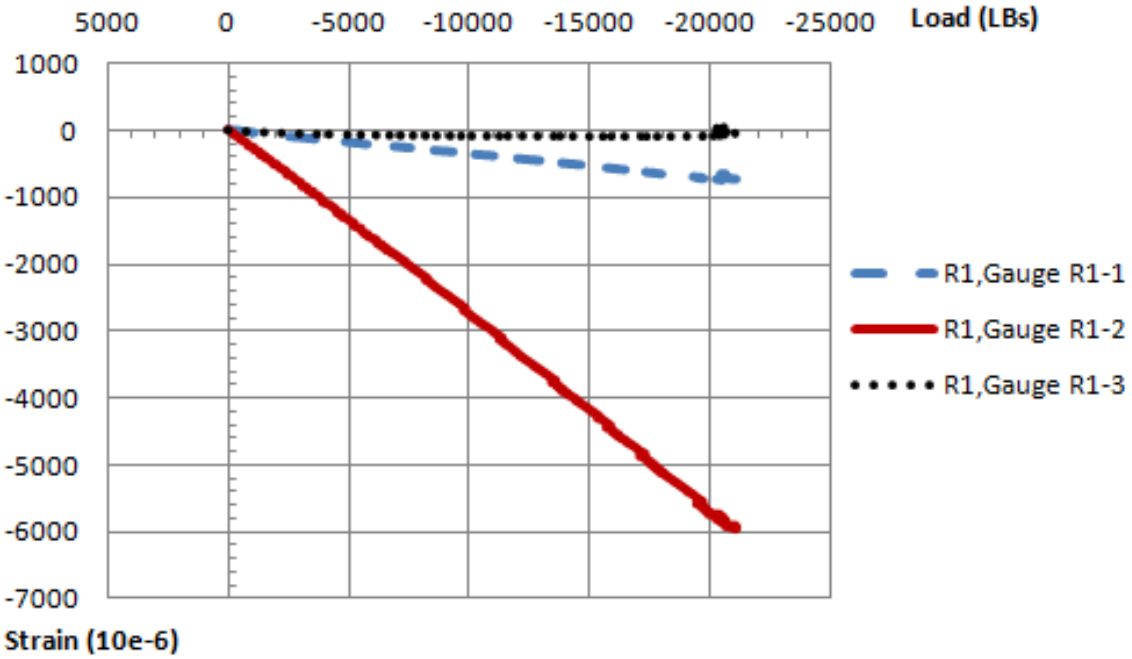

(b) Strains on Rosette R1, tube 2

Figure 4.23 Strains versus load on R1-2 and R3-2 (tube 2)

Rosette R3 is at the right-bottom side showing tensile strains. Strain gauge R3-2 is positioned at center line and showing maximum tensile strain of 6900 micro strain. Strain gauges R3-1 and R3-3 are located at positions symmetrical to center line, and both gauges display small tensile strains.

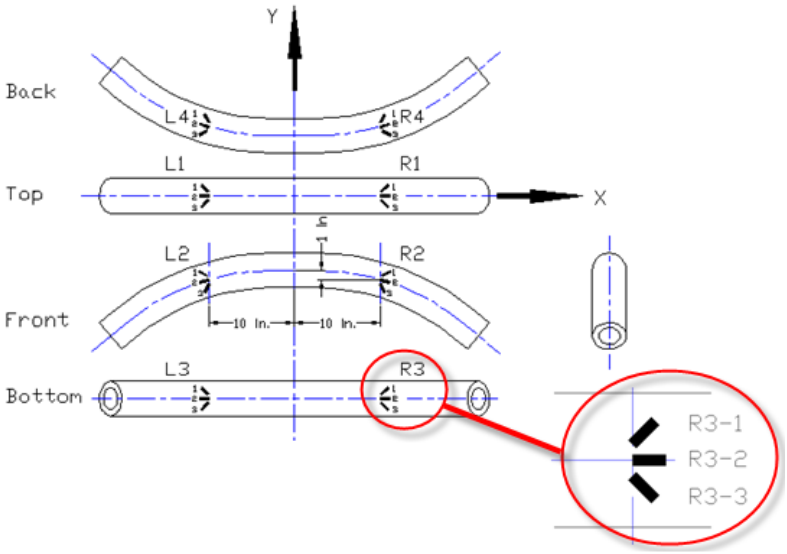

(a) Locations of strain gauges of rosette R3, tube 2

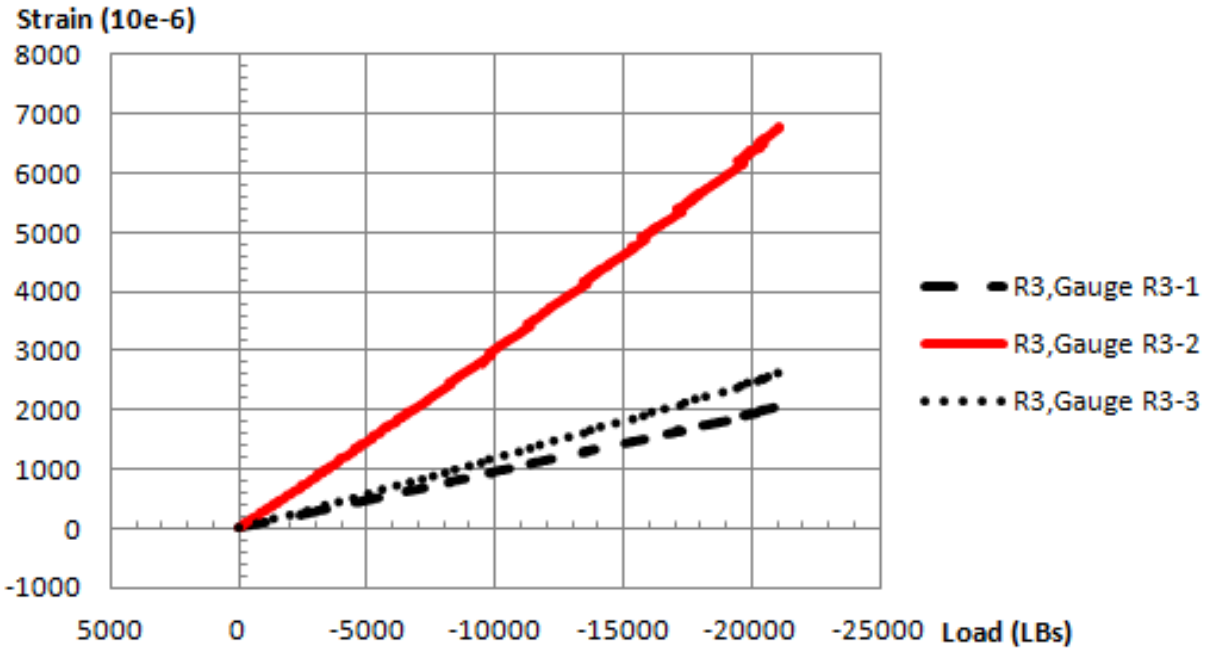

(b) Strains on Rosette R3, tube 2

Figure 4.24 Strains versus load on rosette R3 (tube 2)

Rosette R4 is at the right-rear side. Strain gauge R4-2 is tangent center line. Three strain gauges of this rosette illustrate small compressive strains.

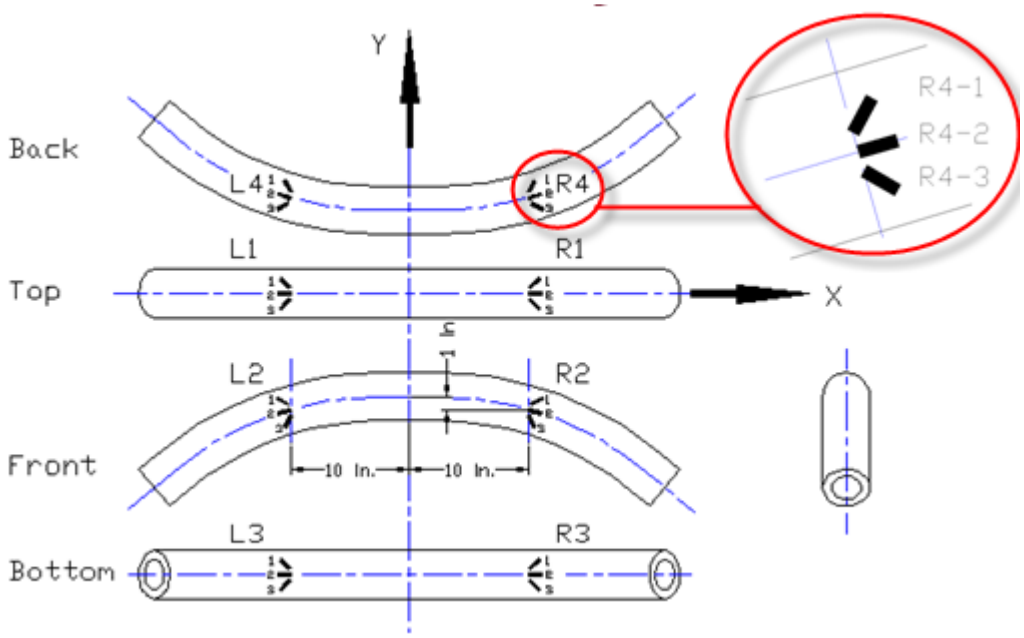

(a) Locations of strain gauge of rosette R4, tube 2

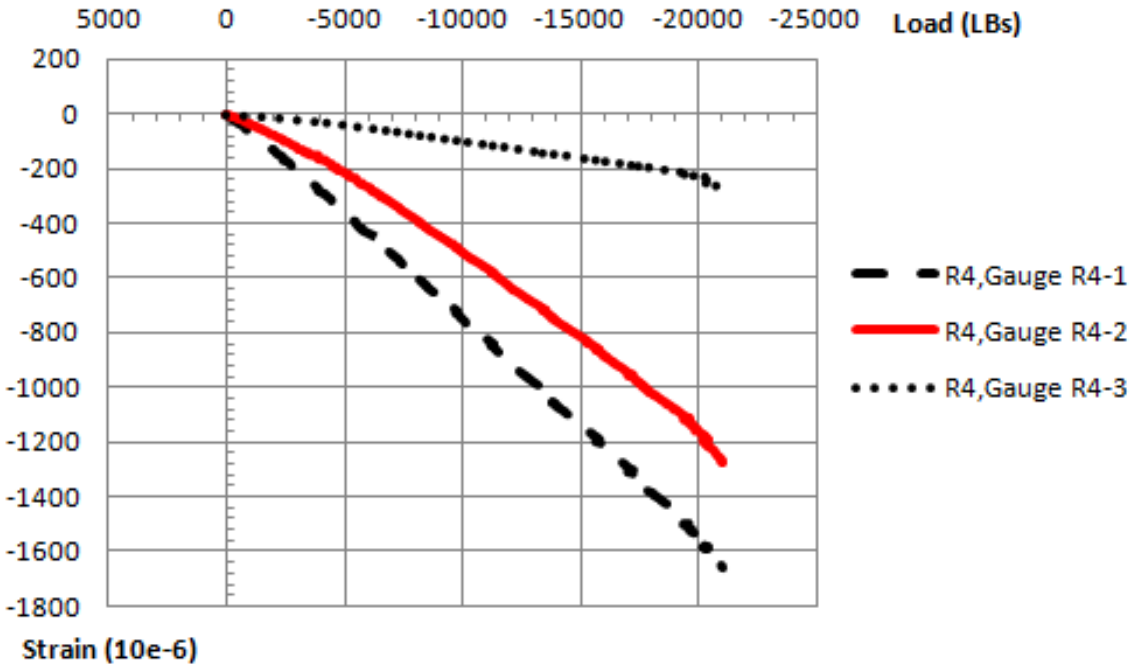

(b) Strains of Rosette R4, tube 2

Figure 4.25 Strains versus load on rosette R4 (tube 2)

Rosette L1 is on the left-top side demonstrating compressive strains. Strain gauge L1-2 is located at the center line and exhibits the maximum compressive strain of 5200 micro strain. Strain gauges L1-1 shows small tensile strain, and L1-3 displays small compressive strains.

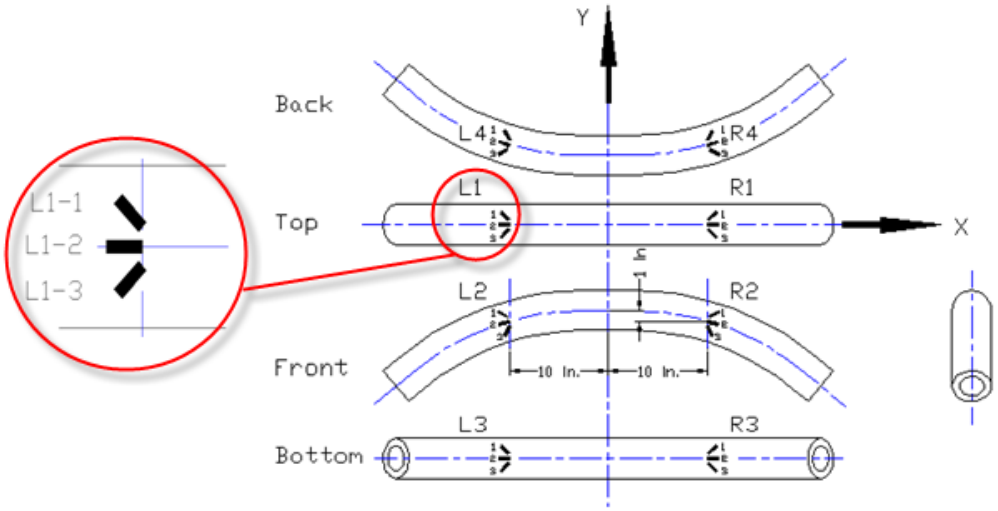

(a) Locations of strain gauges of rosette L1, tube 2

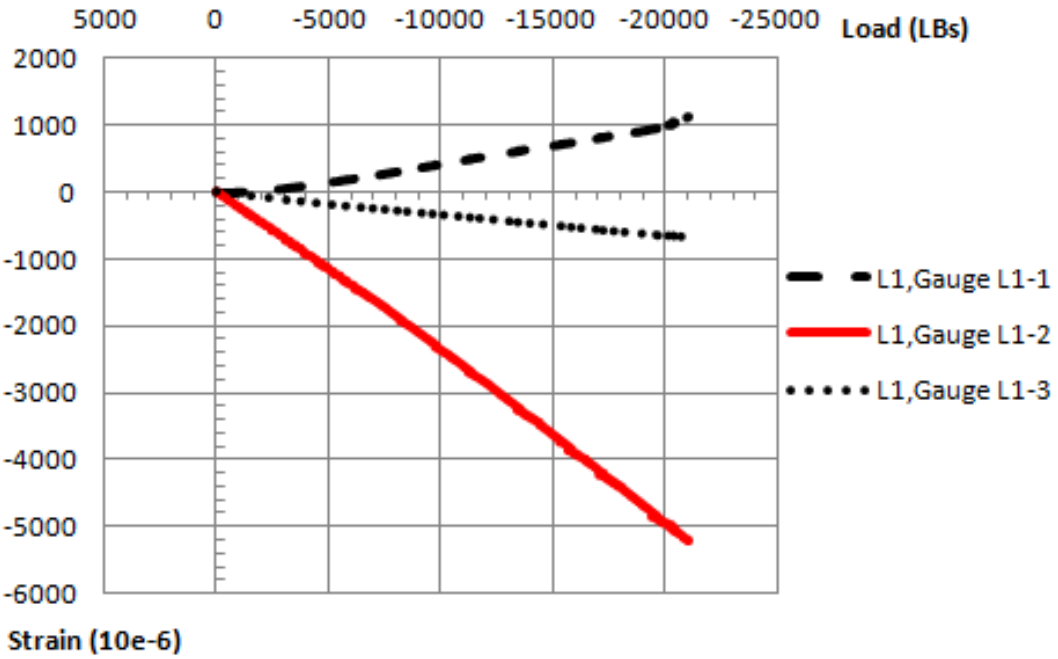

(b) Strains of Rosette L1, tube 2

Figure 4.26 Strains versus load on rosette L1 (tube 2)

Rosette L2 is at the left-front side. Strain gauges L2-1 and L2-2 display very small compressive strains, and strain gauge L2-3 exhibit a maximum compressive strains of 2300 micro strain.

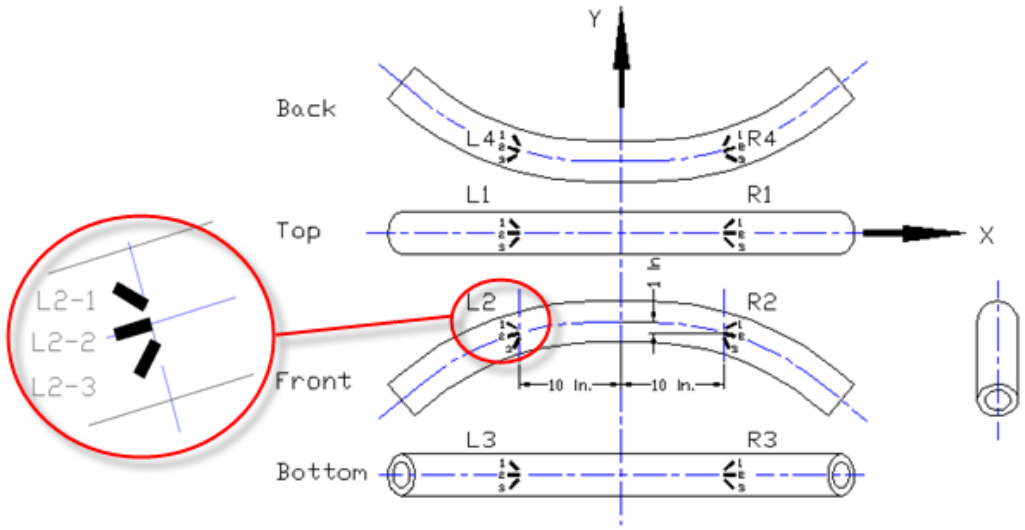

(a) Locations of strain gauges of rosette L2, tube 2

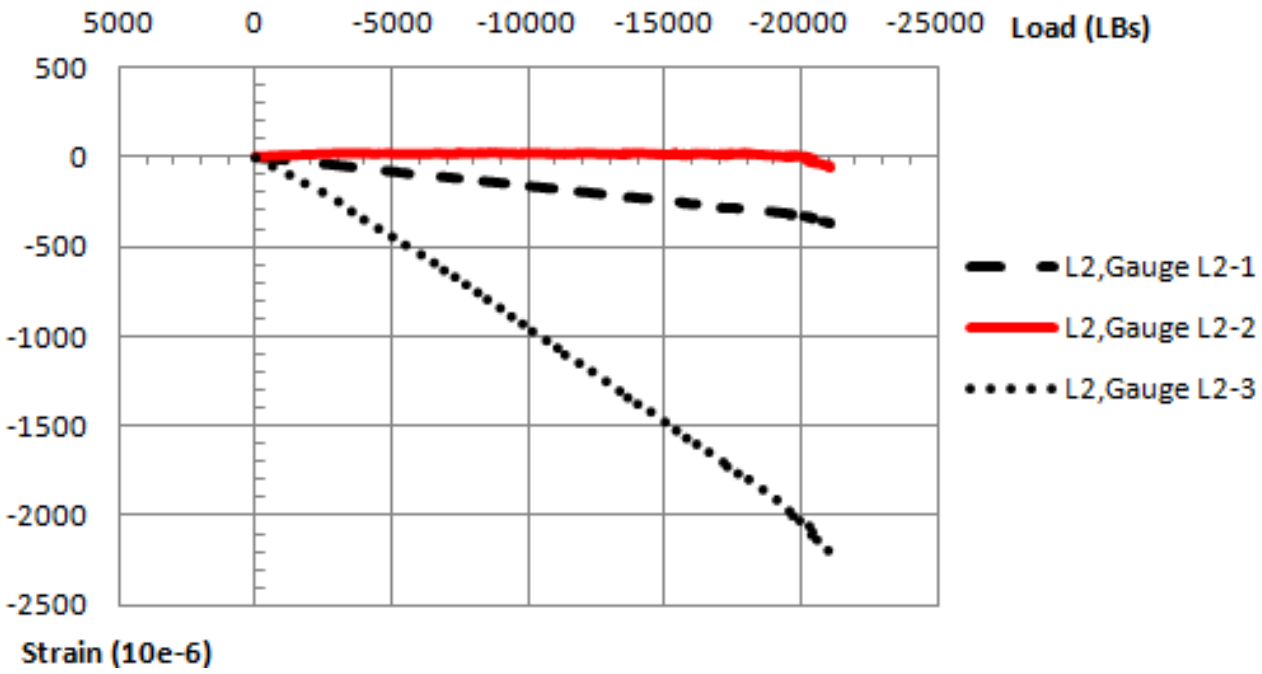

(b) Strains of Rosette L2, tube 2

Figure 4.27 Strains versus load on rosette L2 (tube 2)

Rosette L3 is at the left-bottom side showing tensile strains. Strain gauge L3-2 is positioned at center line and showing maximum tensile strain of 9000 micro strain. Strain gauges L3-1 exhibits maximum tensile strain of 2500 micro strain, and L3-3 displays maximum tensile strain of 3900 micro strain.

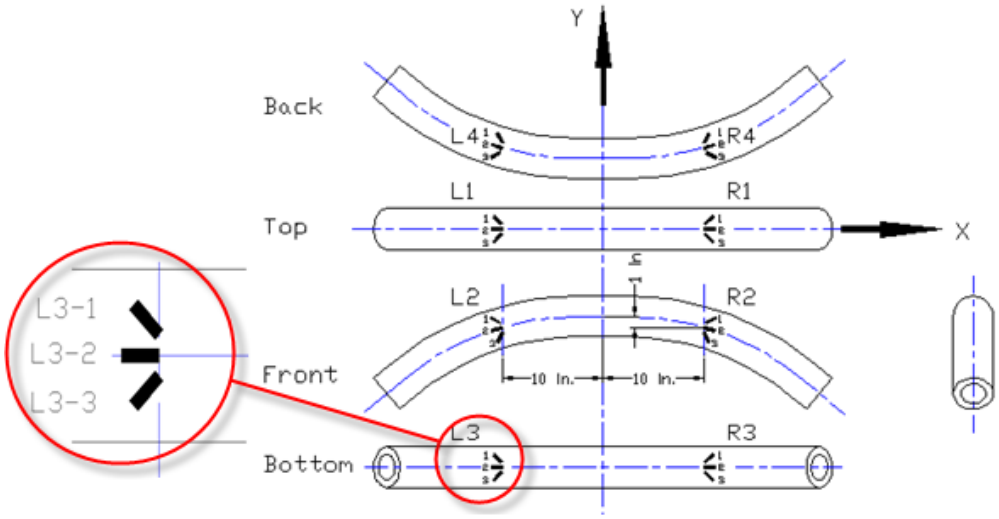

(a) Locations of strain gauges of rosette L3, tube 2

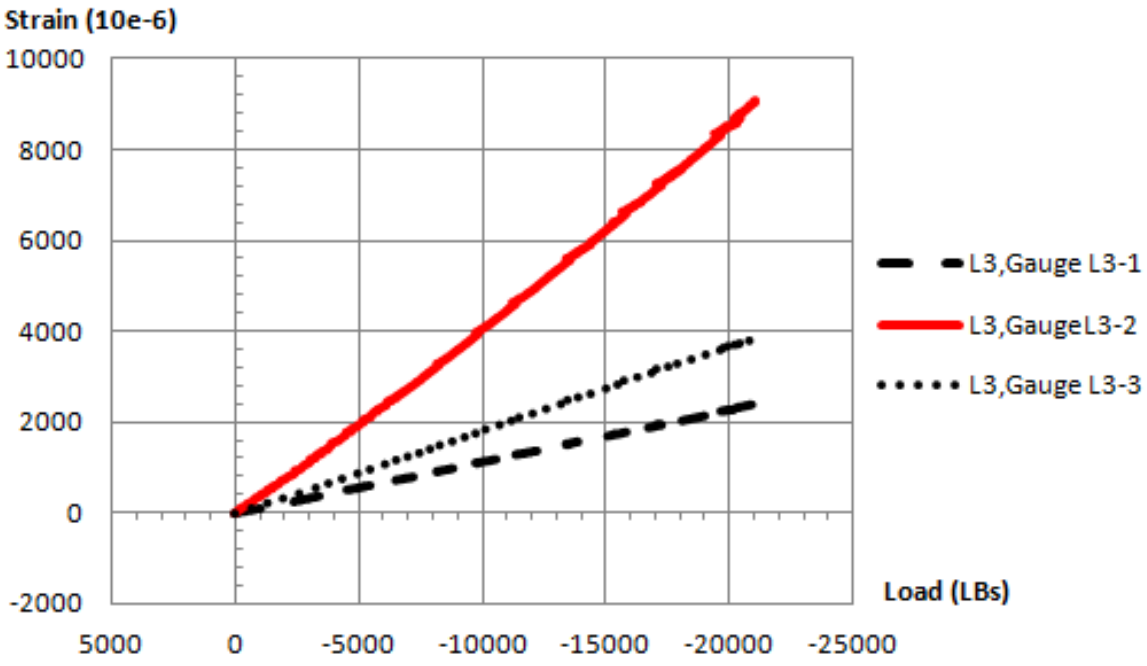

(b) Strains of Rosette L3, tube 2

Figure 4.28 Strains versus load on rosette L3 (tube 2)

Rosette L4 is at the left-rear side. Strain gauge L4-2 is tangent center line. All strain gauges show small compressive strains.

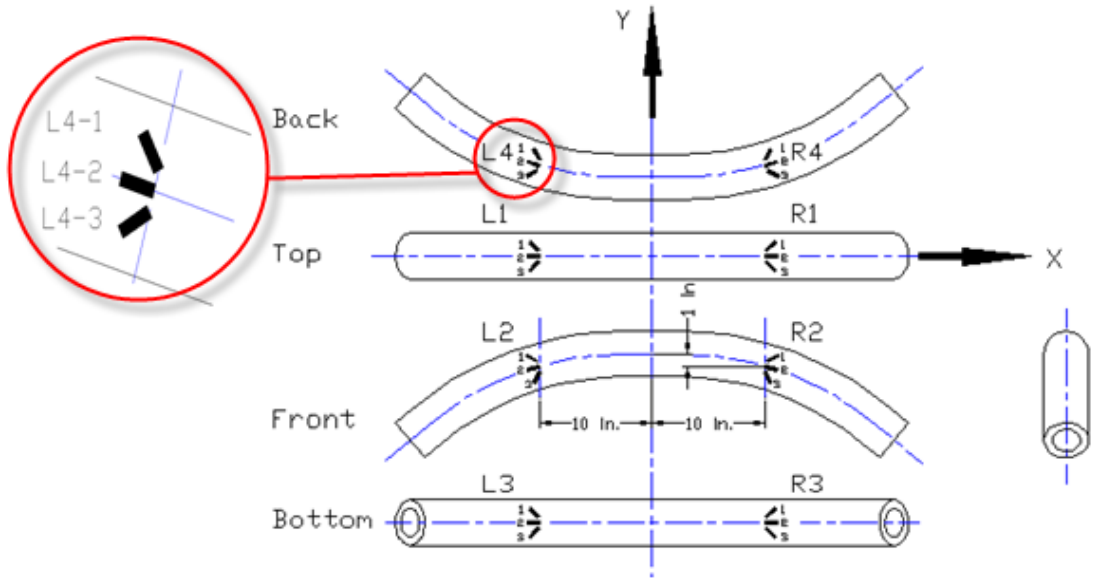

(a) Locations of strain gauges of rosette L4, tube 2

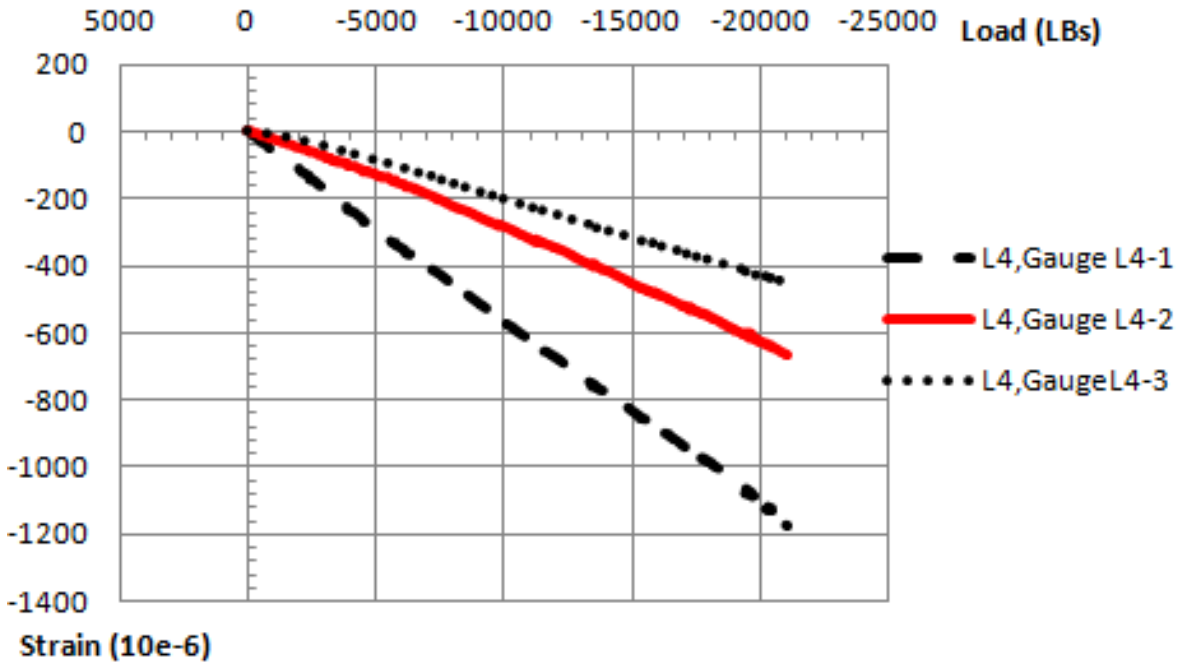

(b) Strains of Rosette L4, tube 2

Figure 4.29 Strains versus load on rosette L4 (tube 2)

4.3.3 Compare the experimental data with FEA

The finite element analysis is performed using ABAQUS. Due to the symmetry of the curved tube, half of the tube is modeled to reduce the number of elements. Only the linear analysis was conducted, so there were only comparison for the linear portion of the load and strains between experimental data and FEA results

As shown in Figure 4.30, the length of line EF represents the holder shown in Figure 4.8(e), which is not deformable during the test.

A 4-node shell element, S4R, is used to conduct the analysis. The element size is 0.2 inches; and there are 6680 elements in total. The displacement of face AB is applied as loading, and only linear analysis was conducted. The reaction force at point F, and the strains on the element located at 10 inches to the middle plane (on top and bottom surface) are recorded.

The following mechanical properties listed are used for this analysis. [13]

(1) $E_{11} = 20000000\ psi$, $E_{22} = 1500000\ psi$, $E_{33} = 1500000\ psi$

(2) $\upsilon_{12} = 0.3$, $\upsilon_{13} = 0.3$, $\upsilon_{23} = 0.33$

(3) $G_{12} = 820000\ psi$, $G_{13} = 820000\ psi$, $G_{23} = 200000\ psi$

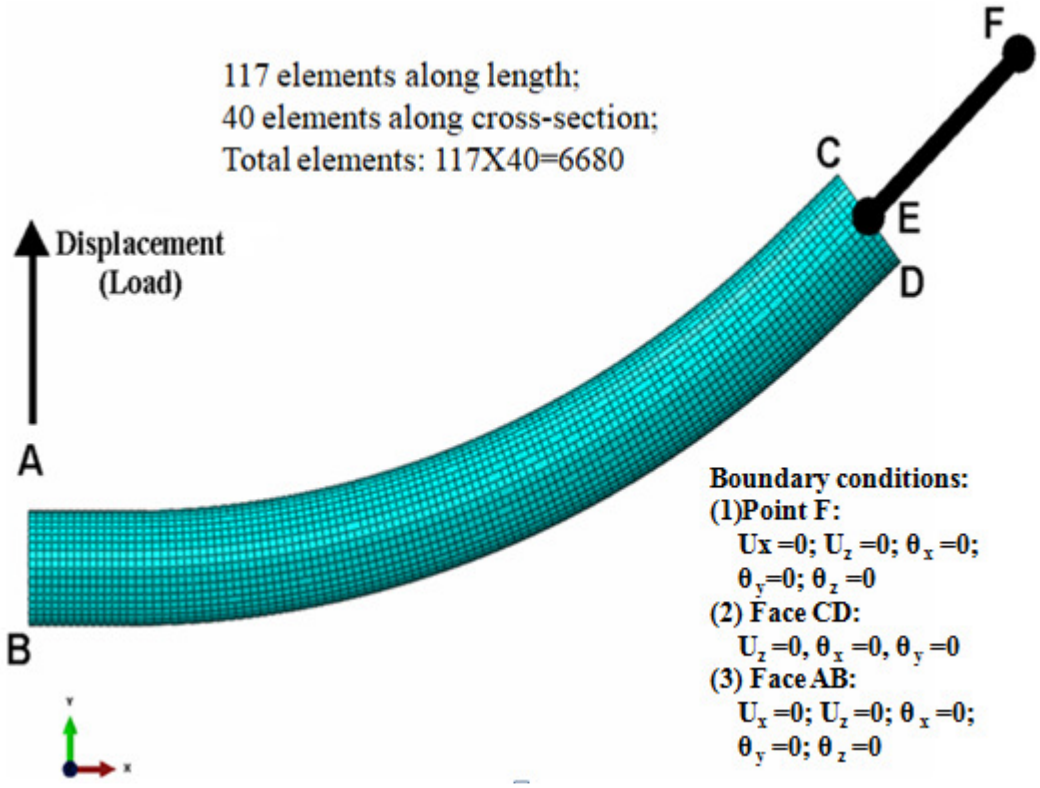

Figure 4.30 FEA model of curved tube

4.3.3.1 Comparison of the result on tube 1 (Constant thickness)

Comprisons of for load versus deflection are displayed in Figure 4.31, good correlation is found at the linear portion of the curve between experimental data and the FEA results.

1) Forces versus deflection (Figure 4.31)

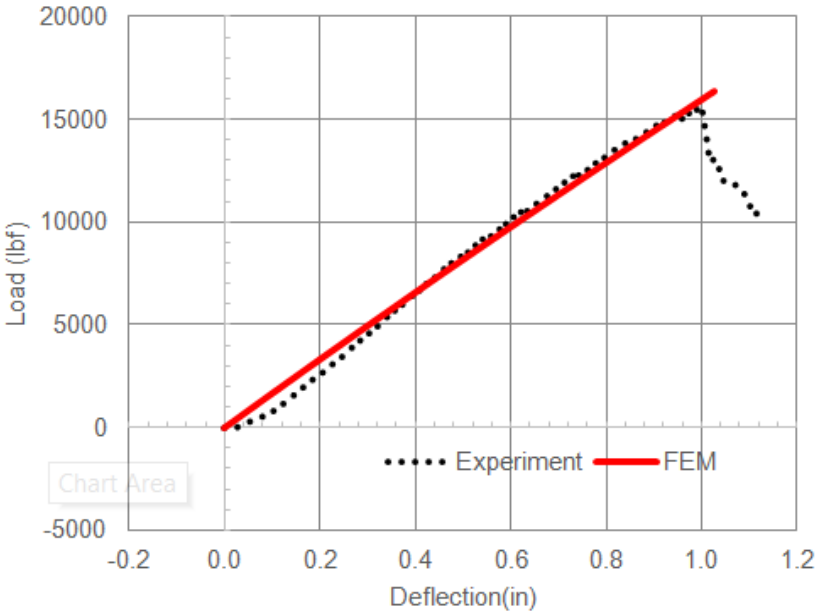

Figure 4.31 Compared with FEA , load versus deflection for tube 1

2.) Strains versus loads (Figure 4.32, compressive strains on gauge R1-2 and L1-2)

As for the strains shown in Figure 4.32, the difference is about 14%.

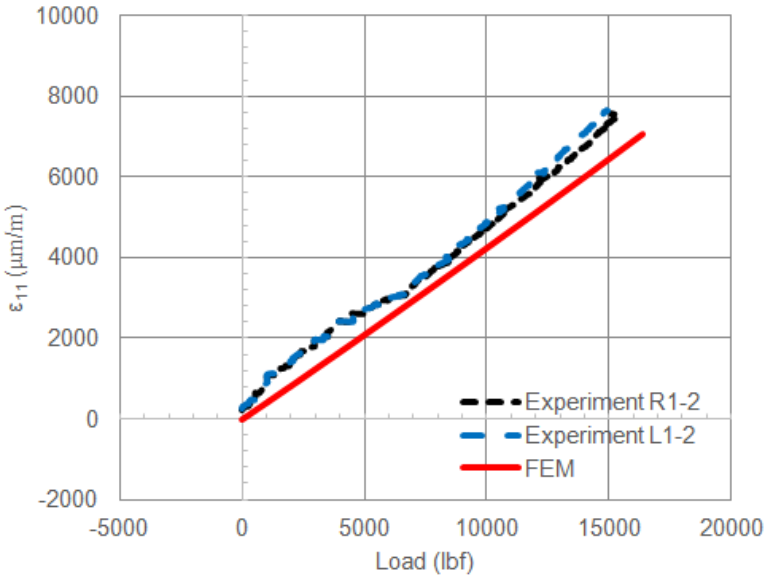

Figure 4.32 Compared with FEA , strains versus load for tube 1

3.) Strain distribution of tube 1 at load of 16000 lbs (from FEA results)

Figure 4.33 illustrate the strain distribution on whole tube at a load of 16000 lbs. Since only half of the tube is modeled, this figure contains a mirror of modeled tube. It can be seen that the maximum tensile strain is about 14800 micro strains (point A on top, 3.0 inches to YZ plane from Figure 4.35) where the tube fails, and the maximum compressive strain is about 8500 micro strains (point B at bottom, 6.0 inches to YZ plane from Figure 4.36).

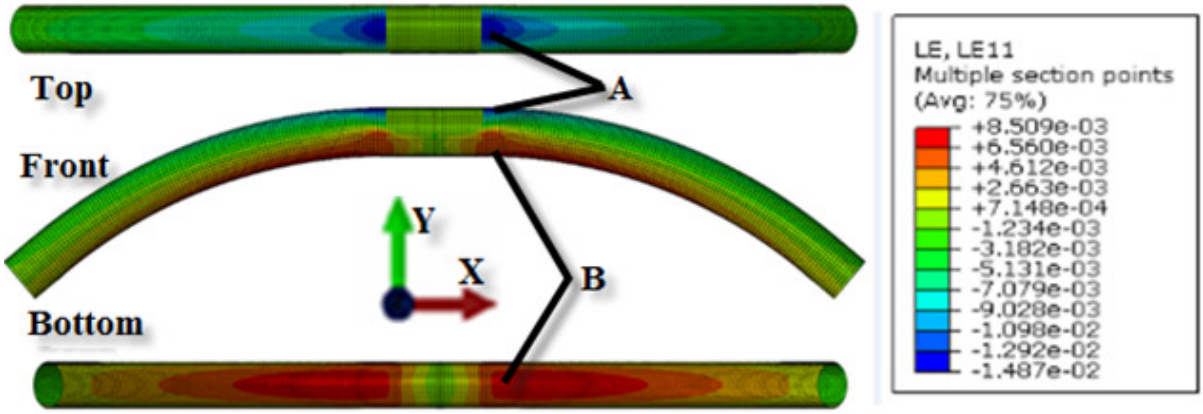

Figure 4.33 Strain distribution on whole tube (tube 1)

In Figure 4.34, a cross section is defined, and strains on half cross section are demonstrated. The axis of distance describes the positions of elements from point A to C, and to B (from top to bottom, or from tension side to compression side). It is found that maximum tensile strain occurs at point B, and maximum compressive strain occurs at point A. Point C is located at the central line where the strain is zero.

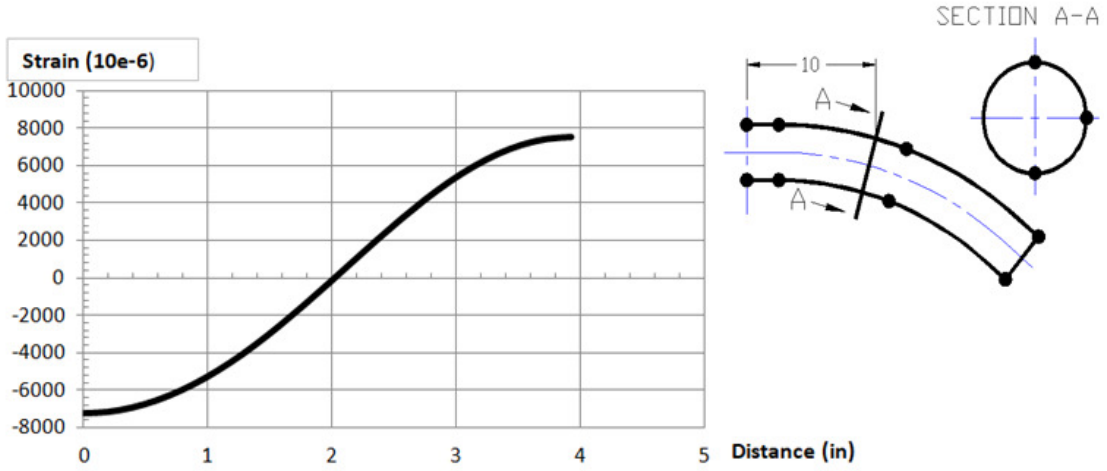

Figure 4.34 Strains at one cross section (tube 1)

Figure 4.35 describes the strains of the elements along center line ABC on top. There is no strain at portion AB, since this portion is defined as the loading area (the displacement of this portion is used as load). It can be found that the maximum compressive strain of 15000 micro strains occurs at the area close to point B.

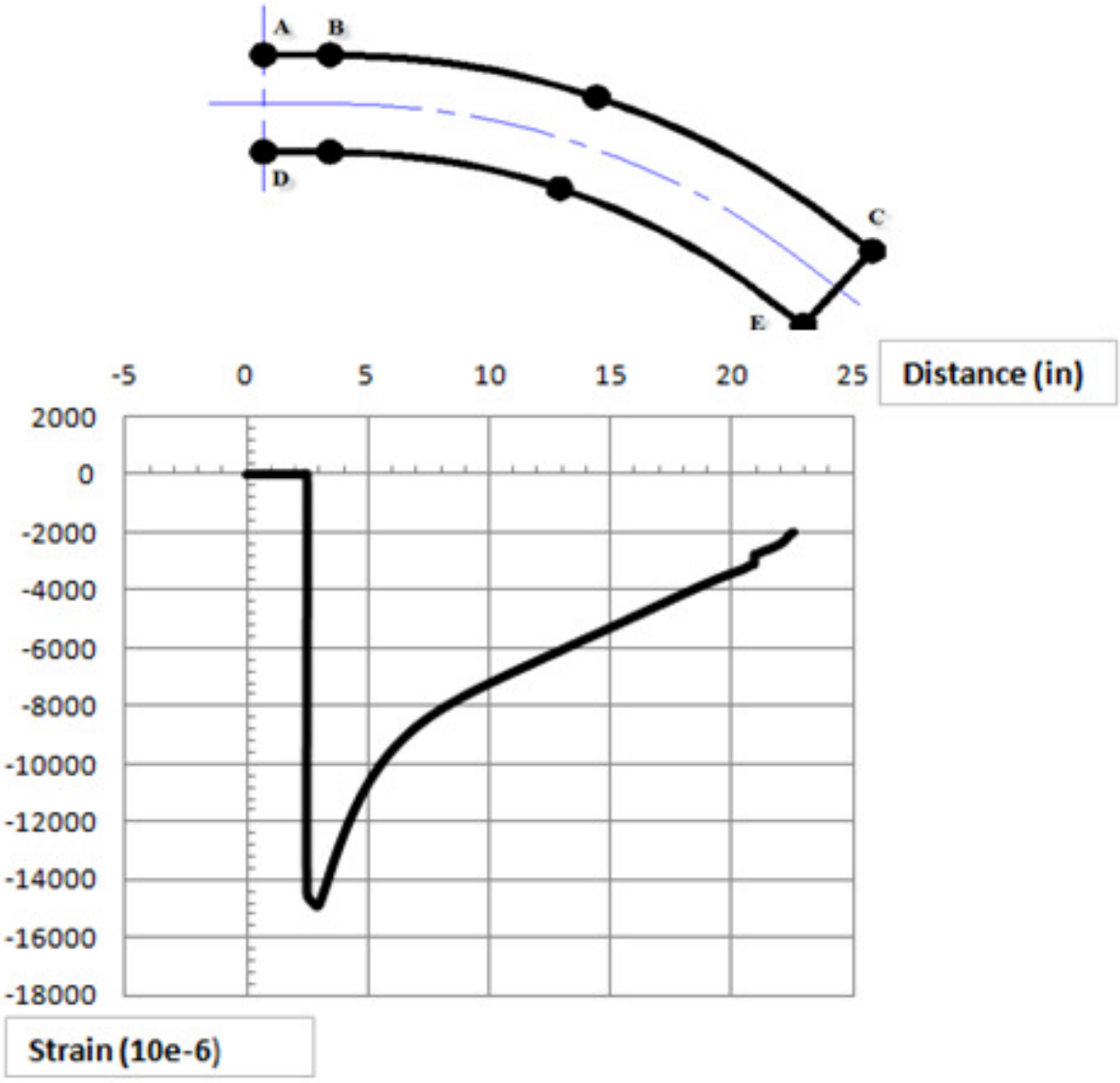

Figure 4.35 Strains along center line ABC on top (tube 1)

Figure 4.36 describes the strains of the elements along center line DE at bottom. It can be found that the maximum tensile strain of 8800 micro strains occurs at the point which is 6 inches to the vertical center line of the curved tube (Y-axis).

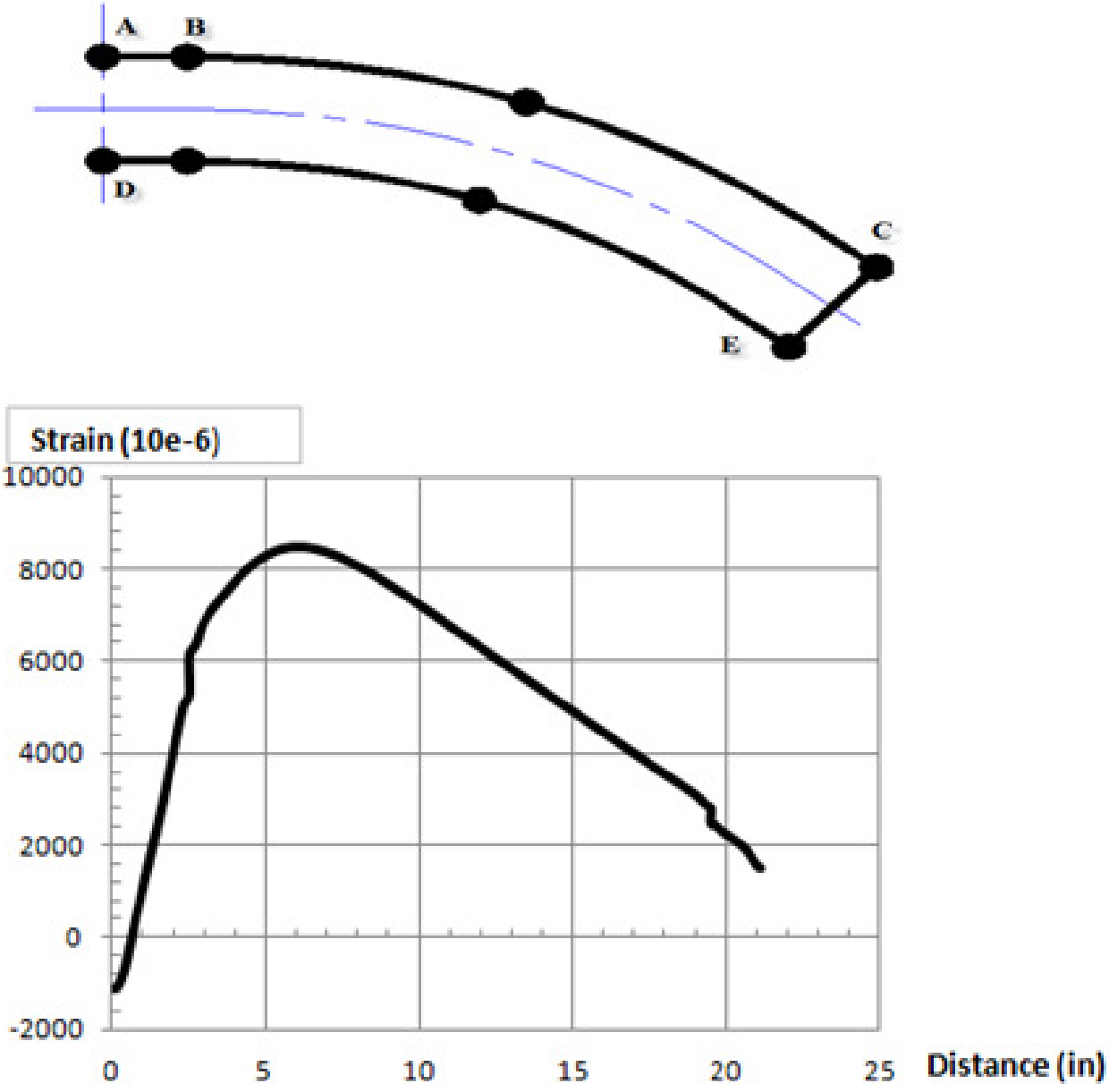

Figure 4.36 Strains at center line DE at bottom (tube 1)

4.3.3.2 Comparison of the result on tube 2 (Variable thickness)

1.) Force versus deflection

Comprisons of for load versus deflection are displayed in Figure 4.37, good correlation is found at the linear portion of the curve between experimental data and the FEA results.

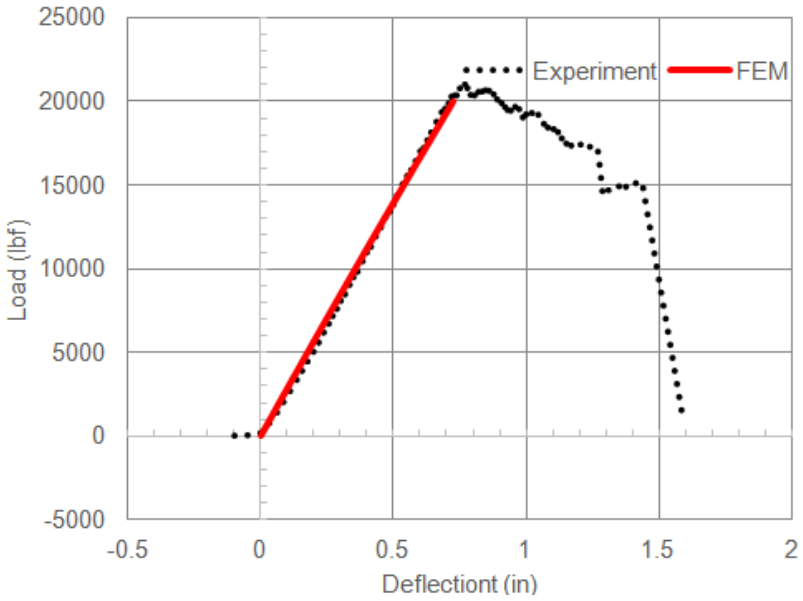

Figure 4.37 Compared with FEA , load versus deflection for tube 2

2.) Strains versus loads (Figure 4.38, compressive strain on gauge R1-2 and L1-2)

As for the strains shown in Figure 4.38, the difference between experimental data and FEA results is about 14%.

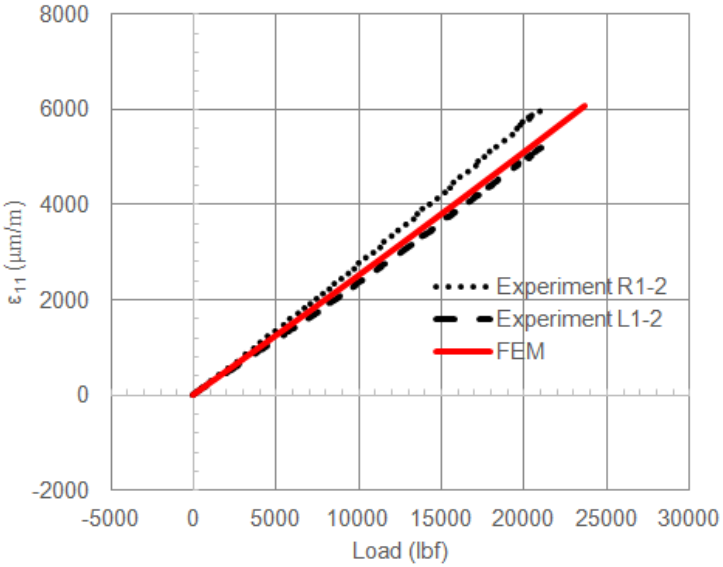

Figure 4.38 Compared with FEA , strains versus load for tube 2

3.) Strain distribution on tube 2 at load of 22000

Figure 4.39 illustrate the stain distribution on whole tube at a load of 22000 lbs. It can be seen that the maximum tensile strain is about 12600 micro strains (at point A on top, 4 inches to YZ plane from Figure 4.41) where the tube fails, and the maximum compressive strain is about 7600 micro strains (point B at bottom, 6 inches to YZ plane from Figure 4.42).

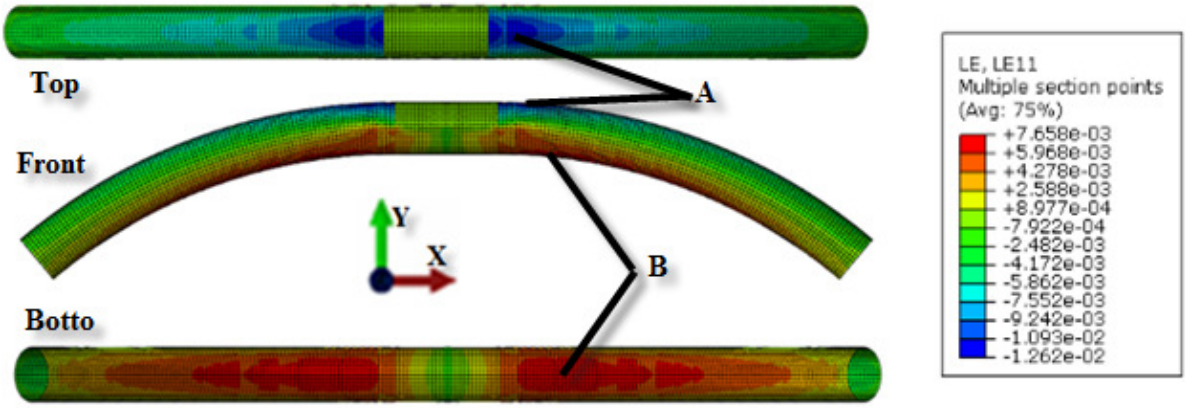

Figure 4.39 Strain distribution on whole tube (tube 2)

In Figure 4.40, a cross section is defined, and trains on path A-C-B are illustrated. The maximum strain of 6000 micro strains is at point, and maximum compressive strain is at point A. The axis of distance describes the positions of elements from point A to C, and to B (from top to bottom, or from tension side to compression side). Point C is located at the central line where the strain is zero.

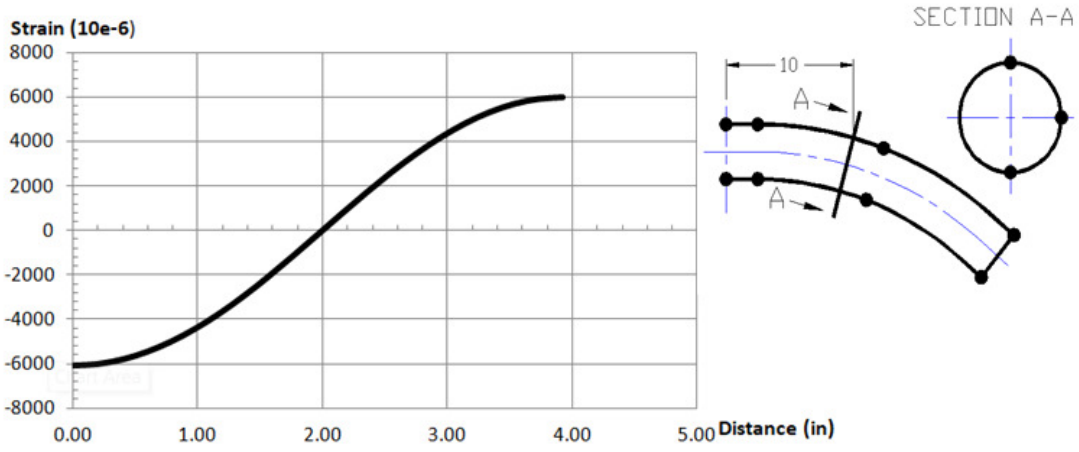

Figure 4.40 Strains at one cross section (tube 2)

Figure 4.41 describes the strains of the elements along center line ABC on top. The portion AB is defined as the loading area (the displacement of this portion is used as load), so there is no strain in the area. The maximum compressive strain of 12000 micro strains occurs at the area close to point B. The zigzags on the curve of strains are caused by the variable thickness. (There are rapid thickness changes between composite layers when the variable thickness is form in FEA model)

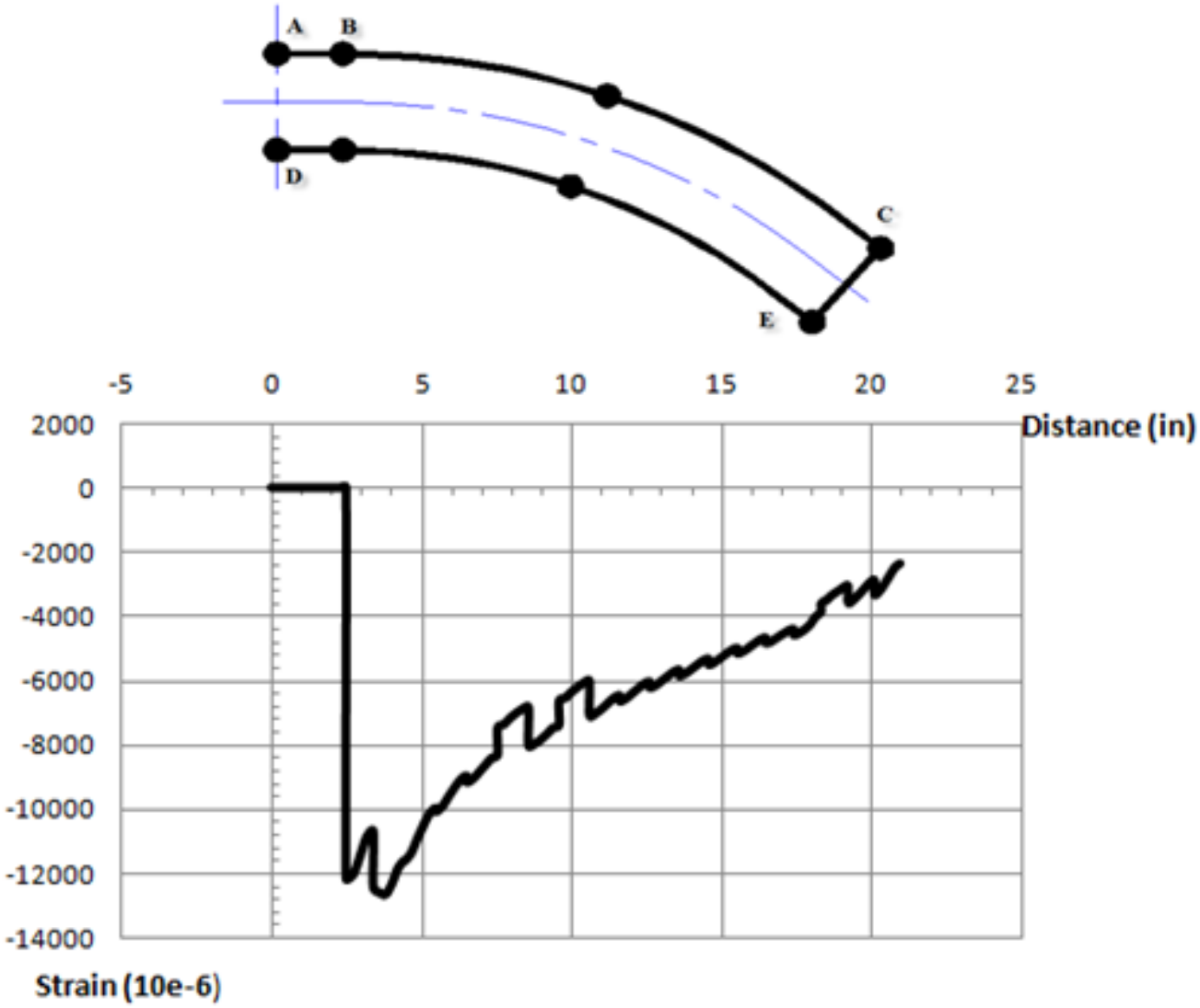

Figure 4.41 Strains at center line ABC on top (tube 2)

Figure 4.36 demonstrates the strains of the elements along center line DE at bottom. It can be found that the maximum tensile strain of 7500 micro strains occurs at the point which is 6 inches to the vertical center line of the curved tube (Y-axis).

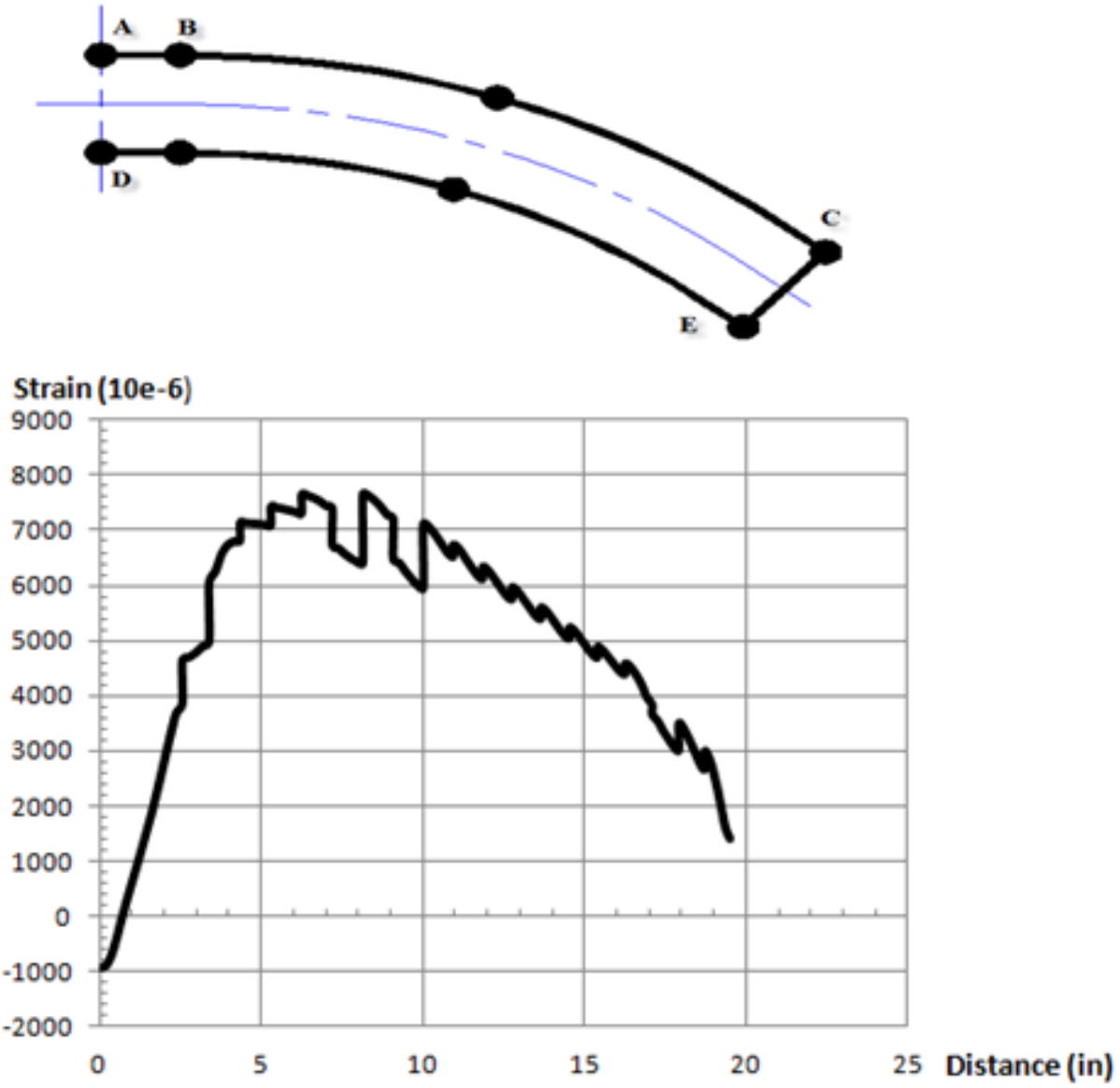

Figure 4.42 Strains at center line DE at bottom (tube 2)

Chapter 5. Discussions, Conclusions and Contributions

5.1 Discussions

(1). Curved thermoplastic composite tubes can be made using automated fiber placement with a segmented mandrel covered with gypsum plaster. Such tubes have good quality and the required strength and stiffness which is mentioned in the research of Bijean Derisi[11].

(2). Combined with segmented metal shaft, gypsum plaster (Plaster of Paris), working as dissolvable or breakable buffer material, provides the most economical and practical way to manufacture thick curved thermoplastic composite tubes.

(3.) According to the experimental results, the maximum strains and stresses are located at the center portion of the tube where the loads are applied, and then variable thickness for the curved tube is required. The maximum thickness should exist at the centre portion and gradually decrease to the minimum at both ends.

(4.) It is difficult to directly deposit thermoplastic composite on to the surface of the plaster, thus thermoset composite layers are wrapped to help the thermoplastic layers to stick on the plaster. It is a preferred choice that coating of epoxy be used to strengthen the plaster and be of assistance to deposit the thermoplastic layers.

5.2 Conclusions

A process for fabricating thick curved thermoplastic composite tubes has been successfully developed by applying a segmented mandrel covered with gypsum plaster as a dissolvable or breakable buffer material. The tubes made with this manufacturing process have the required stiffness and strength. This process offers the possibility to perform further research of the curved composite tubes that will be employed as landing gear in helicopters.

5.3 Contributions

Gypsum phenomenon, which describes a unique property of gypsum that gypsum ($CaSO_4.2H_2O$) loses the water of hydration at elevated temperature to form gypsum plaster (Plaster of Paris, $CaSO_4.0.5H_2O$), and then recombines with proper amount of water at low temperature to attain gypsum, has been successfully employed in manufacturing the thick curved thermoplastic composite tube.

The mandrel for thick curved thermoplastic composite tube is made of segmented metal shafts and then covered with gypsum plaster. This type of mandrel is strong enough to withstand the manufacturing force and high processing temperature. When the curved tube is finished, the whole mandrel can be successfully removed

The thick curved thermoplastic composite tubes made with this type of mandrel have the required strength and stiffness, and the 3-point bending test results have good correlation with the results from finite element analysis.

A conference paper is published:

Chong Hui Song, Jeffrey Fortin Simpson, Suong Van Hoa

"Development of manufacturing process for thick curved thermoplastic composite tubes by using automated fiber placement"

2nd composite symposium, April 2017, Montreal, Canada

5.4 Future works

(1). The gypsum phenomenon or gypsum technology deserves more work, since there are five phases for ($CaSO_4.H_2O$) system and only two phases are used for manufacturing curved thermoplastic composite tubes. More research should be performed to find the best curing time and dehydrated temperature for gypsum plaster.

(2). There is a necessity to design better segmented mandrel that would improve the overall ability of the manufacturing process.

(3). It is desired to optimize the shape of the curved tube considering its dynamic behaviors such as vibration, impact, drop test, etc.

(4). More work needs to be done to search suitable cross section and thickness variation of the curved tube to enhance its overall properties, and to attain more weight saving.

Chapter 6. References

[1] P.K. Mallick,"Fiber-reinforcement composites materials, manufacturing, and design", 3rd edition,CRC Press, 2007, Talor & Francis Group, LLC

[2] Suong Van Hoa, "Principles of the Manufacturing of Composite Materials", 2nd edition Destech publications, Inc., Pennsylvannia, 2017

[3] https://www.google.ca/imgres?imgurl=https://www.1001crash.com/dossier/composite/B787_composite.jpg&imgrefurl=https://www.1001crash.com/index-page-composite-lg-2.html&h=417&w=700&tbnid=26D0TVqw-QiNVM:&tbnh=138&tbnw=232&usg=__LljeqheTswrgDxTrnDOoUFJtJOM%3D&vet=10ahUKEwiEoe3jzezZAhURk1kKHdLMB1oQ9QEIKzAA..i&docid=_bPeV_8IualkRM&sa=X&ved=0ahUKEwiEoe3jzezZAhURk1kKHdLMB1oQ9QEIKzAA

[4] Michael W. Hyer,"Stress analysis of fiber-reinforced composite materials",WCB/Mc-Graw Hill International Editions, 1998

[5] Dan Leeser, "Thermoplastic composites: A proven composite material technology generates new interest", EPOXYWORKS Number 26, 2008, Gougeon Brothers, Inc.

[6] Kendra A. Allen,"Processing of thermoplastic composites", *Polymer and composite processing (2012)*, pp 1-10

[7] Brydson, J.A., "Plastic Materials", 1989, Fifth Edition, Butterworth Scientific, London

[8] Joanna Wong, "Processing of high performance thermoplastic composites", 2 March 2017,131-5048-00L Manufacturing of Polymer Composites
https://www.ethz.ch/content/dam/ethz/special-interest/mavt/design-materials-fabrication/composite-materials- dam/Education/ Manufacturing_of_Polymer_Composites/FS2017/151-0548-FS2017-K5-MATERIALS.PDF
CMAS Lab, ETH Zurich

[9] "https://www.automateddynamics.com"

[10] Xiao Cai, "Determination of process parameters for the manufacturing of thermoplastic composite cones using automated fiber placement", MSc. Thesis, Concordia University, 2012

[11] Derisi Bijan, "Mechanical behavior of tubes made of thermoplastic composites for helicopter applications", Ph.D thesis, Concordia University, 2008.

[12] Derisi, B., Hoa, S.V., Xu, D., Hojjati, M., and Fews, R., "Mechanical behavior of carbon/PEEK thermoplastic composite tube under bending load", Journal of Thermoplastic composites Materials, Vol. 24, No. 1, January 2011, pp. 29-49.

[13] Derisi, B., Hoa S.V., and Hojjati, M. "Similitude study on bending stiffness and behavior of composite tubes", Journal of Composite Materials, Vol. 46, No. 21, 2012, pp 2695-2710.

[14] E, Vargas Rojas, D. Chapelle, D. Perreux, B. Delobelle, F. Thiebaud, "Unified approach of filament winding applied to complex shape mandrels", Composite Structures, 116 (2014) 805-813

[15] V.V. Vasiliev, A.A. Krikanov, A.F. Razin, "New generation of filament-wound composite pressure vessels for commercial applications", Composite Structures, Volume 62, Issue 3-4, 2003, pages 449-549

[16] F. Henninger, K.Friedrich, "Thermoplastic filament winding with online-impregnation. Part A: process technology and operation efficiency", Composite Structures, Volume 33, Issue 11, November 2002, Pages: 1479-1486

[17] Mohamed Ibrahim El-Geuchy, "Bending Behavior of Thick-Walled Composite Tubes", Ph.D Thesis, Concordia University, 2013

[18] Can Hui Zhang, Suong Van Hoa, Pei Liu, "A method to analyze the pure bending of tubes of cylindrically anisotropic layers with arbitrary angles including 0° or 90°", Composite Structures,volume 109, page 56-67, March 2014, ISSN:0263-8223

[19] Ahmed M. Amin, Mithuma Thottethodi, T.N. Vijaykumar, "AquaCore: A programmable architecture for microfluidics", ISCA 07, June 9-13, 2007, San Deigo USA.

[20] Matthias Meyer Dipl. -ing, "Micro wave drying of Aquacore, Aquapour and Aquaseal", www.aero-consutants.ch

[21] "A guide to product lines", www.acmtucson.com,

[22] "Aqua infor and instructions", www.aero-consultants.ch,

[23] Sayonara M. M. Pinherio and Gladis Camanrini, "Characteristics of Gypsum recycling in different cycles", LACSIT International Journal of Engineering and Technology, Vol. 7 N0. 3 June 2015.

[24] Harry B. Weiser and Ferrin B. Moreland, "The setting of Plaster of Paris", J. Phy. Chem. 1932, 36(1) pp 1-30, DOI: 10 1021/j150331a001

[25] P. S. Irabor, S. O. Jimoh, O. J. Omowumi, B S. O. Ighalo, “Physical and chemical analysis of some Nigerian gypsum minerals for application in manufacturing, construction and allied industries”, International Journal of Scientific & Technology Research, Volume 2, Issue 10, October 2013.

[26] Kim A. Cabrera, “Plaster Track Casting Procedure”, www.bear-tracker.com.

[27] “Plaster of Paris”, Transactions of the Indian Ceramic Society, 18:1-2, 35-54, DOI: 10.1080/0371750X.1959.11011909

[28] E. Posnjak, “The System CASO4.H2O”, Am. J. Sci. 1938;5(35A): 247-72.

[29] “http://www.loftingservices.co.uk”

[30] G. Hohne, W. Hemminger, H. –J Fla,,Ershelm, “Differential scanning calorimetry: and introduction for practioners", Belin; New York: Springer-Verlag, 1996

[31] Yunus A. Cengel, Afshin J. Ghajar,“Heat and Mass Transfer: Fundamentals & Applications”, 4th Edition, Mc Graw Hill.

[32] https://www.cytec.com/sites/default/files/datasheets/APC-2_PEEK_031912-01.pdf

[33] Derisi, B., Hoa, S.V., Xu, D., Hojjati, M., and Fews, R, “Composite tube exhibiting large deformation under bending”, Journal of Composite Materials, Vol. 44, No. 16, 2010, pp. 2005-2020.

[34] Captain J.R. Watson, “Building composite tubes with West System® epoxy and braided fibers”, EPOXYWORKS Number 26, Spring, 2008. Gougeon Brothers, Inc.

[35] Nehdi Hajianmaleki, Mohamad S. Qatu, “Vibrations of straight and curved composite tube: A review”, Composite Structures, 100(2013) 218-232.

[36] J.B. Bai, J.J. Xiong, J.P. Gao. X.S. Yi, “Analytical solutions for predicting in-plane strain and interlaminar shear stress of ultra-thin-walled lenticular collapsible composite tube in fold deformation”, Composite Structures 97(2013) 64-75.

[37] G. Minak, S. Abrate, D. Ghelli, R. Panciroli, A. Zucchelli, “Low-velocity impact on carbon/epoxy tubes subjected to torque: Experimental results,analytical models and FEM analysis”, Composite Structures 92(2010) 623-632.

[38] El-Sadig Mahdi, Hany El Kadi
“Crushing behavior of laterally compressed composite elliptical tubes: Experimental and predictions using artificial neural networks”, Composite Structures 83 (2008) 399-412.

[39] E.E. Theotokoglou, “Behavior of thick composite tubes considering of delamination” Theoretical and Applied Fracture Mechanics 46 (2006) 276-285

[40] Dimitrios Karamanlidis, University of Rhode Island, “A simple and efficient curved beam element for the linear and non-linear analysis of laminated composite structures”, Computer &Structures Vol. 29, No. 4. pp 623 - 632, 1988

[41] K.T. KEDWARD, R.S. Wilson and K. McLEAN, “Flexure of simply curved composite shapes”, Composites, November 1989, volume 20, Issue 6, Pages 527-536

[42] Mohamad S. Qatu, “Theories and analysis of thin and moderately thick laminate composite curved beams”, Int. J. Solids Structures, Vol. 30. No. 20. pp. 2743-2756, 1993

[43] Weicheng Cui, Tao Liu, Jianxin Len and Rongbio Ruo, “Interlaminar tensile strength (ILTS) measurement of woven glass/polyester laminates using four-point curved beam specimen”, Composite parts A 2A (1996) 1097-1105.

[44] Adel Zaki EI-Sonbati, “Thermoplastic composite materials”, Intech, ISBN 978-953-51-0310-3, March 2012, Croatia

[45] J. Dweck, E.I.P. Lasota, university of Rio de Janeiro, “Quality control of commercial plaster by thermogravity”, Themochimca Acta 318 (1998) 137-142.

[46] Ahmet Hilmi Kaya, MD, Adnan Dagcinar, MD, Ibrahim Cebeci, MD, “A training model head of plaster of paris for stereotactic localization”, Surgical Neurology 68 (2007) 544-546.

[47] V.Gopal, K.P. Eloang, “Equilibrium, kinetic and thermodynamic studies of adsorption of fluoride onto plaster of paris”, Journal of hazardous Materials 141 (2007) 98-105.

[48] “Composite Thermoplastic: Lightweight, Corrosion-Free, Interconnect Solutions From Glenair”, Glenair, April 2008, volume 12, Number 2

[49] Maxime Roux, Nicolas Eguemann, Lian Giger, Clemens Dransfeld, High performance thermoplastic compoite processing and recycling: from cradle to cradle”, SAMPE 34th International Technical Conference, January 2013

[50] Klpkjian & Schmid, “Plastics & Composite Materials: Forming & Shaping”, Manufacturing Engineering and Technolgy, 6/e, 2010, Chapter 19, Pearson press

[51] P.D. Mangalgirl, “Composite materials for aerospace applications”, Bulletin of Material Science, May 1999, Volume 22, Issue 3, pp 657-664, India Academy of Science

[52] Jasper Cerneels, Andre Voet, Jan Ivens, Jean-Pierre Kruth, "Additive manufacturing of thermoplastic composites", composite week@Luven and TexComp-11 conference 16-20 September 2013, Leuven.

[53] McCool R., Murphy, A., Wilson R., Jiang, Z., Price, M., Butterfield, J., & Hornsby, P. "Thermoforming carbon fiber-reinforced thermoplastic composites", Journal of materials: Design and Applications, 226(2) 91-102. DOI: 10. 1177/1464420712437381.

[54] T.S, Creasy and Y.S. Kang, "Fiber orientation during equal channel angular extrusion of short fiber reinforced thermoplastic", Polymer technology center Texas A&M University M,S. 3123, 100 ENPH, College Station, TX, USA

[55] "Thermoplastic composite materials made from carbon and glass fibers", SGL Group, www.sglgroup.com/cfm

[56] A. J. Parmar, S. K. Tyagi, V.S. Dabas, J.N. Mistry, "Assessment of the physical and mechanical properties of plaster of paris bandage cast used as a splinting and casting materials", www.veterinaryworld,org/vol.7/December-2014/17.pdf.

[57] Nadira A. Hatin, Isam K. AI-Khayat, Mohammed A. Abdullah, "Modification of gypsum products (Part I): physical and chemical propertes of adding some additives on different types of gypsum products", ISSN: 1812-1217.

[58] R. Wytch, C. Mitchell, I. K. Ritchie, D. Wardlaw and W. Ledingham, "New splinting materials", Prosthetics and Orthotics International, 1987, 11, 42-45

[59] Kaven Croft, "Experimental characterization of autoated fiber placement process defects in composite structures", MSc. thesis 2010, Mcgill University.

[60] Parth N. Raval, Pinank A. Patel, "Expandable and collapsible winding mandrel: A literature review", ISSN 0976-6340 (Print), ISSN 0976-6359 (Online), Volume 5, Issue 2 Feb (2014), pp. 143-148

[61] "https://www.engineeringtoolbox.com